COMPUTATIONAL BIOMECHANICS OF BLAST-INDUCED TRAUMATIC BRAIN INJURY: ROLE OF LOADING DIRECTIONALITY, HEAD PROTECTION, AND BLAST FLOW MECHANICS

A Dissertation
Submitted to the Graduate Faculty
of the
North Dakota State University
of Agriculture and Applied Science

By

Hesam Sarvghad-Moghaddam

In Partial Fulfillment of the Requirements
for the Degree of
DOCTOR OF PHILOSOPHY

Major Department:
Mechanical Engineering

August 2015

Fargo, North Dakota

North Dakota State University
Graduate School

Title

Computational Biomechanics of Blast-Induced Traumatic Brain Injury:
Role of Loading Directionality, Head Protection, and Blast Flow Mechanics

By

Hesam Sarvghad-Moghaddam

The Supervisory Committee certifies that this ***disquisition*** complies with North Dakota State University's regulations and meets the accepted standards for the degree of

DOCTOR OF PHILOSOPHY

SUPERVISORY COMMITTEE:

Dr. Ghodrat Karami
Chair

Dr. Mariusz Ziejewski

Dr. Yildirim Bora Suzen

Dr. Kalpana S. Katti

Approved:

8/25/2015
Date

Dr. Alan R. Kallmeyer
Department Chair

ABSTRACT

In this dissertation, blast-induced traumatic brain injury (bTBI) is studied with respect to the blast wave directionality, mitigation capability of helmet/faceshield, and blast flow mechanics using finite element (FE) and computational fluid dynamics (CFD) schemes. For the FE study, simulations are performed on a detailed FE head model using LS-DYNA, and CFD simulations are carried out using the ANSYS-CFX to examine the underwash development by analyzing the behavior of blast flow from different directions. The following tasks are conducted.

First, the effects of the loading direction on the mechanical response of the head and brain is investigated through impact and blast induced loading on the head. Due to the differences in the shape, function, and tolerance of brain components, the response of the head/brain varies with the direction of the impact and blast waves. In identical situations, the head shows to have lower tolerance to side loading.

Second, the inclusion of the faceshield as a potential head protective tool against blast threats is evaluated with respect to blast direction. The helmet-faceshield and helmeted assemblies are shown to be most efficient when the head is exposed to blast from the front and top sides, respectively. Faceshield is observed to be effective only in front blast as it might impose either adverse or no effects in other directions. The shockwaves are seen to form a high pressure region in head-helmet-faceshield gap (underwash effect) which induces elevated pressures on the skull.

Third, the underwash effect's mechanism is investigated through CFD simulations of supersonic shockwave flow around the helmeted head assemblies. CFD results reveals that the backpressure is produced due to the creation of a backflow in the exterior flow on the outgoing

interior flow. The bottom and side shockwave directions predict the highest underwash overpressures, respectively.

Finally, the ICP and shear stress of the brain is evaluated in case of underwash incidence. FEA results show that underwash overpressure greatly changes with the blast direction. It is concluded that underwash clearly altered the tissue response of the brain as it increases ICP levels at the countercoup site and imparts elevated skull flexure.

ACKNOWLEDGEMENTS

A special thank you and acknowledgement first goes to Dr. Ghodrat Karami, my PhD advisor, for supporting me during these past four years. I have gained much over the years from my attendance of his classes, his guidance, his patience and our conversations which guided me on a journey to a new way of living life. Dr. Karami is not only my advisor, he is a great role model and leader for me in my professional and personal life. I hope that I could be as lively, enthusiastic, and energetic as Dr. Karami and to someday be able to command an audience as well as he can.

I would like to thank my co-advisor, Dr. Mariusz Ziejewski, for his continuing support throughout my PhD study, as well as recognition of my work in national and international conferences. His guidance and expertise in the field of biomechanics greatly inspired me for pursuing this field in the future.

I thank my committee members, Dr. Bora Suzen, and Dr. Kalpana Katti, for their time, advice and contribution towards the improvement of my research.

I thank Mr. Asghar Rezaei for helping me with the modeling, as well as cooperating with me on different aspects of the research.

I also would like to thank Dr. Alan Kallmeyer, the Mechanical Engineering Department Chair, for his support and for providing a great teaching opportunity for me in the ME Department.

With immense gratitude, I also would like to thank my group members and friends for their collaborations and encouragement throughout of my research.

I thank the Department of Defense, Army Research Office, and the Mechanical Engineering Department for funding support.

My deepest gratitude goes to my parents and my family for their unfailing love, support and advice. Thank you for being there for me, motivating me, supporting me, showing me the right path, and giving me your unconditional love throughout not only the course of my Ph.D. studies but my entire life. I should say that without my mom and dad, I would have never been able to get where I am today. Without them, I would have never had the peace and courage to keep on.

Finally, I should be very grateful to my beautiful lovely wife, Nassibeh. As I have always said, you have been my inspiration, you have been my biggest motivation to do this, and you have been my best partner of all time. Thank you for keeping up with all my grumping and nagging, thank you for believing in me, and thank you for being with me. You made me believe myself, you made me take the challenges that I would have never taken without you, and you made a better person. We got married four years ago, and that's when we took this path. Without your unconditional inspiring love, I would have never been where I am today.

DEDICATION

This dissertation is dedicated to my beautiful wife, Nassibeh, my parents, Morteza and Masoumeh, for their constant encouragement, unwavering support, love, and pride, and my little angel who is on his way to join us.

TABLE OF CONTENTS

LIST OF TABLES

LIST OF FIGURES

CHAPTER 1. INTRODUCTION

1.1. Background and Significance

Traumatic brain injury (TBI) is defined as a type of acquired brain injury that occurs upon an assault exerted by an external force such as impact or explosion blast waves. Every year, 1.7 million people, only in the U.S., suffer from TBI (Faul et al. 2010). Occurring in the form of closed (blunt) and penetrating injuries, mild, moderate, and severe TBIs represent 75%, 23%, and 3% of the annual incidents, respectively. However, the incidence rate for each type of TBI may change with respect to the epidemiology of the injury (Laker 2011; Tanielian and Jaycox 2008). Falls, assaults, car crashes, and sporting events are the main causes of impact induced TBI (iTBI) which mainly occurs among civilians. Hockey and especially football players are the ones that are most prone to iTBI in sports (Sahler and Greenwald 2012). However, the prevalence of TBI among the military members is mainly due to the ballistic impact of projectiles and fragments, as well as high pressure shockwaves generated by the explosive devices such as Improvised Explosive Devices (IED), grenades, and landmines, i.e. blast induced TBI (bTBI).

TBI mechanisms appear in two general forms, namely, focal and diffuse injuries which are visible and invisible injuries, respectively. While Intracerebral and subdural hematomas, subarachnoid hemorrhage, and contusion are some of the widely known focal injuries, diffuse brain swelling and especially diffuse axonal injury (DAI) are the most common diffuse injuries. While both injury mechanisms can be seen in iTBI and bTBI injuries, they are mainly associated with focal and diffuse injuries, respectively (Meaney et al. 2014). Mild TBI (mTBI), or concussion, is a common form of TBI, DAI is addressed as a severe pathological feature of TBI which usually results from the acceleration-deceleration of the head. DAI usually occurs as a result of the shear deformation of brain tissues which can lead to lifetime impairment of brain

In the past decades, the conflicts in Iraq and Afghanistan have given a significant rise to severe brain neurotrauma among service members, besides the physical injuries and fatalities. It has been mentioned that most of the post-war head injuries are signature wounds of blunt impacts, and they may be perceived as the main cause of about 25% of the mortality rate around the world (Okie 2005; Tanielian and Jaycox 2008). However, it has been reported that out of 1.6 million personnel deployed in the Iraq war, around 19.5% of the members have been recognized as suffering from blast-induced mild TBI (Tanielian and Jaycox 2008). Moreover, many reports has pointed out the prevalence of abnormal behaviors, severe headaches, insomnia, aggression, dizziness, and vomiting among the returning service-members as the consequences of the blast induced brain trauma (Anderson 2008). Although it is believed that most of the soldiers sustain mild TBI, which requires a recovery time up to 3 months, seven to 33 percent also may suffer for a much longer time (Alexander 1995; Belanger et al. 2005). The significance of blast-related injuries became remarkable when US troops and military members were exposed to powerful explosive devices during Operation Enduring Freedom and Operation Iraqi Freedom, which caused 73% of casualties in the US military (Cernak and Noble-Haeusslein 2010; Taber et al. 2006). Soldiers who are influenced by primary blast injuries due to blast overpressure are more susceptible to secondary and tertiary blast injuries which might be caused by shrapnel fragmentation and sudden movement of the head or body, respectively.

Upon interacting with the head, any assault on the head in the form of high pressure gradient blast waves can introduce diffuse axonal injury, subdural hemorrhaging, and contusions (Taber et al. 2006). Moreover, fatal injuries can affect facial parts and gas filled organs, such as lungs, which also may be accompanied by intoxication due to blast explosives.

The high mortality rate, TBI-related disabilities, and the clinical and economic burdens of TBI make it necessary for the fundamental studies to clearly understand the mechanisms leading to brain injuries. In order to prevent the blast and impact induced injuries, effective and improved protective equipment should be designed and tested to reduce the injury levels to the lowest possible limits. Hence extensive efforts can be directed towards understanding the mechanism of the blast wave- head interaction using computational simulations and numerical methods. Accordingly, FE modeling has obtained great attention as it can provide a good solution prediction of the phenomenon. However, the complexity of the geometry and the materials of head, helmet, and the faceshield along with loading scenarios still remains.

1.2. Anatomy of the Human Head

Human head, one of the most important parts of the human body, is highly prone to injury and damage when exposed to impacts as a result of fall, accident, assault, sport contacts and military conflicts. The complex anatomy of the brain involves many different sinus, neurovascular, and membrane systems. Basic knowledge of the anatomy of the head is necessary for understanding the biomechanics of TBI. The structure of the human head in a brief description can be considered as a multi-layered structure with the outermost layer being the scalp, a skull, meninges, brain tissues and the vascular and central nervous system (CNS). Each of the aforementioned components, however, consists of different parts which will are explained as follows:

Scalp is a multi-layered component mainly composed of soft tissues of skin and connective tissues which covers the top portion of the head and extends to neck from lateral and posterior sections while it is bounded by the face at the anterior site. The main 5 layers of the

scalp are the skin, the connective tissues, the epicranial aponeurosis the, the loose areolar connective tissue, and the pericranium.

Skull, the bony component of the human head, which is composed of the cranium and the mandible, acts as the protective element of the facial region, and most importantly provides a protective cavity shell for the brain. There are 8 cranial bones which their main task is to protect the cranium and brain against any sudden load and assault to the head, as well as connect the head to the neck. Moreover, there are 14 facial bones in the skull which construct the human facial structure, the sensory structures and nasal cavities, and the feeding system and teeth (Tse et al.).

CSF is the colorless body fluid produced in the choroid plexuses of the ventricles of the brain and acts as the cushion and damper of the brain. It occupies the subarachnoid space and the ventricular system around and inside the brain and spinal cord. CSF moves the waste products as well as the hormones from and to different parts of the brain and the blood stream, buoy the brain, provides chemical stability and prevents the brain ischemia.

Meninges are referred to the membranes which separates the soft brain tissues from the inner surface of the skull and are arranged as dura mater, archnoidea mater, subarachnoidal space, and the pia mater from the most exterior to the most interior membrane. The outermost membrane, dura mater, is a fibrous tough and dense membrane. Archnoidea mater, on the other hand, is a spider-web structure. The subarachnoidal space is basically the reservoir of cerebrospinal fluid and is occupied by spongy tissue consisting of trabeculae. Finally, the brain tissue is covered with a very thin and delicate fibrous tissue layer, the pia mater, which covers the brain and prevents the direct contact of the brain with CSF as it is impermeable (Tse et al.).

Brain is the major component of the nervous system and the most complicated part of the human body. On average, it forms nearly one one-third (1.5 kg) of the mass of the human head (4.5 kg) and is characterized with the cerebrum, cerebellum, and brainstem (midbrain, pons, and medulla oblongata) as its major parts. Cerebrum is the superior-most portion of the CNS which is considered the largest region of the brain and include the cerebral cortex and subcortical components and controls main functions of such as movement, language and etc. The cerebellum, located beneath the cerebrum in the posterior cranial fossa, is counted as the second largest portion of the brain. The brainstem is the stem-like portion of the brain's base which extends form the posterior site of the brain and is attached to the spinal cord and is responsible for sending messages from the brain to other parts of the body, as well as control functions such as consciousness, heart rate, and blood pressure. The midbrain, located superior to the brainstem is the smallest part of the brain. White and gray matters constitute the brain, where the gray matter develops a cortical layer over the cerebellum and cerebrum, and the white matter forms the deeper masses (Tse et al.). Brain is enclosed by a rigid cranium and is buoyant in the water-like fluid of CSF. Due to the poor structural support from the falx and tentorium in the skull, the lack of supporting fibrous structures and softness of the brain tissue makes it most prone to shear

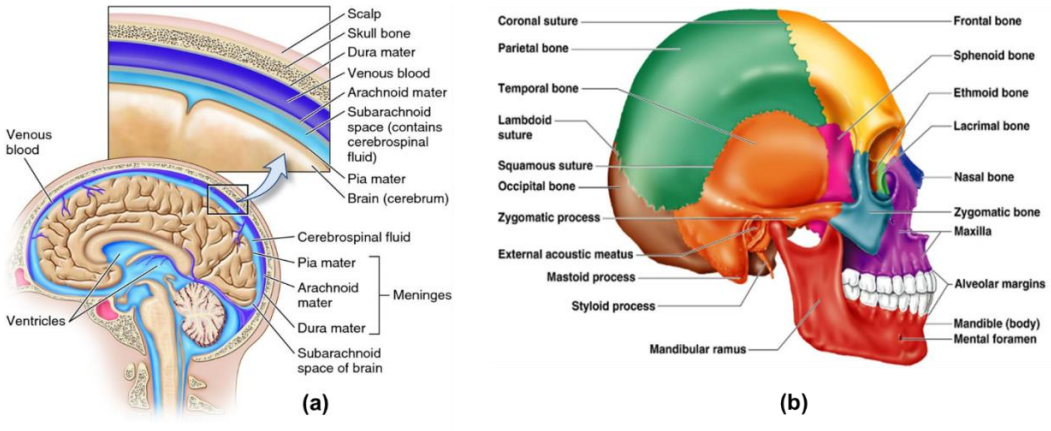

Figure 1.1. (a) Different components of the human head; (b) sagittal view of the human skull (Martini 2005)

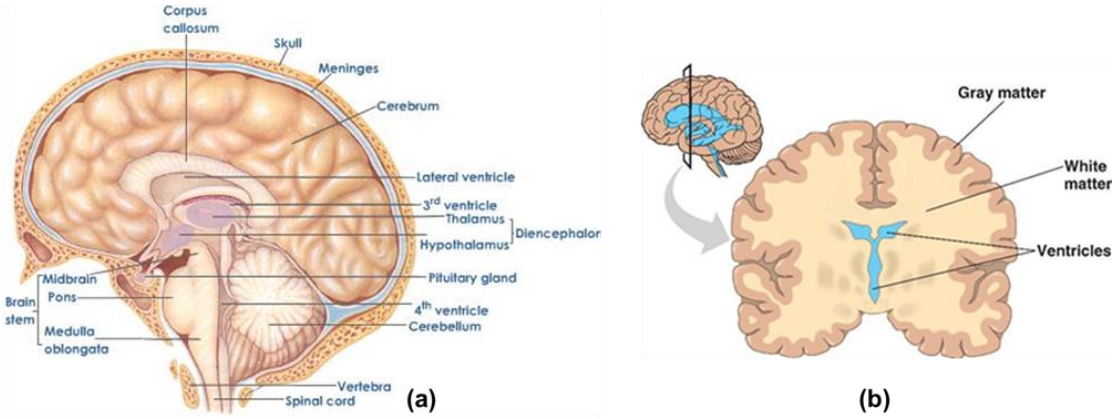

Figure 1.2. (a) Anatomical components of the human brain; (b) coronal plane of the brain showing white and gray matters and the ventricles (Martini 2005)

1.3. Traumatic Brain Injury

The biomechanical response of the head under different impact loadings has been the topic of many experimental and numerical studies. These studies have contributed greatly to the analysis of head injury criteria in terms of the kinematical and dynamical parameters in the head. Blunt and ballistic impacts as well as the blast wave interaction with protected and unprotected human head have been the main subjects of the studies as they are the major factors in causing brain injury. The brain injury analysis ranges from macro-scale (tissue damage) to micro-scale (cellular damage), and even nano-scale (axon neural filaments) (Karami 2011). As mentioned before, the major brain injury mechanisms involve subdural hematoma, diffuse axonal injury, and cerebral contusion.

1.4. Impact Induced TBI

Impact induced TBI which accounts for 75% of the TBI cases, is a localized injury which results in from contact of the brain with the skull due to the relative motion of the brain with respect to skull upon acceleration/deceleration of the head upon impact. This type of brain injury, is visible and can be detected by routine imaging techniques such as Magnetic resonance imaging (MRI) or Computed Tomography (CT) scans. The iTBI can appear in the form of skull

fracture, rupture of blood vessels inside and on the brain surface (intracerebral and subdural hematoma), and cerebral contusion. The severity of iTBI varies by several parameters such as the anatomy of the heads, the intensity of the force applied on the head, and the location of impact. The iTBI mainly involves two stages of brain injury: primary and secondary brain injuries. Primary injury refers to the damage of the brain tissue and blood vessels at the instant of the assault due to the structural displacement of the brain (Scalea 2005). On the other hand, the second injury which is perceived as the indirect mechanism injury, involves the deterioration of the cellular activities such as blood-brain barriers damage and dysfunction of neurons. This injury can happen a day or a month after injury and has a major role in the brain dysfunction and the death of the TBI victims (Sauaia et al. 1995). The common causes of iTBI are the car accidents, falls, and sport-related accidents such as football and hockey. Several in vivo animal studies, in vitro experiments, human cadaver and volunteer tests have been performed on the impact induced TBI (Ji et al. 2014; Zhang et al. 2001b). As kinematic-based metrics rely on the linear and angular accelerations of the head, they neglect the material properties and behavior of different head components, especially the brain. Due to structural inhomogeneity of the human head and the intrinsic differences of head components in terms of shape, material, and tolerance, different parameters such as the impact velocity (intensity), location (directionality), the type of blunt impact (struck against or struck by) can affect the mechanical response of the head. Accordingly, these variations would influence the stress and strain wave propagation, as well as the pressure gradient distribution throughout the brain tissue, which would produce different levels of injury. As a common criterion in the literature, the head acceleration is utilized for defining various injury thresholds. It is postulated, however, that the head trauma, such as diffuse brain injury, subdural hematoma, and contusion, is mainly associated with brain tissue

parameters such as shear stress rather than head kinematics. The tissue level parameters can, therefore, be accounted for as being a more reliable basis for the evaluation of head injury (Sarvghad-Moghaddam et al. 2014b).

1.5. Head Injury Criteria

For the last several decades, the number of criteria for head injuries have increased, as well as improved based on the kinematics of the human head. This has contributed to developing different injury criteria based on biomechanical terms in real life. The criteria have been applied in the design of different safety equipment and have addressed the human factors. This has had a positive effect on reducing the severity of injuries and mortalities. Some of the most applicable criteria are briefly explained below.

Wayne State Tolerance Curve (WSTC) was introduced by Gurdjian et al. (1953) as a human head tolerance limit indicator. WSTC is measured as a relationship between an average translational anterior-posterior acceleration level and the duration of the acceleration pulse. WTSC assumes that the fracture tolerance of the skull is equivalent to the tolerance of brain injury.

Severity Index (SI) was introduced by Gadd (1966) and is based on WSTC by integrating the linear acceleration raised to the power of 2.5.

Head Injury Criterion (HIC) introduced by the United States (US) National Highway Traffic Safety Administration (NHTSA) (Versace 1971) as an alternative formulation of SI, and was included in the Federal Motor Vehicle Safety Standards (FMVSS 208). HIC is heavily used in traumatic brain injury (TBI) diagnosis which may occur as the result of many different types of accidents, including motor vehicle collisions (MVCs), boating accidents, slips, trips, falls,

construction site injuries, and airplane or train accidents. The HIC predicts head injury due to impact with flat objects due to a combination of brain injury and skull fracture. It is defined as:

$$HIC = \left\{ \left[\frac{1}{t_2 - t_1} \int_{t_1}^{t_2} a(t)dt \right]^{2.5} (t_2 - t_1) \right\}_{max} \quad (1\text{-}1)$$

HIC does not take the rotational acceleration into account and this is regarded as a major limitation of the criterion.

a3ms (or cum3ms) is based on WSTC, and is calculated from the maximum value of acceleration during an impact with duration of 3ms. The three milliseconds window should not exceed 80G in the resultant acceleration curve.

The above criteria were all based on linear acceleration of the head and did not include any rotational acceleration. Working on rotational acceleration as an injury mechanism, Melvin and Lighthall (2002) determined human being's tolerance to angular acceleration is 7500 rad/s² with a concussion probability of 99%. Löwenhielm (1974) suggested that the bridging veins, between the skull and brain, start to tear from 400 rad/s² angular acceleration.

Generalized Acceleration Model for Brain Injury Tolerance (GAMBIT) was introduced by Newman (1986) in an attempt to combine the impacts of translational and rotational accelerations. The GAMBIT equation is:

$$G(t) = \left[\left(\frac{a(t)}{a_c} \right)^m + \left(\frac{\alpha(t)}{\alpha_c} \right)^n \right]^{\frac{1}{s}} \quad (1\text{-}2)$$

with $a(t)$ and $\alpha(t)$ as the instantaneous translational and rotational accelerations, respectively, and a_c and α_c as their limiting critical values. n, m and s are empirical constants selected to fit the data by Kramer and Appel (1990). GAMBIT does not account for duration of the time on the head injury process.

Head impact power (HIP) was introduced in terms of the kinetic energy containing combined rotational and translational accelerations as a head protection criterion (Newman et al. 2000b). It is expressed in terms of;

$$HIP = \sum_{i=1}^{3} ma_i \int a_i dt + \sum_{i=1}^{3} I_{ii}\alpha_i \int \alpha_i dt \qquad (1\text{-}3)$$

where *m*, *I*, *a*, and α represent the mass, moment of inertia, linear acceleration, and angular acceleration, respectively. Since *HIP* is a time-dependent function, the maximum value predicted by this function is used as the injury predictor value.

Abbreviated Injury Scale (AIS) was introduced by the Association for the Advancement of Automotive Medicine (AAAM) as an anatomically-based coding system (Pike 1990) to classify and describe the severity of specific individual injuries. AIS codes range from 0 to 6. AIS codes 0 and 1 indicate no injury and minor injury, respectively. AIS 6 indicates non-survivable as the most severe injury. AIS codes have been used widely to correlate levels of injury to different biomechanical criteria such as HIC (Prasad and Mertz 1985).

1.6. Brain Injury Thresholds

As a consequence of sudden head motion or impact, brain stresses and strains that might lead to injury are developed. Several injury criteria have been defined to measure the level of the brain's injury based on both the kinematical and kinetic responses of the human head and brain. The major injury criteria are based on the head linear and rotational accelerations (or the combination of both), the principal and shear stresses and strain, and the ICP of the brain. Although the injury thresholds in terms of brain stress/strain and ICP have not been employed extensively, as compared to the criterion in terms of the kinematics of motion, such thresholds should be primarily correlated to brain injury. In Table 1.1, some of the suggested thresholds are described.

Table 1.1. Different Brain Injury Criteria Based on Mechanical Parameters of Head and Brain

Parameter	Thresholds	Reference
Intracranial Pressure (ICP)	> 235 KPa → Injury <173 KPa → Minor or no injury	(Ward et al. 1980)
	≥ 300 kPa → mTBI	(Newman et al. 2000a)
	66-114 kPa → Injury 44-78 kPa → Non-injury	(Zhang et al. 2004)
Strain	>0.13 → 25% probability of mTBI (conservative) >0.18 → 50% probability of mTBI (optimal) >0.28 → 80% probability of mTBI (liberal)	(Bain and Meaney 2000)
	>0.25 → Structural failure >0.20 → Functional deficit < 0.1 → Reversible injury	(Galbraith et al. 1993)
	>0.14 → 25% probability of mTBI (conservative) >0.19 → 50% probability of mTBI (optimal) >0.24 → 80% probability of mTBI (liberal)	(Zhang et al. 2004)
	≥ 0.18 → Axonal damage	(Deck and Willinger 2008)
Shear Stress	11-16.5 KPa → Severe injury	(Claessens et al. 1997)
	8-16 KPa → Severe injury (mild DAI)	(Anderson et al. 1999)
	> 7.8 kPa → 50% probability of mTBI (Upper brainstem) > 6.6 kPa → Injury (midbrain) 3.3 – 5.7 kPa → Injury (Thalamus) 1.9 – 3.7 kPa → Non-injury (Thalamus)	(Zhang et al. 2004)
Von Mises Stress	≥ 11 kPa → Brain injury (car accident)	(Zhou et al. 1997)
	7 or 8.6 kPa → Contusion	(Miller et al. 1998)
	>27 kPa → 50% probability of moderate neurological injury >39 kPa → 50% probability of severe neurological injury	(Willinger and Baumgartner 2003)
	≥ 26 kPa → Axonal damage	(Deck and Willinger 2008)
Linear Acceleration	>76 g → Closed head injury (20ms duration)	(McElhaney et al. 1973)
	>220g → Injury (2ms duration) >76 g → Injury (9ms duration)	(Ono et al. 1980)
	73 - 133g → Injury 34 - 76 g → Non -injury	(Zhang et al. 2004)
Rotational Acceleration	>1800 rad/s^2 → 50% probability of injury	(Ommaya et al. 1967)
	>4500 rad/s^2 → Gliding contusion	(Löwenhielm 1975)
	>16000 rad/s^2 → moderate to severe DAI	(Margulies and Thibault 1992)
Combined Linear and Rotational Accelerations	≥ 85g → Irreversible brain injury ≥ 6000 rad/s^2 → Irreversible brain injury	(Zhang et al. 2004)

1.6.1. Blast induced TBI

Blast induced TBI, or the blast induced neurotrauma (BINT), refers to the diffuse brain injury caused upon the impingement of the blast shockwaves on the head and consequently, transmission of high pressure waves into the intracranial space and the brain through different pathways such as the cranial orifices as well as the vasculature. Referred to as the invisible wound of war (Tanielian and Jaycox 2008), bTBI usually acts diffusely and triggers different lesions of the brain instead of being focalized. That's probably the reason that the mechanism of bTBI is much more complicated than the iTBI and is yet still unknown. While there are numerous data on the mechanism and mechanics of the iTBI, due to the moral issues and experimental limitations on the blast traumatic injury (bTBI) studies, there are a few studies investigating the mechanisms leading to bTBI. As shown in Figure 1.3, blast induced TBI can occur through four different mechanisms (DePalma et al. 2005; Moore et al. 2009):

1- Primary blast injury: The interaction of supersonic explosion blast waves in the form of a sphere of expanded chemical gases and air, with the head in a matter of few milliseconds during which the individual is still (peak overpressure).
2- Secondary blast injury: Due to the rapid fall of pressure after the peak overpressure, a vacuum is generated which is soon invaded by a supersonic rush of wind flow which throw away and fragments the objects it moves forward, turning the debris into fast moving projectile weapons.
3- Tertiary blast injury: The supersonic wind lifts the individuals hurling them toward the ground, the rocks, and walls.
4- Quaternary blast injury: Everything else: toxic products of explosion, e.g. carbon chemicals which scorch, and dust.

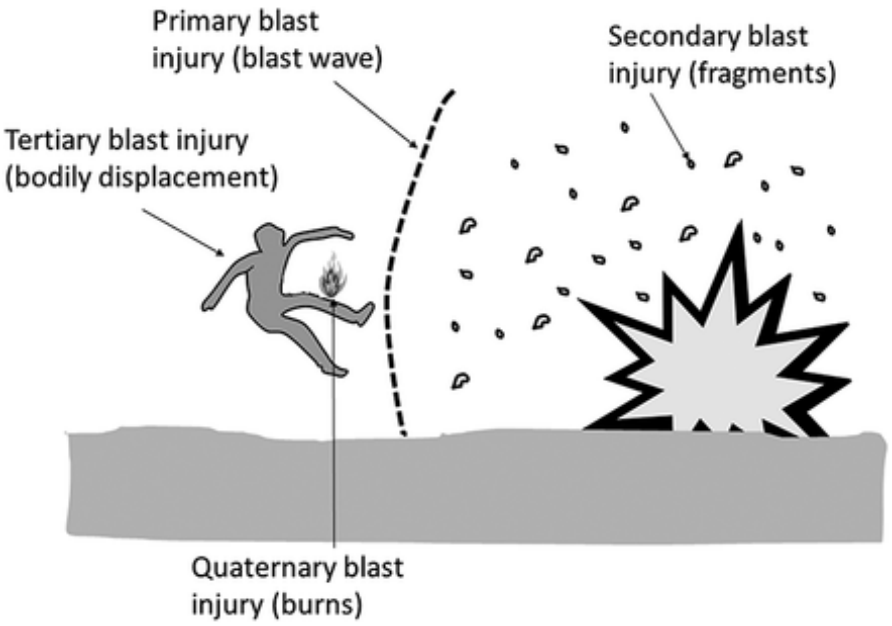

Figure 1.3. Different blast-induced TBI mechanisms (Ramasamy et al. 2013)

Unlike iTBI experimentations, there are so many limitations which prevents the experimental studies of the bTBI. Using human volunteer is unethical and only tests at injury levels much lower than the injury threshold may be possible. Although human cadaveric models provide the anatomical features of the real human beings, it is not possible to recreate the real physiological conditions and hence, evaluation of the tissue responses of the brain as well as analysis of DAI and concussion mechanisms cannot be carried out (Ji et al. 2014). Using in vivo animal models may seem to make up for the physiology issues about the cadaver, but drawing conclusions on the mechanical response of the human brain from animal experimental data may not be accurate due to the different head geometry, anatomy, and mass distribution in the animals (Zhang et al. 2001b). However, several animal models such as mice, rats, porcine, and rabbits have been used to study the bTBI mechanism (Bauman et al. 2009; Bowen et al. 1968; Cernak et al. 2011; Cernak et al. 1996; Courtney and Courtney 2009; Zhou et al. 1994). A summary of the iTBI and bTIB injury mechanisms are shown in Figure 1.4.

Due to the ethical, moral, and experimental challenges of cadaveric tests as well as insufficient accuracy of in vitro and in vivo animal models in studying the iTBI and specifically bTBI, using mathematical modeling and computational algorithms have found a great attraction in the past few decades. One of the most effective and advanced computational methods for studying the mechanical response of the human brain to dynamic loads is the finite element analysis (FEA). FEA codes have been extensively used not only to evaluate the kinematics of the head, but also to assess the deformation of the soft tissue of the brain and different head components to provide estimates of the stresses and strains inside the brain. A major feature of FE solver codes is their ability to model the generation, propagation, and interaction of explosion blast waves with solid bodies such as structures, rigid bodies, as well as human body and head using fluid-solid interaction and multi material arbitrary Lagrangian Eulerian (MMALE) algorithms. LS-DYNA, a nonlinear transient hydrocode developed by the Livermore Software Technology Corporation is a robust finite element software which provides various efficient methods for modeling the blast waves and their interaction with solid bodies (Hallquist 2007).

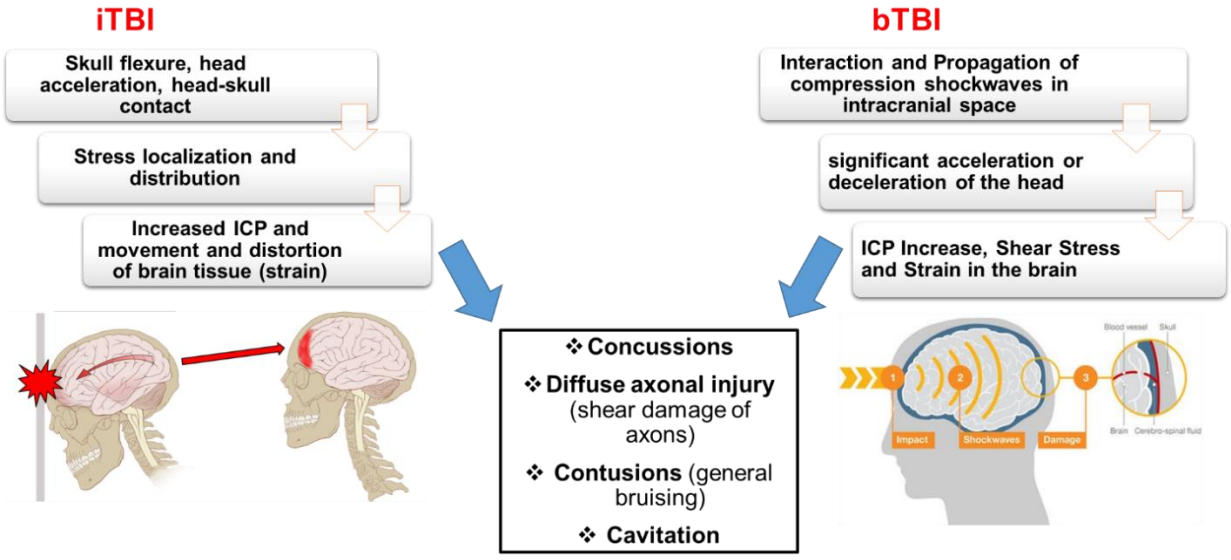

Figure 1.4. Injury mechanisms involved in iTBI and bTBI

1.7. Head Protection Against TBI

Although the pathobiology and the epidemiology of the TBI can greatly help to understand the mechanisms, causes, and the consequences of different brain injuries after the occurrence of TBI, the prevention of head neurotaruma through development of novel and efficient protective tools are vital to reduce the fatalities and the post TBI disorders as well as saving the people's lives. The most efficient head protective tool introduced for the protection of head against impacts is the helmet. Many studies have addressed the use of helmets in sports such as football, hockey, and ski, as well as for motorcyclists (Daneshvar et al. 2011; Daniel et al. 2012; Greenwald et al. 2008; King et al. 2003; Macnab et al. 2002; Post et al. 2013; Viano et al. 2007). Recording the head kinematical metrics such as linear and angular acceleration, many injury criteria as well as injury mechanisms have been proposed for the iTBI. A major part of TBI studies, however, have been addressing the effect of helmets in the battlefields. Although many studies confirmed the high efficiency of combat helmets against high-speed fragmentations and projectiles in the war zone (Aare and Kleiven 2007; Chelluru 2007; Jacobs and Van Dingenen 2001; Jazi et al. 2013a; Lee and Gong 2010; Tan et al. 2012; Tham et al. 2008; Yang and Dai 2010), the efficiency of helmets against blast waves are still questionable (Ganpule et al. 2012; Grujicic et al. 2011; Moss et al. 2009; Nyein et al. 2010; Sarvghad-Moghaddam et al. 2014a; Zhang et al. 2013a). Recently, few researchers have looked into the effect of using faceshield as a protective tool for reducing the risk of bTBI (Nyein et al. 2010; Sarvghad-Moghaddam et al. 2014a). While these protective tools are advantageous in protecting the head against brain trauma, their efficiency should always be studied and improved.

1.8. Current Protective Headgears in Military

Personal Protective Equipment (PPE) are defined as the tools and devices designed to protect the human body from different types of threats. They may include protective headgears such as combat helmets and ballistic faceshields, eyewear such as spectacles and goggles, clothing such as ballistic suit, hearing such as earplugs and etc. Although all these tools are of great importance for the safety of the service members, the protective headgears have attracted the most attention as they are dealing with life-threatening and fatal assaults in terms of the head injury. In this regards, a brief review of the most prominent protective headgears is presented in this section.

1.8.1. Military Helmets

As the major component among all protective headgears, the combat helmet is assumed to be the most effective tool in protecting the head against different ballistic, blunt, and blast assaults. Although the advent of the combat helmet as we know it today, goes back to Adrian helmets for the French army in 1915, but their evolution throughout the years has gone a long a way ahead. A schematic of the helmet design evolution is shown in Figure 1.5. The very first combat helmets, mainly designed to protect against ballistic and fragmentation impacts, were made of steel. However, the growth of assaulting war weapons, fatal ballistic impacts, and ongoing use of Improvised Explosive Devices (IED) led to the development of new designs of combat helmets. Light weight, high ballistic protection capacity, and comfort are the major requirements of a good helmet. In this section quick review of the most recent combat helmets in the US army is presented.

M1 helmet, also named “steel pot” by the military wearers, has been widely used in the US military during World War II until 1985 (Walsh et al. 2005). The unique design of this

helmet was the reason for its popularity. However, its poor fit on the soldier's head and the availability in only one single sizing were the major disadvantages of this helmet. The shell was made of steel to have great protection against ballistic threats. However, the liner system including the chinstrap, nape strap and webbing suspension was embedded in this helmet in order to improve the comfort and wearing efficiency of the helmet resulting in a total weight of 3.3 lbs. for M1 protection unit. In the mid-1980s, M1 helmets were replaced by the Personnel Armor System for Ground Troops (PASGT) protective equipment, also called the "k-pot", to provide much better ballistic protection, lighter weight, and improved ergonomics. The PASGT helmet opened its way in the US military as the standard protective headgear for infantry forces because unlike M1 helmets they were offered in five different sizes weighing from 3.1 lb. for the smallest to 4.2 lbs. for the largest one (Kulkarni et al. 2013; Walsh et al. 2005) Multiple layers of Kevlar/ phenolic composite was used to make the helmet shell in order to provide enhanced ballistic and shrapnel protection. Another improvement of PASGT helmets was the ability to upgrade their webbing suspension system to a padding suspension, hence increasing their performance. However, there was still much more to do in terms of the helmet exterior and interior design; weight should have been minimized to the less possible and padding suspension should have been improved to their highest level.

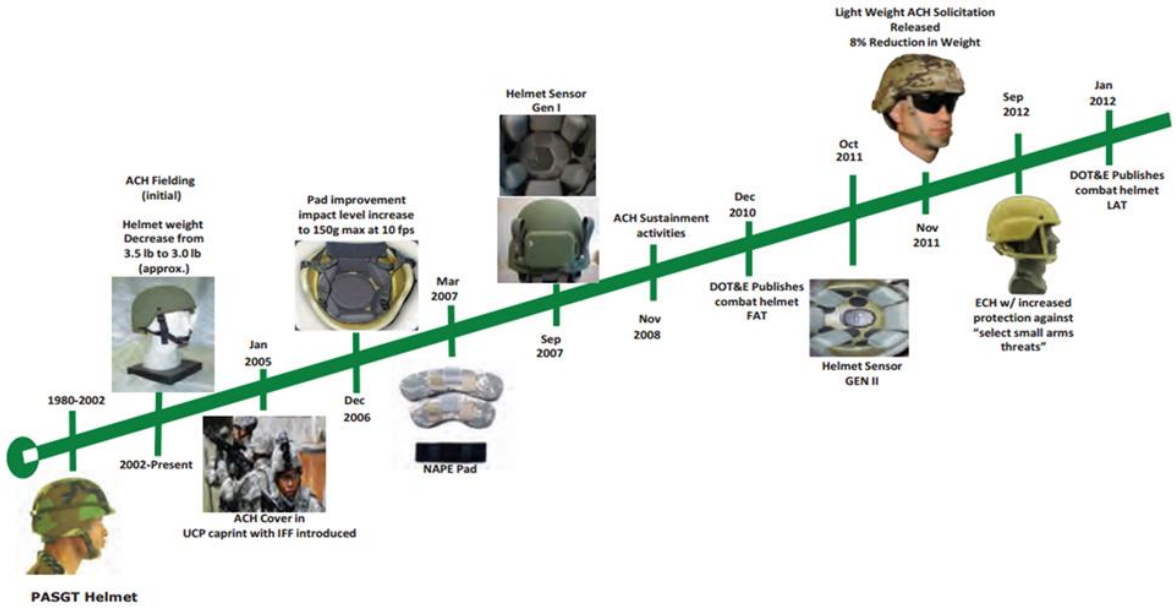

Figure 1.5. Evolution of helmet design (technical assessment of ACH helmets) (Stone 2013)

Accordingly, Modular Integrated Communications Helmets (MICH) which took advantage of a brim-less, high-cut design compared to PASGT helmets, was developed by the United States Army Soldier Systems Center to replace the PASGT helmets. The advanced Kevlar type used in these helmets provided much higher impact protection and a lighter weight (around 3 to 3.6 lbs) with respect to the PASGT (Kulkarni et al. 2013). The Advanced Combat Helmet, which is mainly derived from MICH helmet design, was offered by the US Army as the next generation of helmets and is the one which is currently used by the service members. Improved padding suspension system, enhanced retention system and lighter weight compared to PASGT helmets provides much more ballistic protection capability, comfort, and ventilation for the soldiers (Aare and Kleiven 2007). It was first fielded in 2003 and then some attachments such as the nape pad was added to increase the efficacy of these helmets. It offers equipment for mounting other attachments such as communication devices as well as night vision goggles. Recently, a new combat helmet called Enhanced Combat Helmet (ECH) inheriting a similar profile to the one used for the ACH helmet but thicker has been developed by the US Marine

Corps and is going to be deployed in early 2014. Taking advantage of a "tactical cut" it offers more flexibility to the soldier while it reduces the head coverage. In this generation of helmets, thermoplastics are being used in the place of the ballistic composites, i.e. the shell is made of ultra-high-molecular-weight polyethylene (Zhang et al. 2013b). 3M Company as the manufacturer of this type of helmet declared that it offers 50% higher ballistic protection compared to the ACH helmets (www.mmm.com). It favors the advanced padding suspension system and offers all the characteristics available in the ACH helmets. Figure 1.6 shows the different helmet types that were mentioned above.

Figure 1.6. Combat helmets; (a) M1; (b) PASGT; (c) ACH; (d) ECH (Kulkarni et al. 2013; Sharma 2011; Zhang et al. 2013b)

1.8.2. Faceshield

Faceshields that are mainly designed to protect the soldier's facial parts from any ballistic impacts as well as explosive fragmentations are believed to be a means of reducing blast-induced head injury. This concept studied previously only by Nyein et al. (2010), is one of the main contributions of our work which will be discussed in details later. The shields are usually made of thermoplastic polymers such as polycarbonate, i.e. Lexan which provide excellent impact resistance, optical quality, heat resistance and normal chemical resistance. These polymers are highly durable and are transparent to visible light better than regular glass. As shown in Figure 1.7, they come in different shapes and sizes based on the application and the

corresponding National Institute of Justice (NIJ) standard. Faceshields are widely used as riot shields in the police forces and the main reason mentioned for not using them in US army and Marine Corps is that they reduce the visibility and comfort of the soldiers as well as apply extra loading on the soldiers' head and neck which may limit their maneuverability.

Figure 1.7. Different faceshield configurations (www.paulsonmfg.com)

1.8.3. Liner Systems

Improving the applicability and the protection efficacy of the combat helmets have always been an issue for the department of defense and the US forces. One significant consideration was to add an efficient liner system for the interior design of the helmets. The liner systems may include the webbing or padding suspension system which are employed to fit the wearer's head inside the helmet, the hook discs to attach the pads or webbing inside the helmet, and the retention system, i.e. chinstrap which fixes the helmet on the soldier's head to improve stability. Upon improving the ballistic protection of the combat helmets, padding suspension systems replaced the webbing systems. As the main component of the liner system, the main focus has always been on improving the padding efficiency in terms of arrangement, material, and structure. The current pads used in military forces are mainly manufactured by Team Wendy, Oregon Aero, Skydex, and Gentex. All of these manufacturers offer different types of liner systems with advanced protection capacity with each one being suitable for specific

applications. The stand-off distance of helmet defined as the gap between the head and helmet usually fall between 0.5 to 0.75 inches and it is chosen with respect to the pad thickness and the wearer's head anatomy. The pads are usually made up of Expanded Polystyrene (EPS) which unlike the rigid shell, deforms under ballistic and blast impacts to mitigate the transferred loads to the head. The behavior of the foams are expressed in terms of their plateau (stress-strain curve) which is different based on the type and intensity of the loading. In a study performed by Moss and King (2011) on the behavior of different military and Football pads under blunt impacts they concluded that the behavior of pads differ based on the impact velocity such that soft and hard pads performs much better at lower and higher velocities, respectively. They also mentioned higher efficiency of thicker pads especially at higher impact velocities. Figure 1.8 depicts the different pad types currently used in the military.

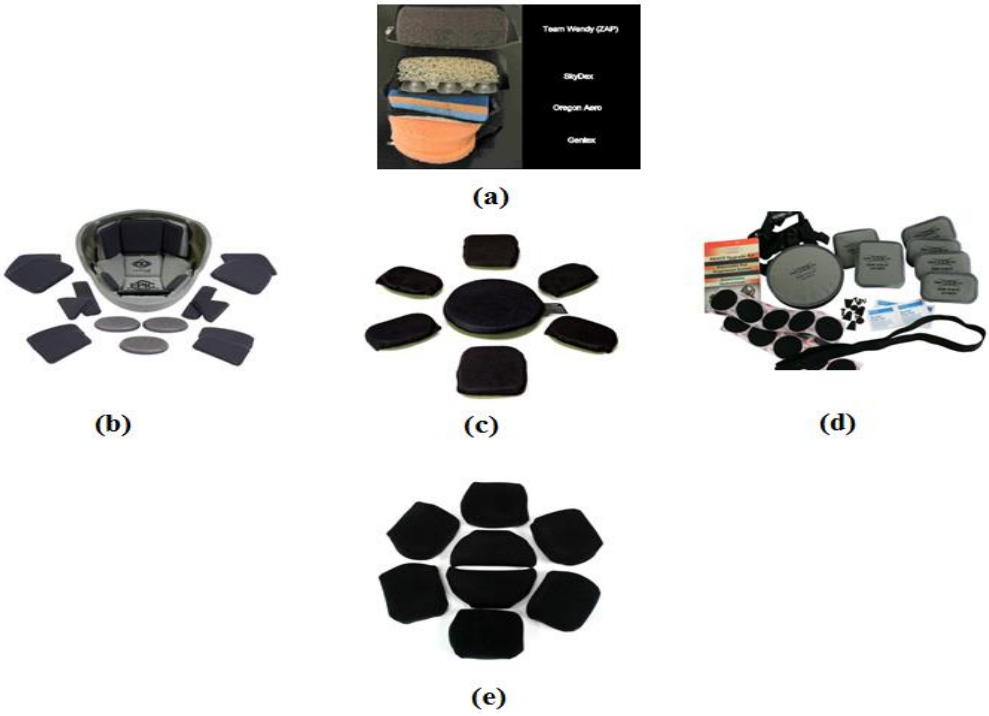

Figure 1.8. (a) Cross-section of different pads; (b) Team Wendy EPIC™ (www.teamwendy.com) (c) Oregon Aero (www.oregonaero.com); (d) Skydex (www.skydex.com) ; (e) Gentex (www.genex.com) padding/liner systems

1.9. Impact Mechanics

Impact is characterized by a great force or shock generated due to the collision of two bodies in a short duration of time. The effect of this type of force depends on the relative motion of the bodies. Physical occurrences such as shock and elastic wave propagation, perforation and fracture may happen in the event of an impact (Meyers 1994).

The classification of analytical impact mechanics falls into four major groups: 1) rigid-body dynamics; 2) propagation of stress waves in perfectly elastic materials; 3) propagation of stress waves through solids which are not perfectly elastic; and 4) non-classical models to describe spallation and fragmentation upon impact. However, another group which is employed to solve for the analytical models is the numerical methods such as finite difference, finite element and mesh free methods. Different numerical approaches such as Lagrangian, Eulerian and Arbitary Lagrangian-Eulerian are employed to implement the numerical algorithms (Qiao et al. 2008). When the collision between two objects is perfectly inelastic, the struck object will deform due to strike by the projectile and most or all the energy is converted into heat and sound due to the vibration and deformation induced in struck object. However, in high-speed impact, there isn't enough time for the deformations to happen. Accordingly, the struck object behaves as a brittle material and the kinetic energy of the applied force is used towards fracturing the struck object. The behavior of objects under high is highly dependent on their material properties (Goldsmith 2001).

1.10. Blast Mechanics

Shock waves are defined as the energy carrying disturbances propagating through different media such as solid, liquid, and gas which are generated through a rapid displacement of the medium. The turbulent nature of these waves can induce sudden changes in the different

properties of the medium they are traveling in. The development of the shock waves is usually accompanied by a rapid increase in temperature, pressure and density of the corresponding medium. Blast waves appear in the form of shock waves propagating through the atmosphere and imposing an overpressure when they hit an obstacle and are reflected off that. The severity of the blast-induced loading is highly dependent on different parameters such as the overpressure, the media of explosion, the stand-off distance, the overpressure duration and the confinement of the space (Cernak and Noble-Haeusslein 2010). A typical time history of the pressure wave generated by a blast is shown in Figure 1.9. The major features of this shock wave illustrated in this figure. can be summarized as: (a) arrival time (t_a) of the blast wave to the object of interest; (b) peak overpressure (p_{max}) representing the maximum pressure generated by the shock wave based on the HE size as well as the distance from explosion; (c) positive time duration (t_P) implying the time it takes for the maximum pressure to fall to the reference pressure (p_0), (d) negative time duration (t_N) refers to the time required for the pressure to reach its maximum negative value after t_P i.e., the maximum negative pressure (p_{min}); and (e) overpressure impulse of incident which is evaluated as the overpressure integral over the t_d range. Based on the parameters defined above, one can describe the blast-induced pressure at a specified location by the Friendler equation (Baker 1973).

Friedlander developed a mathematical formula for the pressure in terms of time in an open-space air blast by assuming air as an ideal gas as follows:

$$p(t) = p_0 + p_{max}\left(1 - \frac{t}{t_d}\right)^{\frac{bt}{t_d}} \tag{1-4}$$

where *b* is the decay constant of the curve and *t* is the time at which the pressure is desired. The parameters utilized in this equation can be obtained through the data from experiments.

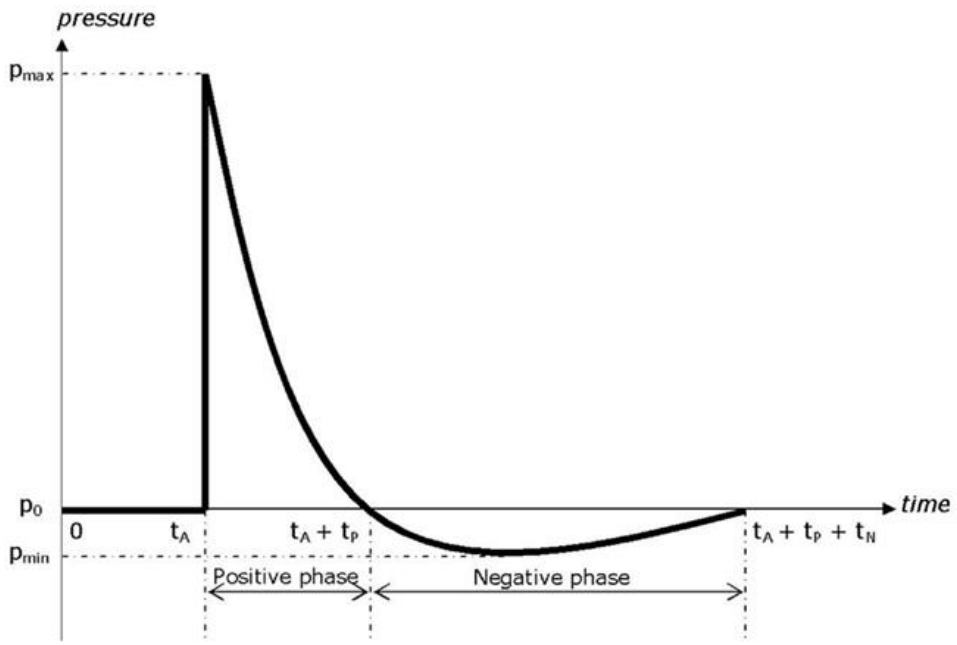

Figure 1.9. Time history of blast-induced shock wave (Baker 1973)

1.11. Underwash Effect of the Blast Shockwaves

The interaction of blast-induced shockwaves with a structure or solid object brings up different behaviors in terms of the wave propagation. The behavior of these blast waves are mainly dictated by the geometry and material of the objects they are impinging on. The geometry plays the main role in determining the blast wave flow around the object. However, the pressure gradient and intensity as well as the mitigation trend of these waves are determined by the material properties of the objects they collide with. In the military and combat scenarios, blast waves are interacting with unprotected or protected bodies.

The military helmets, originally designed for protection against ballistic impacts, show a different behavior under blast loadings. Upon entering this gap, shockwaves start to move in different directions inside the helmet/faceshield gap. Upon exiting, however, these waves meet at the opposite side of the entrance (countercoup site). This will lead to the formation of a localized high pressure region which induces an elevated overpressure on the skull, and is comparable or

higher than the incoming primary blast wave's overpressure. This is in contrary to the fact that the blast overpressure is attenuated upon interacting with and propagating around the head. This phenomenon, called the underwash effect, is believed to be the adverse effect of the head protective tools. The underwash effect is observed through an increase in pressure due to the geometrical constraints along the path of the head-helmet gap. The surface pressure induced by underwash on the skull is believed to have the potential to impose elevated risks of brain injury. The mechanism leading to the formation of the underwash impulse is yet not clearly known. Moss et al. (2009) studied the impact of non-lethal blast waves on unprotected and helmeted heads and reported localized regions of high and low pressures due to the dynamic deformation of the skull. Also, they confirmed the role of the padding system in attenuating the underwash impulse under ACH helmets. In a numerical study, Ganpule et al. (2012) investigated the extenuating effect of the ACH helmet against blast-induced overpressures on the head. Employing three different cases (unprotected, helmeted head, helmeted head with interior foam pads), they observed the intensification of the blast overpressure due to underwash effect for the helmeted case, which was also confirmed by their experimental setup. Moreover, there are many parameters that can cause this effect, exacerbate that, or in some cases prevent that. The blast parameters such as blast intensity and direction, the geometrical features of the helmet/faceshield, as well as the mechanics of the blast flow are some of the detrimental parameters. Figure 1.10a shows a schematic 2-D representation of the blast flow around and inside a helmeted head to better visualize the incidence of underwash. Figure 1.10b also depicts the blast flow streamlines using computational fluid dynamics (CFD).

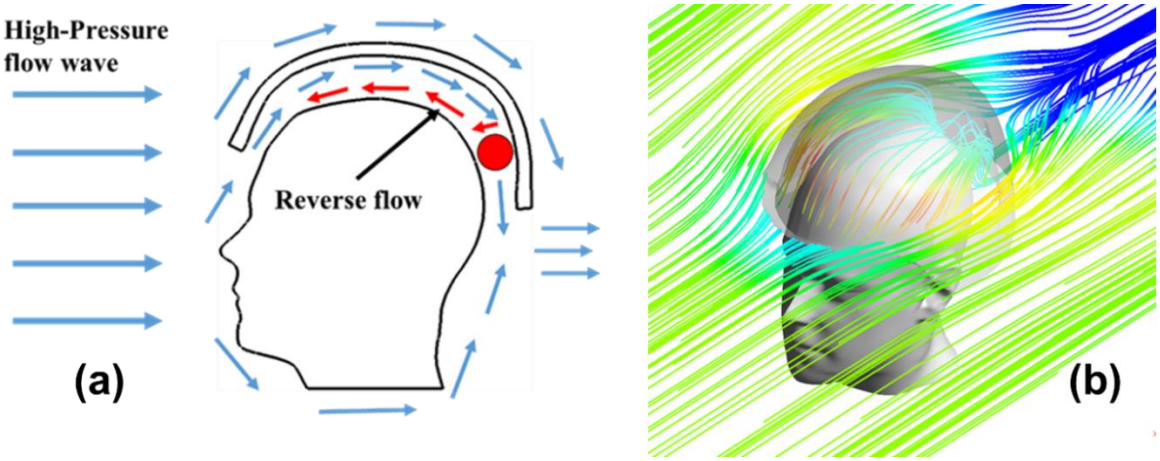

Figure 1.10. (a) Schematic representation of underwash effect; (b) CFD representation of the underwash effect

1.12. Aim and Objectives of the Research

The biomechanics group at NDSU have contributed to the analysis of blast-induced traumatic brain injury using multiscale brain modeling (Chafi 2009; Dirisala 2009; Javid et al. 2014). In the past few years, the material characterization of brain tissue has been investigated using experimental, theoretical, and computational techniques on the animal brain tissue (Abolfathi et al. 2008; Javid et al. 2014; Rezaei et al. 2014a). Moreover, the primary and tertiary blast injuries, as well as the effect of media confinement on the mechanical response of the brain were evaluated using computational analysis of the FE head model (Rezaei et al. 2014b; Rezaei et al. 2014c). Recent studies, however, focused more on investigating the helmet performance against ballistic impacts. Jazi et al. (2013a) closely studied the effect of helmet padding material on the dynamic response of the head to ballistic impacts with different velocities and orientations. They also simulated the interaction of blast waves with the helmeted head and compared the brain response between the protected and unprotected heads, investigated the biomechanics of brain upon exposing the unprotected and helmeted head to blast waves from different orientations, and to further investigate the effect of head/neck boundary conditions,

evaluated the effect of body attachment on brain response (Jazi et al. 2013b; Jazi et al. 2013c; Salimi Jazi et al. 2014)

The current research employs the fundamentals of the TBI study to address the injury mechanisms due to bTBI. To this end, the current research goes above and beyond the previously performed analyses and addresses three major component of bTBI research in a more detailed way. The first contribution of the current study is that it explores the directionality effects of blast waves on the mechanical response of the brain and the head on both qualitative and quantitative levels. In other words, the mechanobiology of brain injury is sought with respect to the injury predictors for real-life blast intensities representing the lung injury threshold. Moreover, for the very first time, the effect of faceshield inclusion in reducing the risk of brain injury with respect to the loading direction is addressed in this work.

The second contribution of the current work is the study of the underwash effect of helmet and faceshield under blast loading. Although this effect has been introduced in very few studies, but it has never been investigated in terms of the causing mechanisms or the possible adverse effect on the brain tissue response. This study take advantage of a novel CFD technique to analyze the interaction of supersonic shockwaves with helmeted head in an attempt to investigate the mechanisms leading to this phenomenon with respect to different flow parameters.

Finally, for the first time, the underwash influence on the brain response is investigated in details and possible injury mechanisms are evaluated under this effect. The study of this effect as well as the directionality effects of the protective tools develop new insights towards understanding the mechanics of blast waves, interaction of these waves with the head, and improvement of the protective tools.

The overall objective of this research is to investigate the effect of loading conditions, as well as the head protection on the response of the human head to impacts and blast waves through evaluating the kinematical and tissue level parameters of the brain using a finite element approach. To achieve this goal, a set of specific goals has been formulated as follow:

- To understand the effect of the impact and blast wave loading directionality on the kinematical and tissue responses of the human brain.
- To investigate the effect of helmet and specially faceshield protective headgears on the transferred mechanical loads to the head in different blast loading orientations.
- To develop a computational fluid dynamics (CFD) approach to study the blast flow mechanics around the protected head.
- To quantify the mechanical response of the brain to blast and impact assaults based on the current injury thresholds and criteria.
- To examine the development of the adverse effect of protective headgears, referred to as the underwash effect, in the gap between the protective tools and the head.
- To quantify the biomechanical insult on the head and brain as a result of underwash effect and examine possible increased injury risk.
- To identify the role of the helmet padding material in increasing the protection efficiency of the combat helmets in the blast theatre.
- To identify the key differences between impact and blast induced injury mechanisms under identical kinematical responses for the head.
- To ascertain the major injury mechanisms involved in the bTBI.

1.13. Outline of the Dissertation

This dissertation is divided into 7 chapters. Chapter 2 presents a comprehensive literature review on the finite element modeling of the human head, experimental and numerical works that have been performed on the analysis of both impact and blast induced TBI. Chapter 3 introduces the computational methodology, finite element analysis, as well as the material modeling for this research. In this chapter, the details of the FE head model used for this study, the specifics about the material models, and the physics of the blast and the corresponding FE approach are presented. Chapter 4 presents a detailed FE analysis of the human head response to dynamic impact loads from different directions in an attempt to highlight the effect of directionality considerations for the TBI analysis, as well as the importance of the tissue level parameters in defining the injury criteria. Chapter 5 involves a comprehensive investigation on the mechanical response of the human head to blast loads with directionality considerations as well as the role of different protective systems such as the combat helmets and the ballistic faceshields. This chapter not only emphasizes on the directional response of the human brain to blast waves but also looks deeply into the blast mitigation capability of current advanced combat helmets (ACH) and the faceshields in the theatre of a blast with directionality considerations. Moreover, the effectiveness of a few commercially available helmet foam pads is evaluated under blast to investigate the bTBI incidence upon using different padding. In Chapter 6, a CFD approach is taken toward understanding the blast flow mechanics around the helmeted head. This is done in an attempt to verify and investigate the underwash effect of the helmets. Moreover, this CFD study can delineate the flow behavior of the blast waves around the head when it is protected by the helmet to better visualize the dynamics of blast flow. Moreover, a detailed FE study is performed to understand the tissue response of the brain upon the incidence of

underwash. The purpose of this work to investigate any possible injury by the underwash overpressure on the brain. Chapter 7 concludes this research with introducing the major findings of this work with respect to the set objectives. Finally, the limitations of this study and possible avenues for future research will be presented.

CHAPTER 2. LITERATURE REVIEW

This Chapter provides a comprehensive review on the current state of the TBI research. As pointed out in the previous section, numerous studies have been carried out on the pathobiology, mechanobiology, mechanisms, and prevention strategies of both impact and blast induced TBI. To explore the current gaps and highlight the novelty of the current research in filling some of these gaps, it's essential to review the related works. This chapter is divided into two major parts: in the first part, the experimental studies on both iTBI an bTBI using in vivo animal models, in vitro models, as well as human cadavers are presented. This parts extensively reviews the development and improvement of experimental techniques for evaluating the mechanical response of the head and the brain to blunt impacts and blast waves. The second part involves a detailed study on the available numerical techniques in studying the TBI, mainly the FE approaches and methodology in assessment of the brain dynamic response. This part looks into the different FE head model used for the iTBI and bTBI studies, as well as the major findings using the FE analysis. As a major part of the current research is dedicated to evaluate the role of head protective tools in preventing the brain injury, a detailed overview of the experimental and numerical works on the evaluation of protective headgears and their accessories such as foam padding is presented in the third part.

2.1. Experimental Works on TBI

Experimental works on TBI involves 1) studies using in vitro models to understand the pathobiological mechanisms leading to the cellular damage and dysfunction of the brain after exposing to mechanical loads; 2) studies using in vivo models to mimic actual head injuries, such as animals (pigs, rats, mice), and surrogate head models such as spherical shells containing fluid, Sylgard gel, and gelatin to investigate the mechanisms involved with the second injury as well as

development of therapeutic strategies for both iTBI and especially bTBI; 3) studies using post mortem human surrogates (PMHS) and human volunteers to simulate the dynamic response of the human head to different loading using the real physiological and geometrical features of the head.

Using the in vitro models of TBI, not only provides a perfect chance for investigating the effect of injury mechanisms through accurate control of the injury biomechanics, but also allows for studying the pathobiology of injury within a particular region of interest. For detailed review on the models and works, readers can refer to the work of Kumaria and Tolias (2008) and Morrison III et al. (2011).

Salvador et al. (2013) introduced the stretch in brain microvascular endothelial cells (cEND) as an in vitro TBI model of the blood brain barrier. They used murine brain cEND that was developed in their lab and applied pressure to the cultured cells in flexible-bottomed wells.

LaPlaca and Thibault (1998) employed a rotating disk situated above a layer of cells to generate fluid shear. Using this technique, they deformed the cells using the fluid shear forces, where they could alternate the shear force through controlling the offset distance and rotation rate. With their appropriate design, they could cause enough cellular deformation for the TBI study.

Morrison et al. (2006) developed a novel in vitro model to study the biomechanics of TBI using organotypic hippocampal slice cultures on deformable silicone membranes, as well as an injury device to generate cellular deformation. They stated that their model is capable of predicting the impacts of a mechanical stimulus in a complicated cellular setting to mimic the in vivo setting.

Other significant works involve development and design of novel in vitro mechanical neurotaruma force to the anterior of the cranium to produce iTBI by causing sagittal and anterior-posterior models using different stimulation and tissue preparation and characterization techniques. Some of the in vitro injury models include cell stretch, transection, compression, hydrostatic pressure, fluid shear stress, shear strain, and stretch injury, acceleration, and hydrodynamic models (Arundine et al. 2003; Cater et al. 2007; Elkin et al. 2010; Geddes and Cargill 2001; Nilsson et al. 1996; Povlishock et al. 1997; Rossaint et al. 2009; Shepard et al. 1991; Yunoki et al. 2003).

The in vivo models provide a convenient and practical means for studying the different types of brain injuries. Various TBI models have been used for animals and humans such as controlled cortical impact (CCI), weight drop, vacuum deformation, fluid percussion injury, penetrating TBI, diffuse, rotational TBI, and blast injury models (O'Connor et al. 2011; Rostami 2012). These models have been used for studying primary and secondary brain TBI, as well as different impact and blast induced injury mechanisms such as concussion, contusion, subdural hemorrhage, diffuse axonal injury, and skull flexure (Finnie and Blumbergs 2002). Moreover, the use of Sylgard gel as well as spherical shells have attracted the attention of researchers as a way to mimic the physical and mechanical attributes of the human head (Zhang et al. 2009).

Animal models such as rodent (mice, rats), rabbits, sheep, monkeys, and pig have been widely used in the analysis of iTBI (Fritz et al. 2005; Gennarelli et al. 1981; Kabadi et al. 2010; Kilbourne et al. 2009; Li et al. 2012; Liu et al. 2012; Sadasivan et al. 2008; Xing et al. 2013) and bTBI (Axelsson et al. 2000; Bauman et al. 2009; Bogo et al. 1971; Cernak et al. 1995; Cernak et al. 1996; Damon et al. 1966; Goldstein et al. 2014; Long et al. 2009; Moochhala et al. 2004; Mundie et al. 2000; Richmond et al. 1966; Säljö et al. 2002).

Kilbourne et al. (2009) carried out a study to replicate the closed head trauma in humans through a frontal impact scenario on a rat's head. They presented an appropriate rodent head model with the ability to replicate closed head injury for the very first time. They applied the acceleration. Although no skull fracture or mortality were not observed, they asserted that the observed diffuse injuries were relevant to the human TBI.

Liu et al. (2012) conducted a study to characterize the pressure response of the pig's head to 48 non-penetrating ballistic impacts. They used a physical head model of the pig as well as a live pig protected by an aramid plate. They performed their tests using a 9 mm standard bullet at different velocities. They found a good correlation between the maximum pressure of the physical and the live pig models, and reported the peak pressure as the main criterion for predicting the severity of the injury.

Richmond et al. (1966) carried out a comprehensive bTBI study by exposing 8 different species of animals, namely, mice, rats, hamsters, guinea pigs, cats, rabbits, dogs, and goats to blast shockwaves with different intensities and from different orientations. Based on the lung injury threshold, they evaluated the chance of petechial hemorrhage. They concluded that the size of the animals has a negligible role in the animal tolerance in long-duration blasts, while it is the opposite for the short-duration ones.

Axelsson et al. (2000) studied the brain activity, circulation, and respiration in the pigs after they were exposed to open field blast waves. They observed that that unlike the control animals, transient flattening of the electroencephalogram was seen in the 4 experimental animals. They concluded that the instantaneous depression of the cortex was due to the influence of the blast pressure waves on the brainstem.

Among all experimental studies, the ones with the PMHS are very rare as there are ethical issues are involved with them. However, they can replicate the same geometrical features of the human and hence can provide valuable information about the mechanism and pathobiology of both iTBI and bTBI. However, there is always the problem of the inconsistency of the physiological conditions of the cadavers. The cadaver experiments mainly involve the iTBI studies as there are much stricter regulations and moral issues are involved with performing bTBI studies on cadavers.

Nahum and Smith (1976) and Nahum et al. (1977) performed cadaveric impact tests on 10 and 8 different seated cases, respectively. They used several impactors with masses ranging between 5.18 to 23.09 kg and constant impact velocities varying from 3.56 to 12.5 m/s. The head was inclined 45 degrees about its horizontal plane and a frontal impact was carried out on the frontal bone. The cadavers' represuurization was done to mimic the real physiological conditions in terms of the in vivo brain pressure. Pressure transducers were implemented in 5 different locations inside the brain to record the ICP. The peak force delivered to the head was reported to be between 2.9 to 12 kN with a duration of 3-18 ms. They reported the peak positive pressure at the coup site and the peak negative pressure at the coup site and reported a linear relationship between the linear head acceleration and the ICP. They also found a good correlation between the recorded ICP and acceleration data and the injury severity criteria such as HIC and GIS.

Stalnaker et al. (1977) carried out cadaveric tests on 15 seated cadavers using a 10 kg impactor. The peak force was recorded as 4.2 and 14.6 kN with the durations of 3.2 and 10.6 ms. They reported a linear accelerations of 140 and 532 G's and reported the peak ICP as 140 kPa. Due to the data scatter, they couldn't obtain a robust correlation between the load intensity and

the injury level was not found. They reported better skull-brain coupling and hence, minimized relative motion of brain with respect to skull for pressurized heads.

Trosseille et al. (1992) performed impact tests on 2 seated cadavers. The heads were impact using a 23.4 kg impactor with velocities of 5 to 7 m/s at the thorax, the forehead, and the face. Using the data acquisition systems, they recorded the linear and angular accelerations, as well as the ICP values at different locations. They reported similar ICP pattern to those reported by Nahum and Smith (1976). Possibly, due to the different setup of the cadavers and the measuring devices, very different linear and angular accelerations were obtained compared to the work of Nahum and Smith (1976). They reported a minimum countercoup pressure of -30 kPa and found no injury for linear accelerations less than 60G and angular ones less than 4300 rad/s^2.

Hardy et al. (2001), employed the neutral density and high-speed x-ray techniques to evaluate the relative motion of the brain with respect to skull for different impact tests. The impacts were performed using a 152 mm diameter impactor at 2 to 4 m/s. Measuring the kinematics of the brain and skull, they reported a 5mm relative displacement between then after 20-30 ms. In another similar experiment they also measured the ICP (Hardy et al. 2007). They also evaluated the average peak principal and shear strain of 8.8% and 8.9% for the brain tissue. They also pointed out that the changing the angular acceleration didn't affect the pressure and strain peak values.

The aforementioned experimental studies are commonly used to in computational studies (FE analyses) to validate the numerical FE head models. However there are several other experimental works in the literature that mainly investigated the correlation between the head kinematics and the tissue response and the injury level, the significance of linear and angular accelerations as injury predictors, and evaluation of ICP and brain strain (Got et al. 1978;

McIntosh et al. 1993; Nusholtz et al. 1984; Rizzetti et al. 1997; Stalnaker et al. 1977; Walsh et al. 1985).

Unlike bTBI experimental studies using PMHS models, there are a few bTBI studies involving PMHS. The major cadaveric experiments on the bTBI are from the researches at Wayne State University biomechanics group.

Bolander et al. (2011) and Leonardi et al. (2011) used PMHS models in their PhD studies at Wayne State University and evaluated the human brain response to shockwaves simulated using a shock tube. They evaluated the effect of different blast directions and intensities through fifteen blast events. Employing a pressure sensors, they measured the ICP values at various lesions of the brain, namely, frontal, parietal, occipital, and ventricles. Moreover, they evaluated the skull strain at five different locations by the strain gauge. They reported that the brain pressure variation is administered by structural response of the skull and brain coupled system. The skull flexure, introduced as one of the major injury mechanisms by Moss et al. (2009), was further emphasized to have prominent role in the ICP distribution inside the cranium. They also asserted that the geometrical features of the human head as well as the orientation of the head had a significant influence on the tissue responses of the brain.

Sharma (2011) validated the Wayne State University Head Injury Model (WSUHIM) against cadaveric test by exposing the cadaver's head to blast shockwaves generated by a shock tube. Their study mainly focused on the validation of their FE model for use in bTBI research. Moreover, they studied the effect of different blast directions and material models of the head components to elucidate the significance of parametric studies for analysis of the blast related injuries.

Rafaels et al. (2010) also employed a PMHS model for their study on the effect of the helmet protection against the blast but didn't look deeply into the tissue response of the brain. The main objective of his work was to evaluate the surface pressure of the skull upon using the helmet. Minor attention was given to the ICP and strain values inside the brain.

2.2. Computational Study of TBI using FE Modeling of the Head

Although experimental tests may lead the most accurate results if they are performed in the current setting, with accurate measuring devices, as well as precise repressurization of the cadavers, there are still many challenges involved with the experiments using PMHS models. The ethical issues of using cadavers, repressurization of the PMHS to mimic the real physiological situations, The number of possible experiments on each cadaver, the credibility of the PMHS models for further experiment, as well as the strict regulation on using these models and hence the time consuming procedure for getting approval, makes it very difficult to employ these models for TBI studies, specially bTBI. Mathematical modeling of the human head is believed to have started using a spherical model of liquid mass (Anzelius 1943). By generating a rapid motion in the model in terms of sudden velocity change, he recorded the pressure distribution and reported positive and negative pressure profiles at the coup and countercoup sites, respectively. Moreover, his model predicted a zero pressure node at the center of the spherical geometry. However, due to limitations of the mathematical models in terms of geometrical regularity, simple material models and boundary conditions, they were replaced by numerical approaches such as FE modeling, which provide approximate analytical solutions using numerical methods. Numerical approaches have found a great attention among the researchers. The fast growing computational technologies in the past few decades has introduced numerical procedures, such as finite element analysis (FEA), as a powerful tool in modeling soft-

tissue behavior. FE modeling serves to study the biomechanical behavior of complex biological components under nonlinear dynamic loading such as blunt impacts and blast waves. It has been shown by many researchers that the intricate material behavior, as well as the geometrical nonlinearities, of these components can be well modeled using FE methods. Many FE animal, human, and physical head models have been developed to study the response of the human head to different dynamic loads such as impact and blast. This section provides a review of the available FE head models in the literature used for the study of impact related and blast related TBIs.

2.2.1. Animal FE Models

2-D and 3-D FE models of animals are commonly used in different studies such as TBI researches. These models can be easily validated using in vivo animal experiments. Lee et al. (1987) used a 2-D FE model of rhesus monkey to predict the injury threshold of subdural hematoma as well as investigate the injury mechanism. Considering a rigid skull and an isotropic homogeneous elastic brain material, they replicated the acceleration experiments of Abel et al. (1978). They found that at lower Poisson's ratios (0.475), both linear and angular accelerations contributed equally to the bridging veins deformation, while for higher Poisson's rations (0.49), angular acceleration had the major contribution. Using the acceleration data, they defined threshold values for Hematoma. Using this 2-D model, Ueno et al. (1989) performed a FE study on the impact responses of the human brain. As the major outcome of their study, the scaling law applicability was investigated. Pena et al. (2005) used a controlled cortical impact (CCI) model in their numerical study to examine the ability of FE modeling is predicting the primary brain neurotaruma using a 2D finite element approach. Their effort was mainly pointed out towards finding a relationship between the injury mechanism and the biomechanical parameters of brain

such as displacement as well as mean and shear stresses. They reported that the elastic nature of the regional tissue plays an important role in transfer of load from the initial tissue to the surrounding tissues. Shreiber et al. (1997) developed a FE model of cerebral contusion in rats and compared their results with injury maps of blood brain barrier (BBB). They found good correlation between numerical and experimental results for the maximum principal stress and strain, strain energy density and von Mises stress, and reported that the BBB was most sensitive to maximum strain. Mao et al. (2006) developed a detailed 3D model of rat's head consisting of more than 250000 hexahedral elements (100-300 microns). Using a six different CCI cases, they evaluated the mechanical brain parameters such as strain, strain rate, and the ICP in the rat's brain. The head model was validated against in vivo test results and it was found out that the high strain regions correlated well with the contusion, axonal dysfunction, and the cell injury reported in experimental studies. Miller et al. (2000) developed a nonlinear 3D model of the swine brain in order to analyze the experimental data. They carried out a comprehensive study on the accuracy of brain constitutive material models for FE simulation of brain neurotaruma. They showed that the use of a hyper-viscoelastic model can be reasonable to simulate surgical procedures. They reported that the forces obtained in the numerical analysis were 31% of those predicted in the experiments. In another study, Miller et al. (1998) performed a FE analysis in conjunction with their experimental study to evaluate the FE modeling capabilities in understanding different forms of TBI. Using a pig's head model under rotational acceleration, they reported several injury mechanism at different lesions of the brain. Comparing the numerical results of two FE approaches with the experimental injury data of the pig, they found that the modeling approach representing the relative motion between the cortex and the skull provided the best agreement. Coats et al. (2012) carried out a FE study to predict the intracranial

hemorrhage in infants. To this end, they used the FE model of a 3-5 day piglet. They simulated rapid head rotations capable of inducing intracranial hemorrhage of various severity to find out the mechanical parameters and injury thresholds for predicting intracranial hemorrhage. They reported that the FE models showing pia-arachnoid complex, cerebrospinal fluid and cortical vasculature (PCC) with spring connectors between skull and brain predicted relative displacements and peak strain as those obtained in situ. In a novel study, Jean et al. (2014) examined the accuracy and feasibility of the animal model's results in predicting the brain injury among humans under blast waves using a FE modeling approach in an attempt to derive a scaling law to correlate these mechanical parameters. They used image-based FE models of the mouse, pig, and human and compared the peak stress values of the brain for different blast intensities. They stated that while mass scaling failed to capture the biomechanical response of the brain to pressure waves, the peak stresses induced by the shockwaves showed to a power function of the scaling parameter. They also found that the human brain was the most vulnerable to the blast induced TBI among other species. Lamy et al. (2011) studied the biomechanics of mild TBI using both experimental and FE approaches. They found the region specific stress response of the brain to mild TBI conditions using the FE model of a rat's skull and brain. Being exposed to angular accelerations, the predicted von Mises stresses correlated well with the changes in the severity of injury. Moreover, they concluded that the time history of the stress variation in the brain is a more credible measure than the peak values for the prediction of the mild TBI. Zhou et al. (1994) developed a 2D FE model of the porcine head including major anatomical features such as skull, dura, CSF, white matter, gray matter and ventricles. At a given applied angular velocity, they evaluated the mechanical response of the brain in terms of peak shear stress and reported a good agreement between their numerical and a counterpart experimental study. They

asserted that the DAI can occur at regions exposed to high shear stress/strain. Antona-Makoshi et al. (2013) developed a 3D FE model of the head-neck of a Macaque monkey to study the correlation between the peak values of the biomechanical parameters of the brain and different injury mechanisms. They validated the FE head model against the experimental results. They reported high correlation between the maximum principal strain in the brainstem and concussion.

2.2.2. Physical FE Models

Besides the animal FE models for the TBI studies, there are many FE physical models that have been used to address the biomechanics of the brain under dynamic loading. These models usually take advantage of the CAD models of simple geometries, such as sphere or ellipsoid shell and solid models, to replicate the geometrical features of the main head components such as the skull and the brain. For instance, Kenner and Goldsmith (1972) employed a 3D FE model of a spherical elastic shell to represent the skull, filled with inviscid, compressible fluid to account for the brain. They modeled the skull as an elastic material while they considered a viscoelastic constitutive model for the brain (fluid). They compared their numerical results with the experimental test's data from an impact test on an aluminum shell with and without distilled water inside. They observed that the FE model predicted principal strains 20% higher than those predicted by the aluminum spherical shape. In another study, Chan (1974), studied the injury mechanism for a closed head impact using a FE displacement formulation method. They modeled the brain and skull as a viscoelastic core and a thin viscoelastic shell, respectively. They employed a prolate ellipsoid and a sphere as two different geometries representing the human head. Using injury-related parameters such as tensile stresses and shear strain, they investigated possible injury mechanisms such as cavitation and rotation. They concluded that both the ICP and the shear strain have significant contribution in iTBIs.

Khalil and Hubbard (1977) carried out a FE study on the impact induced brain injury mechanisms using three different axisymmetric physical models of the human head. They used a single-layer spherical shell, an oval shell consisting of two spherical caps and a cone frustum, and a three-layer spherical shell to represent the skull and covered them with a skin flesh layer as the scalp, while they used an inviscid fluid as the brain to fill the interior cavity in all models. They investigated the effect of the head geometry, material modeling of the skull, as well as the load characteristics on the mechanical response of the skull and brain in terms of the strains and stresses, respectively. They found out that the spatial of the load significantly affected the skull strains. Hardy and Marcal (1973) developed a 2D model of the skull and considered linear elastic material properties. A symmetry boundary conditions was assumed at the mid-sagittal plane and the back of the skull was fixed in all degrees of freedom (DOF). A pressure load of 1000 lb. was applied on different but pretty similar surface areas (1.1 and 1.4 in^2) on the front and side of the skull and the displacements of the skull in horizontal and sagittal planes were recorded. An isotropic and a composite shell were used for the skull. They concluded that the skull showed a high durability to front loads with respect to side loads. Moreover, they proposed a threshold loading value of 1400 and 3500 lb. (based on the side and front load, respectively) for the initiation of crack on the skull which was in agreement with the experimental results on cadavers. Finally, the composite shell model was introduced as the appropriate model in the skull analysis under impact loads. In a similar study, Nickell and Marcal (1974)used a thin, triangular shell element formulation to examine the role of support systems in the frequency response and modal shapes of the head. They used a 2D FE model of skull to find the lowest natural modes of vibration. They observed good agreement between their numerical results with the experimental ones. Moreover, based on their modal shapes, they concluded that the cavitation and skull

rotation both contributed to the injury mechanism. Shugar (1975) added an elastic fluid-like brain model to the 2D three layered skull model of Hardy and Marcal (1973) to make a 2D plane strain model of the human had for studying the response of the head to impact loads. They considered free and fixed boundary conditions for the skull and observed higher stress levels in the brain for the case of a free skull. Moreover, they reported that for non-impact loading, the stress and strain at the brain surface was lower, while the shear stress reached its maximum value. One of the earliest comprehensive 3D FEHM was developed by Hosey and Liu (1982). Their homeomorphic FE model included a layere skull, CSF, dura, falx and tentorium, spinal cord, cervical column, and brain. They emphasized the importance of meninges and membranes on the pressure distribution inside the brain. The complexity of their model made it impossible to perform parametric studies due to the limited computational capabilities at that time. Moreover, they didn't provide numerical validation of their model against the available experimental data at that time.

There are many other works which used different simplified geometrical and material models to investigate the mechanisms of brain injury by assessing the biomechanical responses of the head to impact loads (Ruan et al. 1991; Shugar and Katona 1975; Ward and Thompson 1975).

2.2.3. Review of Major FE Head Models

In the following, a comprehensive review of the major finite element human head models (FEHM) that have been used so far in the study of the traumatic brain injury is presented. The geometry of the FEHM can be constructed from databases, anatomy atlases, and medical images such as magnetic resonance imaging (MRI) or computed tomography (CT) scans.

2.2.3.1. Wayne State University Brain Injury Model (WSUBIM)

Due to the improvement of the computational techniques in the 90's, more realistic 3D FEHMs were developed based on the real geometrical data. The very first version of the WSUBIM is probably the primary most comprehensive and detailed FEHM in the 90's that was employed by Ruan et al. (1993). This model comprised of 6080 nodes, 1895 shell elements, and 5456 brick elements. It included most of the major anatomical components of the head such as scalp, a three-layered skull, dura mater, CSF, falx, and brain. Other than the scalp and the brain that were modeled as viscoelastic materials to account for the strain rate dependency of soft tissues, all the other components were considered as linear elastic materials. They partially validated their head model against the cadaveric experimental data of Nahum et al. (1977) in terms of coup and countercoup ICPs as well as the head acceleration. They studied the injury severity by evaluating the mechanical response of the brain by using different impact directions, velocities as well as impact intensity and measured the HIC criterion to provide an injury measure based on the head kinematics. They observed that HIC was proportional to the ICP and shear stress of the brain as well as the skull von Mises stress. In the second version of WSUBIM, a sliding interface was introduced between the brain and the skull. The head model was further improved by refining the mesh size to element sized of 2mm which increases the total element number to 314500 elements. Using MRI and CT images, a smoothed facial structure was added to the head and meshed with 1mm shell elements. In WSUBIM, CSF was discretized using brick elements and a sliding interface was defined between the arachnoid membrane and dura. The current WSUBIM, developed by Zhang et al. (2001a), is discretized using 330,000 shell and solid elements ad is being used in numerous impact, and particularly blast studies, and quoting Sharma (2011) "includes scalp, skull with an outer table, diploë, and inner table, dura, falx,

cerebri, tentorium, pia, sagittal sinus, transverse sinus, cerebral spinal fluid (CSF), hemispheres of the cerebrum with distinct white and gray matter, cerebellum, brainstem, lateral ventricles, third ventricles, and bridging veins for cranial part, with the facial part consists of 14 facial bones, nasal cartilage, temporal mandibular joint, ligaments, facial flesh and skin", as shown in Figure 2.1(a). Viscoelastic material was considered for the brain, gray and white matters were differentiated to count for the stiffness of the white matter, and both cortical and cancellous bones were included in the facial bones.

2.2.3.2. University College Dublin Brain Trauma Model (UCDBTM)

This model is a detailed high resolution FEHM that was first developed by Gilchrist et al. (2001) at the University College Dublin as a 2D plane strain FE model (12,081 4-node quadrilateral elements) including the skull, brain, and CSF and assigned linear elastic material properties to skull and CSF, while they considered brain as a viscoelastic material. The 3D UCDBTM model was developed later by Horgan and Gilchrist (2003) by employing interpolation and thresholding methods on the segmented CT data of a male cadaver model provided by the Visible Human Project. Then, a smoothed and decimated polygonal model of the skull was created, where planes and curves were defined around 2 different axes of the skull using the MSC/PATRAN software to represent the inner and outer layer surfaces of the skull. The 3D FEHM were discretized with meshes ranging from 9,000 to 50,000 elements and consisted major anatomical components of the head such as scalp, 3-layered skull, dura and pia mater, CSF, tentorium, falx, cerebral hemispheres, cerebellum, and the brainstem. A representation of this head model is shown in Figure 2.1(b). The brain mechanical behavior was modeled using a linear viscoelastic constitutive law which characterized the tissue of the brain as viscoelastic in shear and elastic in compression. CSF. To overcome the inability of the software

in modeling the fluid elements for CSF, it was modeled as solid elements with low shear modulus. They employed the ABAQUS software for their numerical simulations to validate the UCDBTM against the experiments of Nahum et al. (1977) and observed very good agreements between numerical and experimental results in terms of the peak values and temporal variations of the mechanical responses. Horgan and Gilchrist (2003) carried out a parametric High/Low study to examine the effect of the shear modulus of the CSF and brain tissue, different meshes for the skull, and different mesh densities on the brain's dynamic response. They reported that the short-term shear modulus of the neural issued played a significant role in the ICP and von-mises stress predictions. Moreover, based on bulk modulus of the CSF, and the skull topological features greatly affected the pressure responses of the brain at both coup and countercoup sites.

2.2.3.3. Université Louis Pasteur Model (ULP) FEHM

The ULP FEHM developed by Kang et al. (1997) at the Université Louis Pasteur. While the skull geometry was reconstructed by digitization of the interior and exterior surfaces of the skull, the other head components, including scalp, brainstem, cerebellum, falx, cerebrum, tentorium, and the subarachnoid space, were developed using an anatomical atlas data. The model was then exported into HyperMesh and 13,208 elements were generated to discretize the model (Figure 2.1(c)). The skull was modeled using a 3-layered composite shell, the falx and tentorium were meshed using shell elements, and the rest of the components were discretized using solid elements. The mechanical behavior of the skull was modeled as elastic-plastic to be able to capture the fracture, the brain tissue was characterized by a viscoelastic model, and other head components were considered as linear elastic materials. RADIOSS CRASH software was employed for carrying out the simulations with UCDBTM and this head model was validated against the cadaveric experimental data of Nahum et al. (1977) and Trosseille et al. (1992). The

model was later coupled with motorcycle helmets to evaluate the brain tolerance limits for motorcycle accidents.

2.2.3.4. Politecnico di Torino FEHM

This FEHM was developed by Belingardi et al. (2005) in an attempt to improve the HIC criterion for evaluating TBI. The cranium and facial structure were replicated using the CT data of a patient, while soft tissue surfaces were reconstructed from the MRI data of another patient and were scaled to match the cranium of the first patient. The main focus in the development of this model was on the differentiation between white and gray matter, as well as inner elements at ventricles to assess the injury related parameters. The Politecnico di Torino FEHM included main head anatomical features such as scalp, skull, facial bones, dura mater, CSF, falx, tentorium, ventricles, and the brain tissue (Figure 2.1(d)). The model was discretized in HyperMesh with a total of 55,264 elements. The facial bone and the membranes were modeled with shell elements, the intracranial soft tissues with tetrahedral elements, and the scalp, skull, and CSF with brick elements. Except for brain which was modeled as a viscoelastic material, other head components were modeled as linear elastic materials. LS-DYNA nonlinear FE solver code was employed to perform the simulations and the head model was validated against the experiment no. 37 of Nahum et al. (1977). High shear stress regions were found in the corpus callosum and brainstem in this model which are very important the analysis of DAI. While the significance of ventricles in the protection of the midbrain region was highlighted upon using this mode, no alternative injury criteria to HIC was provided.

2.2.3.5. Kungliga Tekniska Högskolan (KTH) FEHM

Kleiven and Hardy (2002) developed a detailed head model consisting of scalp, skull, meninges, brain, CSF, dura mater, spine, muscle, skin, and a simplified neck model and

discretized it using 18,400 elements. The model was reconstructed from the MRI and CT data from Visual Human Project (Figure 2.1(e)). The brain tissue was modeled by a homogenous nonlinear viscoelastic material model (Mooney-Rivlin constitutive law) and linear elastic models were considered for other head components. They used LS-DYNA for performing the simulations and validated the KTH FEHM against the experimental pressure results of Nahum et al. (1977) as well as the relative displacement data of Al-Bsharat et al. (1999) to verify the FEHM for the analysis of shear injuries such as DAI, as these injuries are related with the strain and not the pressure. To further complement the KTH head model, the geometry of the vasculature was obtained from 3D CT data, discretized, and was included the FEHM, where it was reported that the vasculature had a minimal effect on the dynamic response of the brain (Ho and Kleiven 2007). Using KTH model, the kinematical responses of 58 NFL accidents were studied and eight different injury predictors were proposed for 6 different portions of the brain, including a 50% probability of concussion for principal strains greater than 0.21 in the corpus callosum, and 0.26 in the grey matter (Kleiven 2007).

2.2.3.6. Simulated Injury Monitor (SIMon) FEHM

SIMon FEHM was developed by Takhounts et al. (2003) to be used with the SIMon software package in which kinematic and kinetic data are obtained from test dummies are given as inputs to the mathematical model. SIMon FEHM was discretized with 7852 element and only the necessary components of the head were included for injury prediction: rigid skull, dura, CSF, brain, falx, brain, and bridging veins. The bridging veins were modeled by beam elements, while hexagonal elements were used to model other components (Figure 2.1(f)). The SIMon FEHM was validated against the displacement data of brain particles in the cadaveric tests of Hardy et al. (2001). Three major mechanisms for brain injury were proposed: cumulative strain damage

measure, or CSDM, as a correlate for DAI; dilatation damage measure, or DDM, as a correlate for contusions; and relative motion damage measure, or RMDM, as a correlate for acute subdural hematoma.

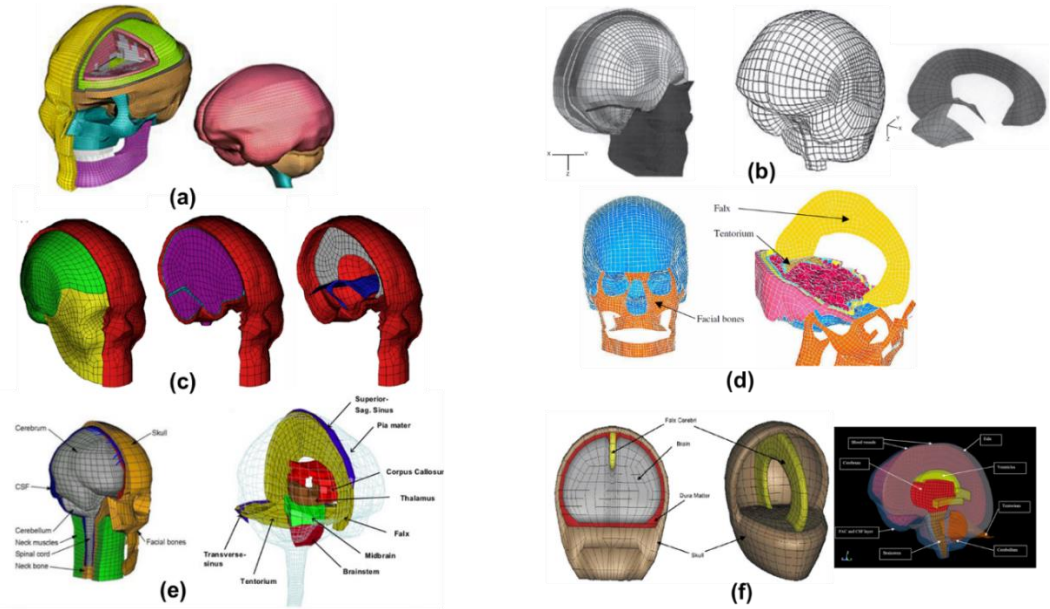

Figure 2.1. Major FEHM in the study of brain injuries; (a) WSUBIM (Zhang et al. 2013a); (b) University College Dublin Brain Trauma Model (UCDBTM) (Horgan and Gilchrist 2003); (c) Université Louis Pasteur Model (ULP) (Marjoux et al. 2008); (d) Politecnico di Torino FEHM (Belingardi et al. 2005); (e) Kungliga Tekniska Högskolan (KTH) FEHM (Kleiven 2007); (f) Simulated Injury Monitor (SIMon) FEHM (Marjoux et al. 2008; Takhounts et al. 2003)

There are many other FEHMs that have been developed by different researchers to study the mechanisms of TBI. These head models have been developed to study both iTBI (Claessens et al. 1997; El Sayed et al. 2008) and bTIBI (Chafi et al. 2010b; Ganpule et al. 2013; Moore et al. 2009; Moss et al. 2009; Sharma 2011; Taylor et al. 2014).

2.2.4. Impact-induced TBI Studies

Ruan et al. (1994) used the very first version of WSUBIM including the facial bone but excluding the falx, dura, tentorium, the spinal cord, and the neck in this model. Linear elastic material properties were considered for all the components. Using Poisson's ratios of 0.489 and 0.4996 for the CSF and brain, respectively, they addressed the compressibility issue of these

components in their study. The main objective of this study was to perform a parametric study to evaluate the pressure response of the brain when the head was exposed to identical impacts from different directions. They reported that while the coup pressure exceeded the countercoup pressure in frontal and occipital impacts, a more symmetric pressure response was observed for the side impact. They reported that while the pressure peak values didn't change much with the impact direction the location of the peak pressure profiles did. Moreover, by changing the Young's modulus of the skull as well as the Bulk modulus of the brain and CSF, they concluded that the material properties of these components affected the pressure response of the brain.

Zhou et al. (1995) used WSUBIM head model to evaluate the impact response of the brain tissue assuming both homogenous and inhomogeneous materials for the tissue. They validated against the experiments of Nahum et al. (1977) and two impact scenarios, a frontal impact, and a rotational impact about sagittal plane were carried out. They concluded that including the ventricles, as well as distinction of gray and white matters in the brain tissue serve as necessary requirements for the recognition of high shear stress regions for understanding the DAI mechanisms. Using homogenous and inhomogeneous models for the brain, they observed that unlike the ICP response of the brain, the brain's shear response had a significant variation with the homogeneity of the brain. Based on the mechanical responses of the brain they drew some conclusions about different iTBI mechanisms: they concluded that the coup-countercoup injuries are related with the ICP variations, the brainstem injuries are induced by the shear stress/strain, DAI can be a result of the shear strains at the corpus callosum, and the subdural hematoma can be induced as a result of the rupture of the bridging veins are they are most prone to high tensile strains.

Zhang et al. (2004) reconstructed actual American football field incidents and used their kinematical data, as the input for their complex FE head model, to evaluate the mechanical response of the head. They recorded the shear stress and pressure response of the brain to several impacts and proposed some injury predictors and mTBI thresholds based on both kinematical and tissue-level parameters of the head. They fully validated their FEHM against different cadaver tests such as Nahum et al. (1977) and Trosseille et al. (1992). High shear stress levels were observed at the brainstem and thalamus locations. The linear head acceleration was found to have a greater effect on the ICP response of the brain. Finally, a threshold value of 7.8 kPa for the shear stress was asserted as the tolerance level for 50% probability of mTBI.

Franklyn et al. (2005) used WSUBIM and SIMon FEHMs to investigate the role of the whole motion (not only the linear acceleration) in the evaluation of the brain injury base on the injury metrics such as AIS. They reconstructed four real-world crashes and used the kinematical data from these events as the inputs to the head models. The tissue responses of the both head models were compared with each other. WSUBIM was observed to predict higher injury thresholds than the SIMon which was believed to be due to the software and the mesh sizing.

Dirisala et al. (2012) used a 3D FEHM consisting of major head components and employed a viscoelastic neck (using spring-damper system) to model the head-neck boundary conditions in order to evaluate the brain response to impact loads. They considered linear viscoelastic material modeling for the brain and assumed linear elastic material for other head components. They compared the predicted biomechanical parameters of their model in terms of the pressure, shear stress, and shear strain with models with an elastic neck and without a neck. They observed that at a later stage of the simulation, the tissue responses of the brain decreased with increasing the damping coefficient of the neck. Comparing the results of heads with

different head models, they concluded that the neck boundary conditions play an important role in the mechanical response of the brain.

Tabacu (2015) developed a numerical dual mode head model capable of being used with both rigid body and FE applications. The main objective of the research was to investigate the capability of the rigid model in acquiring specific injury data from impact analyses. The rigid body model used in their study, was declared to be able to be used in the lumped mass models. He introduced spring connections for the rigid model and identified the required stiffness by comparing their results with the literature. He stated that the rigid model can provide accurate results as well as input data in different brain analyses studies. He reported good agreement between their numerical results in terms of the pressure and the displacement with those obtained using the UCBDTM They also validated numerical results were compared against the experiments of Nahum et al. (1977) and Hardy et al. (2007).

Zong et al. (2006) employed a 3D FEHM to study the mechanical response of the brain to impact loads. They FEHM include a three-layered skull (outer table, diploe, and inner table), CSF, brain, and neck (spinal cord, cervical bone, and disc). As one of their main objectives, they validated the head model against the experimental data of Nahum et al. (1977) and Trosseille et al. (1992). Linear elastic material modeling were used for all the components. Moreover, they introduced a structural intensity (SI) approach, which characterized the power flow inside the head, to evaluate the risk of injury. They computed the SI for frontal, occipital, and lateral impacts and reported power flow path in all cases, as well as observed that the skull was a good channel for energy flow. High chances of neck injury was reported due to the head impact.

El Sayed et al. (2008) employed the 3D FEHM, created by University of Salerno (from MRI images at the Harvard Medical School), and carried out impact simulations for frontal and

oblique impacts to evaluate the brain tissue response. The head model used in this study included scalp, skull, CSF, gray and white matter, cerebellum, corpus callosum, brainstem, telencephalic nuclei, and the ventricles. The main focus of the study was to develop a biomechanical model for assessing TBI and tissue damage by employing a constitutive model capable of capturing injury elastic/plastic deformation injury mechanisms of the brain tissue to evaluate different injury risks such as DAI and cavitation. The skull and the CSF were model by a hyperviscoelastic constitutive model. They reported that with respect to the frontal impact, the brain tissue predicted higher pressure responses at both coup and countercoup sites for the oblique impact, which was indicative of focal and diffuse damages in these sites. Likewise, it was concluded that the brain was most prone to DAI in oblique impact as shear stress levels 10 times greater than those observed in frontal impact was predicted in the oblique impact.

For further studies regarding the iTBI, the readers can refer to the literature provided in the last section on different FEHMs. The development of the FEHMs have been described within the context of the related work and the finding of the corresponding research have also been provided.

2.2.5. Blast-Induced TBI Studies

Chafi et al. (2010b) employed a validated 3D FEHM to conduct a parametric study on the biomechanical response of the brain exposed to different high explosive charge sizes at a fixed stand-off distance. They developed a bTBI model to study the brain ICP, maximum shear stress and principal strain as the determinative parameters for defining TBI at the early stages of the blast. The head model consisted the major anatomical components such as the scalp, skull, dura and pia mater, CSF, falx. Tentorium, and brain and was discretized using 27,971 elements. All the head components were modeled as elastic, except for the brain which was modeled using

both viscoelastic and hyperelastic Mooney-Rivlin model. Using LS-DYNA for performing the simulations, they reported higher biomechanical parameters for the brain at larger explosive amounts. Their results suggested that the transition of shockwaves throughout the cranial space could induce high pressures even before head movement. Based on the available injury thresholds, they evaluated the region-specific brain injury risks such as concussion and DAI based on the pattern and peak values of the ICP, shear stress, and shear strain at different lesions of the brain and correlated them with the amount of the explosives.

Taylor and Ford (2009) developed a high resolution FEHM for studying the bTBI mechanism. Their head model was developed using the high-resolution data of a frozen human female that was provided by Visible Human Project. The FEHM was constructed with a resolution of 1mm cubic and included the white and gray matter, the skull, and the CSF. The had model was discretized using 6,850,560 elements Exposing the head to front, back and side blast loading, they concluded that the focal injuries may occur as a result of blast shockwaves. Skull was modeled as a compressible linear elastic perfectly plastic material to be able to capture the fracture. White and gray matters, on the other hand, was represented as compressible viscoelastic materials. They concluded that based on the head and intracranial components geometries, as well as the direction of the blast wave, elevated levels of pressure, shear stress, and strain can develop at the focal areas of the brain.

Ganpule et al. (2013) replicated the blast wave loading on the brain using a dummy and a real head model through experimental and numerical approaches. They used a shock tube setup for the experiments and FEA for the numerical study. They constructed their 3D FEHM by segmenting high-resolution MRI data from Visible Human Project. The head model included the skin, skull, brain, subarachnoid space (SAS), and neck and was discretized in HyperMesh

software using 10-Noded tetrahedron and 8-noded brick elements into a total of 255,626 elements. Except for the brain that was modeled as a viscoelastic material, the other head components were considered as linear elastic. The main objective of their work was to understand the biomechanical response of the human head upon interaction with high pressure blast waves. To this end the head models were exposed to blast waves from the front. Amplification of coincident blast waves around the head and the unique flow dynamics of the blast were among the major results of their work. They also reported that the mechanical responses of the brain is governed by several parameters such as structural deformation, reflection of shockwaves from material interfaces inside the brain, and direct transmission of shockwaves. Moreover, they elucidated that the tissue cavitation and the skull deformations can be regarded as bTBI mechanisms.

Moore et al. (2009) developed a 3D FEHM, called DVBIC-MIT by segmenting the high-resolution T1 MR images from the Montreal Neurological Institute with 1 mm cubic resolution, and discretized the head model with a total of 808,766 elements in ICEMCFD software. The main goal of their study was to evaluate the blast wave-head interaction to investigate whether shockwaves can propagate through the skull and find out if the lung injury thresholds can be employed toward the assessment of bTBI. They employed the lung injury threshold, as well as the 50% lethal injury threshold to compare and examine similar currently survivable blast exposure on the head, and then compared their blast brain responses to the one corresponding to concussive injuries among NFL players. They compared the ICP response for two different overpressures, 5.2 and 18.6 atm, and found out that the ICP increments was nonlinear in the order of 4-6 times. Comparing the blast results from the 18.6 atm with the one from the 5 m/s

impact, comparable ICP values were reported. They major contribution of their results was towards the development of personal protective equipment against blast assaults.

Panzer et al. (2012) developed a detailed plane-strain FE model of the human head and brain to study the tissue response of the brain when the head was exposed to blast waves with different incident overpressures ranging from 50 to 1000 kPa. The FEHM was developed from an axial slice photo of a female head available from Visible Human Project. The head was scaled to match the size of a 50^{th} percentile male US Army personnel. The FEHM consisted of brain (white and gray matter), CSF, nervous tissue, ventricles, skull (inner table, diploe, outer table), and scalp, and was discretized using a total of 29,088 single-layer hexahedral elements (1mm thick). They employed a linear viscoelastic material model to represent the deviatoric response of the brain, skull, and scalp. However, to describe the volumetric response of the scalp, brain, and CSF, the Mie-Gruneisen equation of state (EOS) was used, while a linear elastic model was used to describe the volumetric response of the skull. As one of their main objectives, they developed a cavitating (including CSF), and non-cavitating (without CSF) to investigate the incidence of cavitation in bTBI. They asserted that while the peak brain ICP was dependent on the peak incident overpressure of the interacting blast waves, the maximum strain depended on the impulse of the shockwaves. They also reported that the cavitation had a significant effect on the tissue response of the brain as it elevated the brain's strain in the cerebral cortex.

2.2.6. FE Modeling of Protective Headgears in TBI Studies

Aare and Keleiven (2007) employed the KTH FEHM to carry out a numerical study to investigate the effect of different helmet shell stiffness on the mechanical response of the head. Moreover, by studying different angles of the ballistic impact, they observed that the oblique impacts may induce larger shear strains on the brain compared to the radial ones. Pointing out

the importance of the helmet shell stiffness in preventing the worst loading scenario due to head-helmet contact, they also concluded that 45 degree impacts impose the highest shear stain on the brain tissue.

Jazi et al. (2013a) studied the effect of different padding material on the mitigation efficacy of ACH helmets under different ballistic impacts. Using a detailed 3D FEHM, they evaluated the tissue responses and the kinematics of the brain and head when the head was protected with a ballistic helmet embedded with foam pads with different material properties. The FEHM included major head components such as the scalp, skull, falx, tentorium, brain, CSF, facial bone and skin, neck bone and skin, and dura and pia mater. The model was discretized using a total of 28,705 shell and brick elements. All the head components except for the brain which was considered viscoelastic, were modeled as linear elastic materials. In terms of the biomechanical parameters of the brain, they found the front impact as the worst scenario in which brain undergoes the highest ICP and shear stress levels. Moreover, foam with lower stiffness transfer less loads to the head.

Grujicic et al. (2011) employed a 3D head model purchased from 3DCAD.com and generated the mesh using HyperMesh software. Their head model included the brain (cerebrum, cerebellum, and brainstem), pituitary gland, CSF, and skull. The FEHM was meshed using 510,000 solid finite elements. Nonlinear Neo-Hookean hyperelastic model was employed to model the deviatoric response of the brain tissue. The skull behavior was characterized using Mie-Gruneisen equation of state for the hydrostatic part, and a linear elastic model for the deviatoric part. They studied the role of the ACH protection system in blast-induced injuries. Applying two different overpressures of 5.2 and 18.6 atm in lateral blast scenarios on unprotected and ACH-protected head models, they observed a significant reduction in the ICP

and maximum shear stress. They observed that shockwaves transmitted within the intracranial space and were reflected at the material interfaces, which gave rise to complex spatial distribution. They tried to provide a correlation between the peak ICP values and different injury mechanisms such as DAI, contusion, and concussion. They stated that the ACH helmets provided significant protection against all types of mTBI.

Nyein et al. (2010) added a conceptual faceshield to the protection system of the pad-supported helmet to evaluate the behavior of the brain under blast loading. Using a biofidelic model of the human head, they replicated the injury mechanism for blast-induced neurotrauma based on the fluid-solid interaction coupling. The frontal blast loading was applied to the head for three cases: an unprotected head, a head with helmet and a head with helmet and faceshield. They observed significant mitigation in transferred load to the head in the case of the faceshield because unlike the helmet, faces shields impeded the stress waves flowing inside brain.

Ganpule et al. (2012) carried out a computational study to investigate the shockwave-head interaction for unprotected and helmeted heads only in a frontal blast using a 2D plane strain FE model of the helmet and the head. They reported an amplified pressure region inside the helmet gap (underwash effect) and explained the incidence of the underwash effect based on the geometry, surface curvature and the gap size of the helmet.

Moss et al. (2009) were among the very first studies to evaluate the efficiency of combat helmets to in protecting the head against blast waves. They employed a simplified head/brain model to including a hollow elastic ellipsoid as the skull, a viscoelastic fluid as the brain, and a layer of CSF surrounding the brain. They also used a simplified neck, face, and body. Using a helmet supported by webbed suspension system, they observed the underwash impulse inside the helmet gap of 1.3 cm. In their second helmet model, the helmet was supported by foam pads and

they asserted that while the use of foam pads eliminated the underwash effect, they caused a stronger coupled motion of the helmet to the head, hence forming localized pressure regions due to the skull deformation.

Sarvghad-Moghaddam et al. (2014a) did a comprehensive study on the protection capability of helmet and helmet-faceshield systems. Using the same head model used by Jazi et al. (2013a), elastic material modeling for the head components and a hyper-viscoelastic constitutive law for the brain tissue, they evaluated the mechanical responses of the head in terms of the tissue and kinematic responses to blast waves approaching from four different directions. An incident overpressure of 5.2 atm was used in their study based on the lung injury threshold. They observed that the brain mechanical responses, as well as the protection capability of both faceshield and helmet significantly changed with the blast direction. The studies on the underwash effect of protective headgears have neglected the effect of a major blast parameter, the blast direction, as well as inclusion of faceshield, on the incidence of the underwash.

CHAPTER 3. FE DISCRETIZATION, MATERIAL MODELING, AND NUMERICAL METHODOLOGY

3.1. FE Discretization

3.1.1. Human Head Model

This human head model for this research was originally developed by Horgan and Gilchrist (2003) from the Computed Tomography (CT) data provided by Visible Human Project, by 0.3 mm increment in the coronal plane. After stacking up the CT data, thresholding and interpolation techniques were performed to identify the voxels representation of the tissue. Smooth triangle surfaces of the head were then created by interpolation through the voxels. The CT data was employed to make a polygonal model of the head using VTK software (Kitware Inc, 2001). After smoothing the polygonal model, it was converted into IGES format and was imported in the MSC/Patran for meshing. The details of the original head model is provided in Horgan and Gilchrist (2003). The North Dakota State University Finite Element Head Model (NDSUFEHM), was developed in 2010 by adding the neck bone and skin, facial skin. The head model was discretized using HyperMesh (HyperWorks, 2011) using a total of 38,379 shell and brick elements. The anatomical components, as well as the discretization properties of all the head/neck components are presented in Table 3.1. NDSUFEHM includes the major anatomical features of the human head and neck such as scalp, skull, dura mater, falx, tentorium, pia mater, CSF, brain, neck bone, neck muscle, facial bone, and facial skin (Figure 3.1). The scalp is represented by two layers of eight node, skull is represented by four layers of solid elements (4-7 mm thickness), brain, CSF, facial bone and skin, and neck bone and skin are molded using 4-noded solid elements, and membranes such as dura and pia mater, as well as falx and tentorium are modeled using 4-noded shell elements.

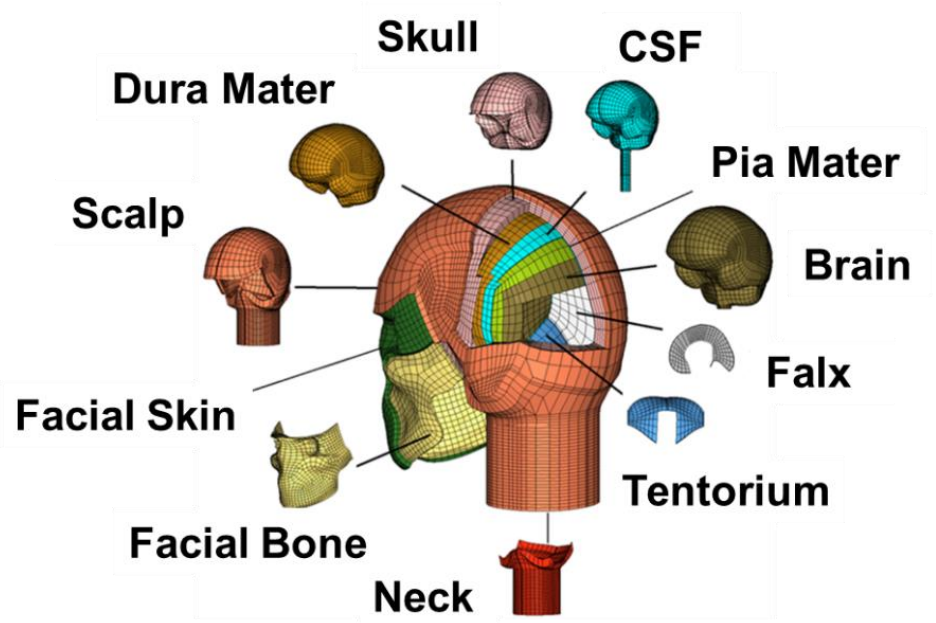

Figure 3.1. FE discretization of human head components for NDSUFEHM

One of the challenges in developing exact FE models of the human head is the accurate modeling of the interfaces among different head components. To this end, it is very important that the CSF layer is properly modeled. As mentioned before, CSF is a water-like fluid layer which surrounds the cranial space and separates the skull from the brain. It acts as a natural shock absorber which provides the relative displacement of the brain with respect to the skull (Bradshaw and Morfey 2001). In our research, CSF was modeled using 8-noded brick elements with fluid-like properties, which allows for the relative skull/brain motion, agrees with impact experiments (Chafi 2009). To comply with the anatomical characteristics of the head, while tied surface-to-surface contact algorithm was employed to replicate the interfaces between the scalp and skull, the skull and dura, and the brain and pia, tied node-to-surface was employed for defining the contacts among the dura-falx-tentorium components, which provides an application of both compressive and tensile loads on the brain.

Contact algorithms are mainly used for defining contact between two parts that are push or slide against each other, as well as the parts that are tied to each other. LS-DYNA provides an extensive library of contact types which can be used for particular use. Through definition of part, segment, and node sets, slave and master parts are checked for possible penetration of slave parts through the master sections. In penalty–based methods, proportional to the depth of the penetration, a force is generated and applied to resist and eventually eliminate the penetration (Bala 2001).

3.1.2. ACH Helmet, Padding System, and Faceshield

The ACH helmet was replicated using digital 3D scanned images. Based on the real-life dimensions and sizing, a 6” x 15” NIJ (National Institute of Justice 1985) standard level II faceshield was developed for the current study using Solidworks. The padding system includes seven pads which is the most common form of their arrangements inside the head-helmet gap (approximately 1 inch spacing).The ACH helmet, faceshield, and the foam pads were modeled using 8-nodded solid elements. The ACH helmet and the faceshield were discretized using 3768 (4 layers) and 2303 (2 layers) solid elements, respectively. They both have a thickness of about 13 mm.

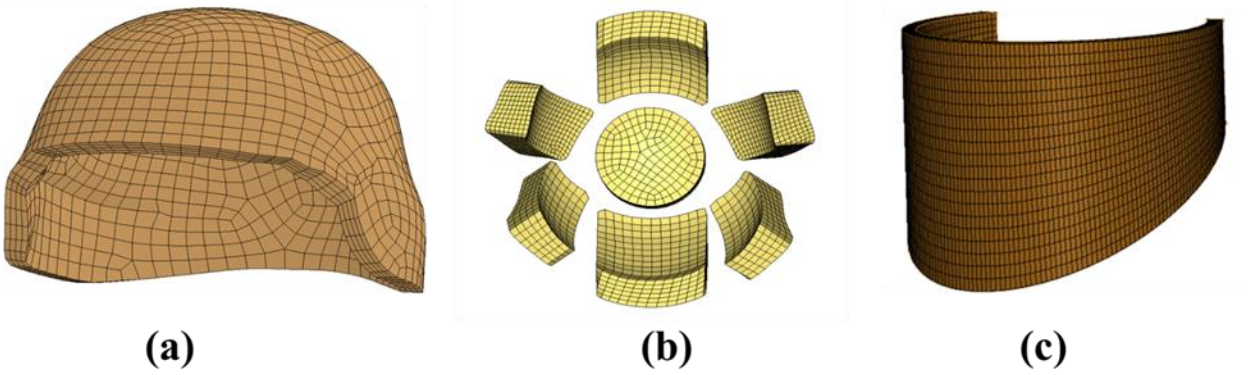

Figure 3.2. FE model of (a) ACH helmet; (b) common 7-pad suspension system; (c) faceshield

The FE model of the padding system was represented using 8663 hexahedral elements. The head-helmet/face shield gap allows for evaluation of the underwash effect which serves as a major goal in this study. The discretization and meshing procedure was carried out in Hypermesh® (Altair Hyperworks 2011) and a total of 53113 Lagrangian elements comprising the head components along with the padded helmet and the faceshield. The FE discretization of the protective headgears used in the current study including the helmet, face-shield, and the padding system is shown in Figure 3.2.

3.2. Material Models

3.2.1. Head Components

Developing an accurate constitutive model for the brain tissue has always been a challenge and numerous studies have been performed to improve the modeling of head components in order to better predict the human head behavior under different loading conditions (Mendis et al. 1995; Ruan et al. 1991).

Panzer et al. (2012) performed an FE analysis on the response of the brain under different blast overpressures. They employed linear elastic and viscoelastic models as well as the Mie-Gruneisen equation of state to approximate the deviatoric and volumetric responses of the brain tissue, scalp, skull and CSF. Taylor and Ford (2009) utilized a linear elastic model for the skull and CSF and considered viscoelastic properties for white and gray matters in an effort to visualize the dynamic response of the brain under the blast loading. In another study, Grujicic et al. (2011) used a linear elastic model for the skull and the Neo-Hookean hyperplastic constitutive law for modeling the brain. In the current study, linear elastic properties used for scalp, skull, pia and dura mater, tentorium, CSF, as well as the neck bone and muscle are adopted from the works of Zhang et al. (2004), Zhou et al. (1995) and Horgan and Gilchrist (2003).

Table 3.1. Finite element characteristics and employed material models for head components

Tissue	Anatomical structure 50^{th} perc. male	Constitutive model	FE model	# of Elements
Scalp	5-7 mm thick	Linear elastic	6 mm Solid element	5938
Skull	195 mm length, 155 mm breadth,225 mm height,4-7 mm thick.	Linear elastic	Solid element	8305
Dura, falx, tentorium	1 mm thick	Linear elastic	1 mm thick shell element	2590
Pia	1 mm thick	Linear elastic	1 mm thick shell element	2754
CSF		Linear elastic & Viscoelastic	1.3 mm thick solid element	3354
Spinal cord		Linear Elastic	Solid elements	496
Brain	165 mm length 140mm transverse diameter	Hyperviscoelastic	Solid element	7302
Neck bone		Linear elastic	6 mm thick solid element	496
Neck Muscle		Linear elastic	Solid element	3772
Facial Bone		Linear elastic	2mm Solid element	1124
Facial Skin		Linear elastic	Solid element	2248

The mechanical properties of these components are described in Table 3.2. However, a hyper-viscoelastic material model is utilized to better capture the nonlinear behavior of the brain tissue. This model, as also employed by (Chafi et al. 2009; Chafi et al. 2010b), develops effective constitutive properties in terms of the large deformations due to the dynamic blast loading. Intracranial pressure, defined as the pressure imposed by CSF, and blood on the brain is

one of the major parameters in evaluation of the TBI as elevated ICP can induce severe neurological damages. However, external loadings on the skull from blunt impacts or blast can result in increased ICP in the CSF and as a result in the brain tissue. Intracranial pressure is defined as the hydrostatic pressure imposed on the brain mainly due to the fluid-like behavior of the tissue. The hydrostatic pressure, P, is the mean stress of three principal stresses, $\sigma_1, \sigma_2 \; and \; \sigma_3$ (Ruan et al. 1994):

$$P = -\frac{\sigma_1 + \sigma_2 + \sigma_3}{3} \tag{3-1}$$

Table 3.2. Mechanical properties of the elastic head components

Head Component	Density (g/cm^3)	Elastic Modulus (GPa)	Poisson's Ratio	Bulk Modulus (GPa)
Scalp/ Skin	1.2	0.0167	0.42	
Skull	1.21	8.0	0.22	
Dura, falx, tentorium	1.133	0.0315	0.45	
Pia mater	1.133	0.0115	0.45	
Facial bone	2.10	5.54	0.22	
Cervical Vertebrae	2.5	0.354	0.3	
CSF	1.004	----	0.499	2.19

In current material modeling, the Mooney–Rivlin formulation is adopted for describing the hyperelastic nonlinear behavior of the brain tissue while the Maxwell constitutive law is applied towards modeling the linear viscoelastic behavior of biological tissues. Accordingly, the resulting Cauchy stresses from both approaches are employed to describe the brain response under applied loadings. The material model used in this study correlated perfectly to the intrinsic behavior of the brain regarding its mostly incompressible behavior and sustainability under large deformations. The parameters for the Mooney-Rivlin constitutive equation are determined from the work of Mendis et al. (1995).

The strain energy density function governing the Mooney-Rivlin constitutive approach for the incompressible, homogenous and isotropic materials is described by:

$$W = C_{10}(\bar{I}_1 - 3) + C_{01}(\bar{I}_2 - 3) + \frac{K}{2}(J_3 - 1)^2 \tag{3-2}$$

where C_{10} and C_{01} and K represent the material constants evaluated experimentally, $\bar{I}_1$ and $\bar{I}_2$ are the first and second invariants of the Cauchy tensor and J_3 is the elastic volume ratio. The Cauchy stress corresponding to the nonlinear hyperelastic model is obtained as:

$$\sigma = -\frac{\partial W}{\partial \varepsilon} \tag{3-3}$$

where W is the strain energy potential of Mooney-Rivlin and ε represents the Green's strain tensor. The parameters for the Mooney-Rivlin constitutive equation is determined from the work of Mendis et al. (1995) and are shown for the brain tissue in Table 3.3. On the other hand, applying the Maxwell model for the linear viscoelastic behavior of the tissue, one can find the resulting Cauchy stress tensor as:

$$\sigma_{ij} = JF_{ik}^{T} \cdot S_{km} \cdot F_{mj} \tag{3-4}$$

where J depicts the transformation Jacobian, F indicates the gradient tensor of deformation and S is the second Piola–Kirchhoff stress tensor. The rate effects captured by this constitutive model are formulated using a convolution integral in terms of the second Piola–Kirchhoff stress tensor, S_{ij} and the Green's strain tensor, E_{kl} as follows:

$$S_{ij} = \int_0^t G_{ijkl}(t-\tau)\frac{\partial E_{kl}}{\partial \tau}\, d\tau \tag{3-5}$$

with $G_{ijkl}(t-\tau)$ indicating the relaxation functions at various stress levels.

The Prony series can be used to describe the relaxation functions which are employed to evaluate the Cauchy stress tensor:

$$G(t) = G_0 + \sum_{i=1}^{n} G_i e^{-\beta_i t} \tag{3-6}$$

where G is the shear modulus and β is the decay parameter. (Nahum and Smith 1977; Willinger et al. 1995; Zhou et al. 1995). The data has been widely used in related literature and has shown to provide reasonable results (Chafi et al. 2009; Chafi et al. 2010b; Gu et al. 2012). In order to prevent the rigid body motion and keep the stability of the solution, the inferior surface of the neck is constrained in all directions.

Table 3.3 Mechanical properties of hyper-viscoelastic brain material

C_{10}(Pa)	C_{01}(Pa)	G_1(kPa)	G_2(kPa)	$\beta_1(s^{-1})$	$\beta_2(s^{-1})$	K (GPa)
3102.5	3447.2	40.744	23.285	125	6.6667	2.19

3.2.2. ACH Helmet, Foam Pads, and Faceshield

A composite material of KEVLAR® 29 with type II fabrics and a phenolic resin is utilized for modeling the current helmet and faceshield. The constitutive properties are adopted form the work of (Van Hoof et al. 2001) and are represented in Table 3.4. The transversely isotropic linear-elastic constitutive law which is a special case of orthotropic model is employed for modeling their material. A brief description for constitutive modeling of orthotropic materials is provided here to delineate the procedure involved in the evaluation of the pressure in these materials. The general Hooke's law is employed to represent the constitutive properties of elastic materials. Accordingly, the stress-strain relations are defined as (Tham et al. 2008):

$$\sigma_{ii} = \frac{1}{3}(C_{i1} + C_{i2} + C_{i3})\varepsilon_{vol} + C_{i1}\varepsilon_{11}^{d} + C_{i2}\varepsilon_{22}^{d} + C_{i3}\varepsilon_{33}^{d} \quad (3\text{-}7)$$

for i = 1,2,3. ε_{vol} and ε_{ij}^{d} are volumetric and deviatoric components of the strain tensor, respectively and both contribute to evaluation of the pressure . The coefficients of the stiffness matrix C_{ij} are defned in terms of the Poisson ratios ν_i's, Young's Moduli, E_i's and shear Moduli,

G_i's, as explained in the work of Xia Huang (2011). Pressure is defined as the negative of mean stresses (average of normal stress components) as: $p = -\frac{1}{3}(\sigma_{11} + \sigma_{22} + \sigma_{33})$. For small strains, the corresponding components can be decomposed into the deviatoric strain, ε_{ij}^{d}, and the average strain, ε_{ave}, such that : $\varepsilon_{ij} = \varepsilon_{ij}^{d} + \varepsilon_{ave}$. Introducing the volumetric infinitesimal strain as the trace of strain components, $\varepsilon_{vol} \approx \varepsilon_{11} + \varepsilon_{22} + \varepsilon_{33}$, the average strain is expressed as: $\varepsilon_{ave} = \frac{1}{3}\varepsilon_{vol} = \frac{1}{3}(\varepsilon_{11} + \varepsilon_{22} + \varepsilon_{33})$. Inserting equation (6) in the pressure equation, we will have (Xia Huang 2011):

$$P = -\frac{1}{9}[(C_{11} + C_{22} + C_{33} + 2(C_{12} + C_{23} + C_{31})]\varepsilon_{vol} \\ -\frac{1}{3}[(C_{11} + C_{12} + C_{13})\varepsilon_{11}^{d} + (C_{21} + C_{22} + C_{23})\varepsilon_{22}^{d} + (C_{31} + C_{32} + C_{33})\varepsilon_{33}^{d}] \quad (3\text{-}8)$$

The three last terms on the right hand side of the above equation are ignored for the elastic isotropic materials. The model employed here as the transversely isotropic elastic material would follow the same procedure as the one explained above.

Foam pads are usually made of energy absorbing materials and help to significantly mitigate the applied load to the head. Different parameters such as the geometry, layout and particularly the material of the padding affect the efficiency of them under dynamic loads. The behavior of the foam is defined using its stress-strain diagram. The expanded polypropylene (EPP) foam was chosen for this study based on the work of Jazi et al. (2013a). The mechanical behavior of the foams is characterized by three different regions in its stress-strain curve, namely linear elasticity, plateau and densification (Figure 3.3a). At small strain, the foam response is linear elastic and its Young's modulus is also defined by the slope of this region. However, as the energy absorption capability of the foam is defined by evaluating the area under the stress-strain curve, the plateau region dictates the main contribution of the foam in energy absorption.

The mechanical behavior of the foam material is adopted from the work of Kleiven (2007) and is shown in Table 3.4. The stress-strain curve used for the EPP foam is shown in Figure 3.3b.

The mechanical behavior of Polycarbonate, a durable thermoplastic with high impact resistance commonly used to make faceshields, was modeled using linear elastic material and the material properties are presented in Table 3.4 (Dwivedi et al. 2012).

Table 3.4. Mechanical properties of helmet, faceshield, and padding material (*E*: Young's modulus, *v*: Poisson's ratio; *G:* shear modulus; ρ: density)

Helmet shell (Kevlar)

$E_{11} = E_{22}$ (GPa)	E_{33} (GPa)	ν_{12}	$\nu_{23} = \nu_{31}$	G_{12} (GPa)	$G_{13} = G_{23}$ (GPa)	$\rho(g/cm^3)$
18.5	6.0	0.25	0.33	0.77	2.715	1.23

Faceshield (Polycarbonate)

Density (g/cm^3)	Elastic Modulus (GPa)	Poisson's ratio
1.197	2.59	0.39

Padding material (Foam)

Density (g/cm^3)	Yield Strength (GPa)	Plateau Strength (GPa)	Tangential Modulus (GPa)
0.031	0.1×10^{-3}	$(100 - 250) \times 10^{-6}$	1.9×10^{-3}

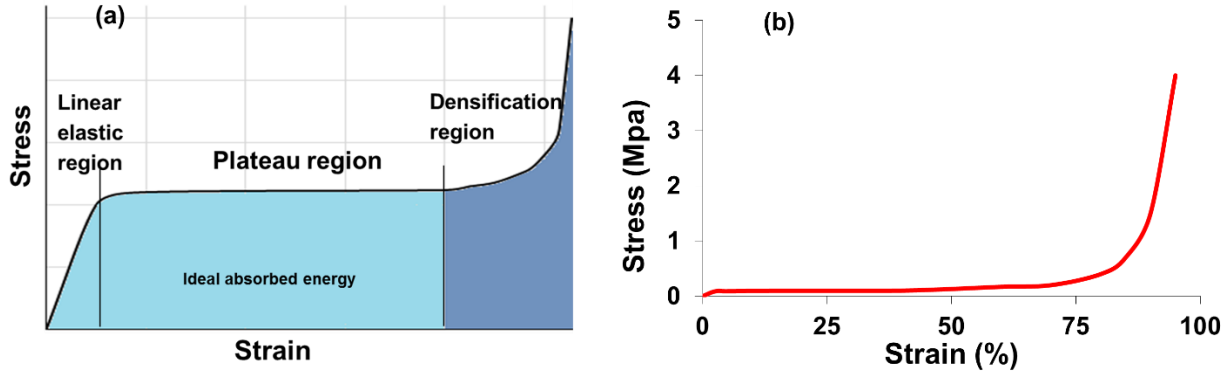

Figure 3.3. (a) Typical stress-strain curve of foam material with three characteristic regions; (b) Stress-strain behavior of EPP foam for the helmet pads in this study (Jazi et al. 2013a)

3.3. Numerical Methodology and Validation Studies

3.3.1. Blast Modeling and Validation

Finite element methods can be employed to simulate the generation, propagation, and interaction of blast shockwaves with solid objects. One of the robust software in modeling blast waves is LS-DYNA, which is a transient, nonlinear, explicit, and dynamic FE hydrocode. The domain in which the blast occurs plays an important role in simulating the fluid - solid interaction between the head and shock waves. In this work, air is chosen as the medium and open space blast scenario is performed. Purely Lagrangian method called Load_Blast_Enhanced (LBE), and Multi-Material Arbitrary Eulerian-Lagrangian (MM-ALE) formulation are the two main numerical techniques in LS-DYNA that have been used for modeling the blast (LS-DYNA 2007). However, low-accuracy as well as the inability of LBE method to model the shockwave reflections at the corners and the huge computational cost of MM-ALE method have led to the advent of the coupled method. This recent feature of LS-DYNA inherits the advantages of LBE and MM-ALE techniques in order to provide an accurate simulation of blast waves with a reasonable computational cost (LS-DYNA 2007). This is achieved through skipping the discretization of the domain between the explosive and the Lagrangian domain. Hence, the simulation can be carried out for any size of the HE charge at any stand-off distance. Figure 3.4 shows the accuracy of the coupled methods when compared with experimental results and the numerical result obtained using MM-ALE method. The details of Lagrangian, Eulerian, ALE, and MM-ALE methods can be found in Chafi (2009).

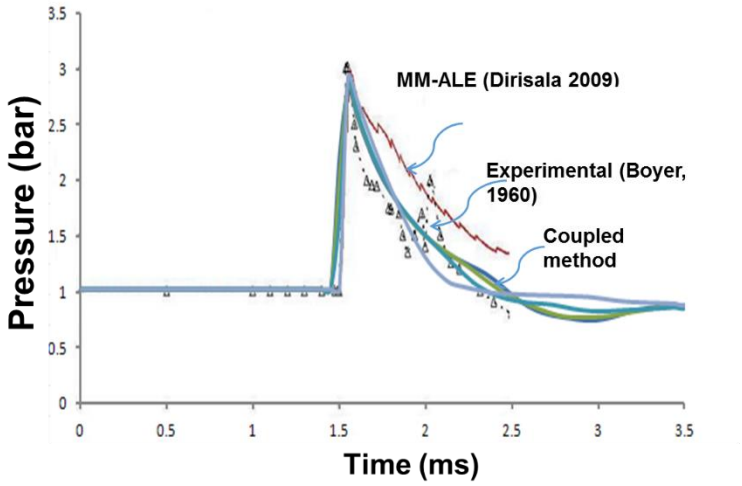

Figure 3.4. Comparison of the coupled method for simulating blast waves with MM-ALE (Dirisala 2009) and Experimental methods (Boyer 1960)

In the coupled method, the blast pressure is calculated using LBE method and is then applied on the surface facing the detonation, i.e. ambient surface (Figure 3.6). The Eulerian domain was filled with air, which was modeled as an ideal gas at $25^{o}C$ and 1 atm using the equation of state (EOS):

$$p = (\gamma - 1)\frac{\rho}{\rho_0}E \tag{3-9}$$

where p is the pressure, $\gamma = \frac{C_p}{C_v} = 1.4$ is the specific heat ratio for air, ρ and ρ_0 are the current and initial air density, respectively and E is the volumetric energy density. In order to implement open-space blast scenario, non-reflecting boundary conditions are assumed for all other surfaces of the media. The domain, including the helmeted head model as well as the boundary conditions and loading are all shown in Figure 3.6. Employing a 50 x 50 x 50 cm computational cubic domain around the model, the pressure wave propagation is modeled in the open space media. To comply with the 50% LD_{50} (lethal dose) of lung injury survival suggested by Bowen et al. (1968), using 70 grams of TNT at a stand-off distance of 58 cm, an overpressure of 520 kPa is generated around the head model and all the studies are performed for the same overpressure.

Figure 3.5 shows the time history of the blast pressure around the head used for the most parts of the current research. As it can be seen, the time history perfectly replicates the Friedlander shockwave's behavior and had an incident overpressure of 520 kPa.

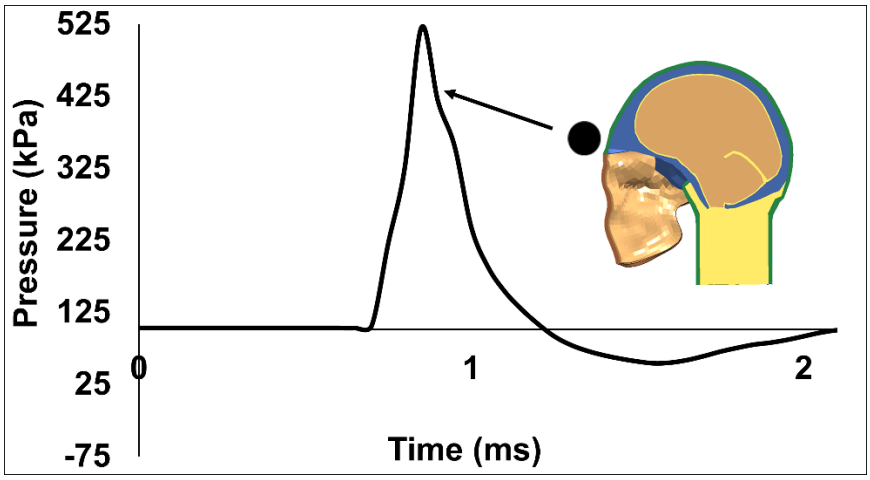

Figure 3.5. Time history of the shockwave generated around the head for current study

3.3.2. Fluid-Solid Interaction (FSI) Analysis

FSI refers to the coupling of the structural mechanics with the unsteady fluid mechanics, which in essence provides a two-way coupling between the structural deformations and the fluid-pressure. Constraint-based and penalty-based formulations are the two commonly used algorithms that are employed by LS-DYNA to implement the FSI coupling. The constraint-based method uses an implicit algorithm to alter the nodal velocities of both shell and solid elements, forcing them to follow each other. This approach is assumed to be quite stable as it only conserves the momentum equation. On the other hand, the penalty-based method is an explicit algorithm which applies forces at nodes by tracking the relative displacement of specific points. Although this formulation conserves energy, it is less stable than the constraint-based formulation (Souli et al. 2000). The fluid-structure interaction between the Lagrangian domain (FEHM) and the Eulerian domain (ALE media and blast pressure waves) is implemented through penalty based methods. In the ALE method, the Navier- Stokes equations (continuity and

momentum) along with solid material constitutive relationships are solved simultaneously. This approach accounts for the response of the fluid flow, structural framework and their interaction with each other. The numerical approach is performed using the Operator Split method (LS-DYNA 2007). Including a Lagrangian step in which the solid deforms and an advection step where element state variables are mapped back onto the original meshing. The multi material ALE method employed here enforces an effective approach for conducting large-deformation analysis such as the impact on soft-tissue materials like brain. The procedure can be simply summarized as follows: the intersection of ALE and Lagrange parts are found, the coupling points are recognized, the displacement of ALE fluid through Lagrange segments is marked as the penetration distance and the loading is evaluated based on this distance.

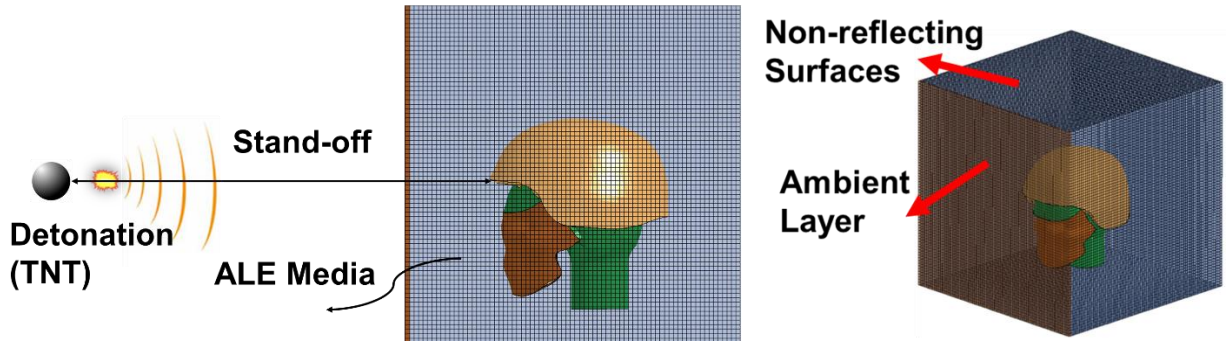

Figure 3.6. Discretized Eulerian and Lagrangian domains along with boundary conditions for the current study

3.3.3. Numerical FE Head Model/PPE Models

In this research, three different models of the FEHM/PPE are employed. The first model, shown in Figure 3.7a, is referred to as the "unprotected head model" which basically is the FEHM introduced earlier. The second model, shown in Figure 3.7b, represent the assembly of the FEHM, ACH helmet and padding system and is called the "helmeted head model". Two different versions of this model is used throughout this study, one without the inclusion of the

padding system, and the other one including the padding system. Finally, the third model which is called the "fully-protected head model", is the assembly of the FEHM, ACH helmet, and ballistic faceshield (Figure 3.7c). This model also has two versions, one with the inclusion of the padding system and one without the padding system.

Different contact algorithms were used for positioning the PPE on the FE head model. A standard gap size of 1 inch was provided between the head and the helmet. The foam pads were fixed on the interior of the helmet shell using the tied-surface to surface contact algorithm, while a surface-to-surface contact was used between the pads and the scalp. Moreover, the faceshield was pinned to the helmet using tied-surface-to-surface contact algorithm.

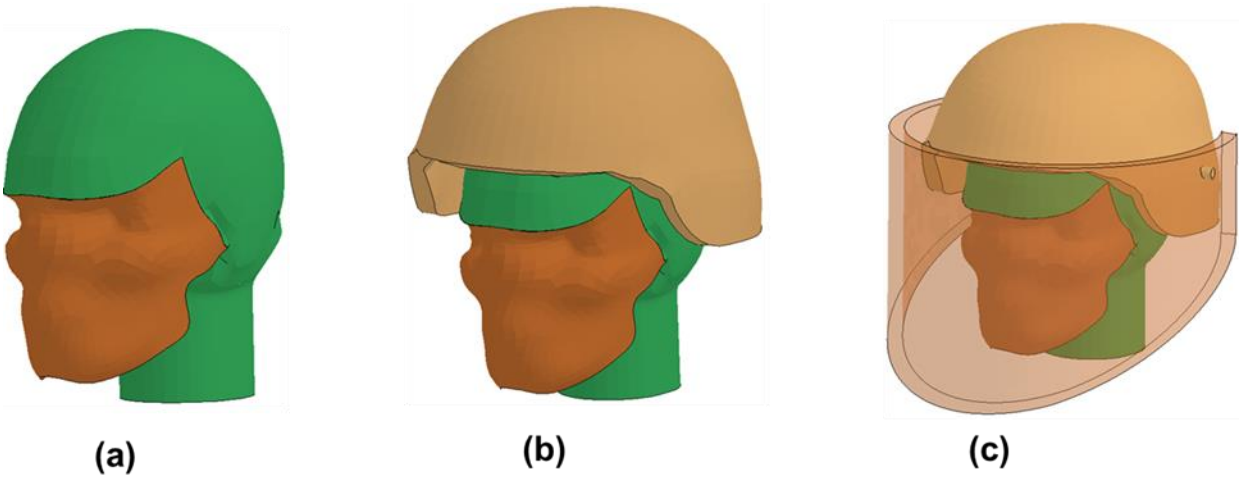

Figure 3.7. Numerical Models of FEHM/PPE used in the current research; (a) Unprotected; (b) Helmeted; and (c) Fully-protected head models

3.3.4. Validation of NDSUFEHM

An important aspect of every numerical work is the validation of the work in terms of result accuracy and reliability. The ethical issues encompassing the human biomechanical studies, restricts the experimental analysis in major areas such as the heart and brain. Accordingly, as mentioned earlier the animal models, as well as the cadaveric experiments, are the major available options in validating the numerical results. One of the signature studies in the

field of head injury biomechanics is the work performed by Nahum et al. (1977). Using an impactor, they applied a frontal impact force to the anterior-posterior orientation of the head in the mid-sagittal plane of the seated human cadaver head. They compared the experimental coup-countercoup pressure gradient in the brain with their FE results for experiment 37 in which they used a 5.59 kg impactor with an initial velocity of 9.94 m/s. To inhibit a skull fracture, the impactor was supported by a padding foam. Due to the lack of data on the pad used by Nahum, the impact force time history was applied for the same experiment (no. 37) at the frontal bone of our FE head model. The force time history used for our simulation is shown in Figure 3, from which the force data was extracted and applied as the input at the frontal bone. Nahum et al. (1977) measured the ICP at 5 different locations inside the intracranial space. To verify the head model used for this study, it was validated against Nahum's data in all 5 locations. However, we only provided the validation results for the coup (frontal lobe) and counter coup (occipital lobe) sites (Figure 4). As shown in Figure 4 (a,b), the results compared well with the experimental data for both the coup and countercoup pressure time histories. The slight differences between the numerical and experimental data may be due to simplifications employed in making the FE model, the mesh size, or differences in the replication of exact experimental conditions. According to the injury threshold proposed by Ward et al. (1980), based on the ICP (234 kPa for coup pressure and -186 kPa for countercoup pressure), no injury was predicted based on the computational results which was consistent with the autopsy results issued after Nahum's experiment (Willinger et al. 1999).

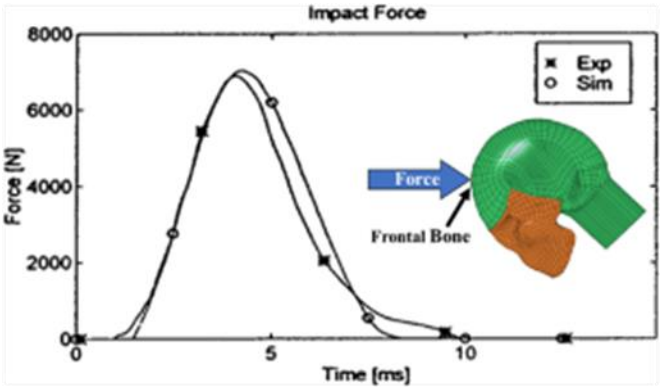

Figure 3.8. the impact force time history used for validation of current FE head model against Nahum's experiment. [19] and the location of impact on the head (frontal bone)

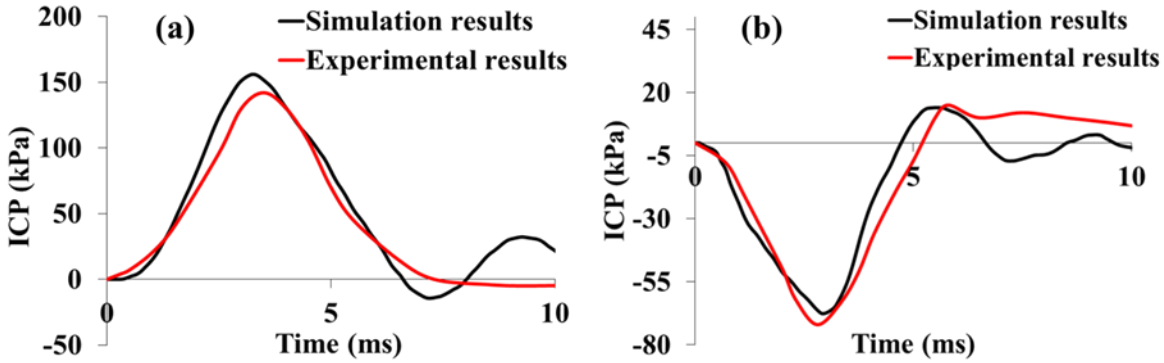

Figure 3.9. Comparison of (a) coup ICP; (b) countercoup ICP between the current numerical results and the experimental result of Nahum et al. (1977)

CHAPTER 4. THE EFFECT OF THE LOADING DIRECTIONALITY ON THE DYNAMIC RESPONSE OF THE HEAD UNDER BLUNT IMPACT

Due to structural inhomogeneity of the human head and the intrinsic differences of head components in terms of shape, material, and tolerance, different parameters such as the impact velocity (intensity), location (directionality), the type of blunt impact (struck against or struck by) can affect the mechanical response of the head. Accordingly, these variations would influence the stress and strain wave propagation, as well as the pressure gradient distribution throughout the brain tissue, which would produce different levels of injury. As a common criterion in the literature, the head acceleration is utilized for defining various injury thresholds. It is postulated, however, that the head trauma, such as diffuse brain injury, subdural hematoma, and contusion, is mainly associated with brain tissue parameters such as shear stress rather than head kinematics. The tissue level parameters can, therefore, be accounted for as being a more reliable basis for the evaluation of head injury.

4.1. Impact Modeling

Different impact modeling scenarios have been carried out on the head using impactors of different sizes and velocities. As a benchmark, most of the studies have validated their head model against Nahum's experiment (Nahum et al. 1977) and have used his impact conditions for their study. These numerical works have either used an impactor similar to the one used in Nahum's experiment (Willinger et al. 1999; Zhang et al. 2001b), or have applied Nahum's impact force on the specified region on the head (Ruan et al. 1994) to replicate similar impact conditions. In the study presented here, however, front, back, and side head impacts against a rigid wall were performed. Using identical boundary conditions in all directions, the head impacted the wall with the same velocity of 2.2 m/s. The head was inclined 45 degrees about its

horizontal plane for the front and back impacts and about its sagittal plane for side impact, as shown in Figure 4.1. The velocity of the head was chosen such that the predicted tissue response would approach the injurious tolerance levels proposed by Ward et al. (1980) Zhang et al. (2004) for the coup-countercoup pressure and shear stress, respectively. The impact simulations were carried out using LS-DYNA, a powerful nonlinear explicit FE solver code, for the duration of 10 milliseconds. Due to the short duration of impact in the simulations, the free boundary condition was considered at the inferior surface of the neck. This assumption has been justified by many researchers (Ruan et al. 1994; Willinger et al. 1999; Zhang et al. 2001b). However, to further verify this assumption, the current simulations were replicated using constrained boundary conditions for the neck in all degrees of freedom and as expected, no significant difference were observed. This would assure that the results were not artifacts of the boundary conditions. A rigid wall was considered for all the scenarios in order to provide a more realistic situation of head impact such as the impact of pedestrian/bicyclist against the ground upon fall or traffic accidents. This would provide a different head impact scenario compared to available literature, which may allow for more concise evaluation of head injury risk based on the injury responses of the head and the brain. As mentioned before, due to the geometrical and behavioral differences of the head components, the initial conditions for the head were intrinsically different at each direction. The aforementioned studies and other research works on brain injury have evaluated the ICP and the maximum shear stress inside the brain to assess the risk of injury based on the proposed injury thresholds. However, in current study, besides considering these two parameters as potential injury predictors, the head kinematics, in terms of linear acceleration of the brain, was also assessed to examine any possible correlation among the tissue and kinematic responses of the brain.

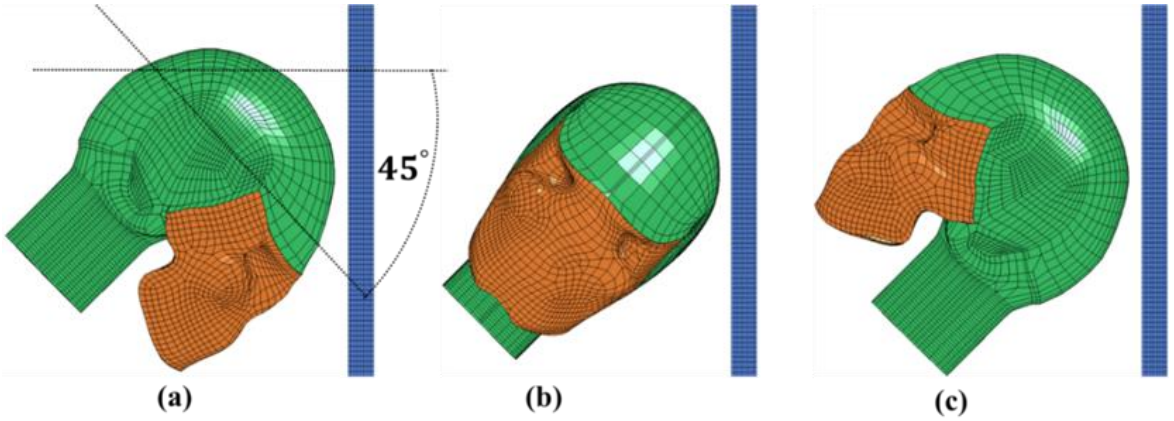

Figure 4.1. Scenarios for the head impact against the rigid wall; front impact; (b) side impact; and (c) back impact

4.2. Results

The tissue responses of the brain in terms of the shear stress and ICP, along with the brain kinematical response in the form of linear acceleration, were evaluated as the main injury predictors in the study presented here. As a major brain injury indicator, Zhang et al. (2004) proposed that when shear stress exceeded a threshold level of 7.8 kPa, there would be a 50% chance of mTBI. However, the peak values for the maximum shear stress in our study were much lower than the proposed tolerance level (around 4 kPa).

Focal brain injuries, such as coup-countercoup injuries and contusion, are believed to result from the ICP profiles inside the cranium. However, diffuse injuries, such as concussion and axon deformations are the outcomes of the tissue deformations under local shear stresses (Ruan et al. 1994; Willinger et al. 1999; Zhang et al. 2001b; Zhang et al. 2004). The brain acceleration is also used as an important parameter in defining injury criteria, such as HIC, and is used in many studies. The ICP, as well as the shear stress distribution, were recorded for all impact scenarios and are presented in the next sections of this paper. Based on the specific impact scenarios performed in this analysis, several results and conclusions were made. It's

worth mentioning that the conclusions provided here are unique to the case studies performed and should be validated through experiments before any general conclusions can be made.

4.2.1. Intracranial Pressure Profile

The temporal evolution of ICP gradients at the coup and countercoup sites were recorded to simply provide a baseline for evaluating the impact related injury based on ICP levels. As shown in Figure 4.2, a peak overpressure of 236 kPa was observed at the coup site while the peak negative pressure at the countercoup site was found to be -196 kPa for the frontal impact. Coup and countercoup pressures were seen to reach their extremes at about the same time. Furthermore, these pressures showed a nearly symmetric behavior due to the symmetric nature of the model. To better visualize the pressure wave distribution inside the brain caused by the focal impact mechanism, the spatial variation of ICP profile inside the brain was obtained, as shown in Figure 4.2 for the front impact at 2.4 ms. The continuous variation of pressure across the mid-sagittal plane clearly delineated five distinct pressure levels at different lesions of the brain with the maximum and minimum being at the coup and countercoup sites, respectively. The corpus callosum and the brain stem also showed peak pressure values of 175 kPa and 50 kPa, respectively.

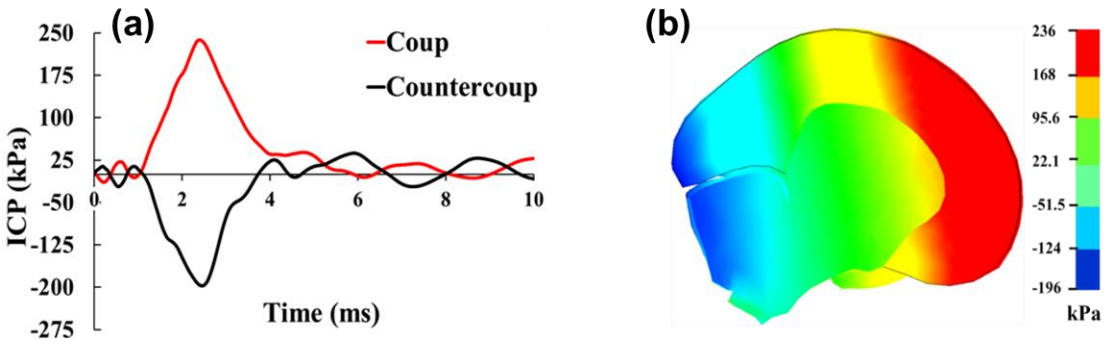

Figure 4.2. (a) Time history of coup-countercoup pressure for the front impact; (b) ICP profiles inside the brain at 2.4 ms for the front impact scenario showing five distinct pressure regions with maximum and minimum at coup and countercoup, respectively

The coup-countercoup pressure time histories along with the developed pressure gradients inside the brain are shown in Figure 4.3 for the side impact. As the temporal lobe was mainly assaulted in the side impact scenario, the maximum coup pressure was experienced by the brain in the right lobe close to the temporoparietal lesion. Similar to the front impact, the peak values for the coup and countercoup pressures were observed at the same time and were nearly symmetric. The peak positive (228 kPa) and negative (-186 kPa) pressure values for the side impact, which was obtained at the coup and countercoup sites, respectively, didn't show a significant difference from the ones observed for the front impact. These pressures were slightly lower than the predicted ICP levels for the front impact. The pressure wave distribution throughout the brain clearly indicated the development of three distinct regions with two transition regions (yellow and light below regions). The continuity of this pressure wave propagation was disrupted in the middle where it was interrupted by the falx. The pressure profiles were observed to for at the left temporal lobe, where it had its maximum value, and moved toward the right temporal lobe where the minimum occurred.

Next, the ICP gradients and the temporal evolution of coup-countercoup pressure for the back impact are presented in Figure 4.4. The maximum positive (221 kPa) and negative (-131 kpa) pressures were again observed at coup and counter coup sites, respectively. The peak positive and negative pressures in the back impact decreased by 6.3% and 33.2 % with respect to their counterparts in the front impact. The maximum pressure values at the coup and countercoup sites occurred around the same time. The higher coup pressure observed in the front impact, with respect to the back impact, can pertain to the fact that the occipital region of the head has a larger radius of curvature compared to the frontal region. Moreover, the bone stiffness is higher in the

frontal area and this would result in a higher stress level in the front region when subjected to a dynamic load such as a blunt impact.

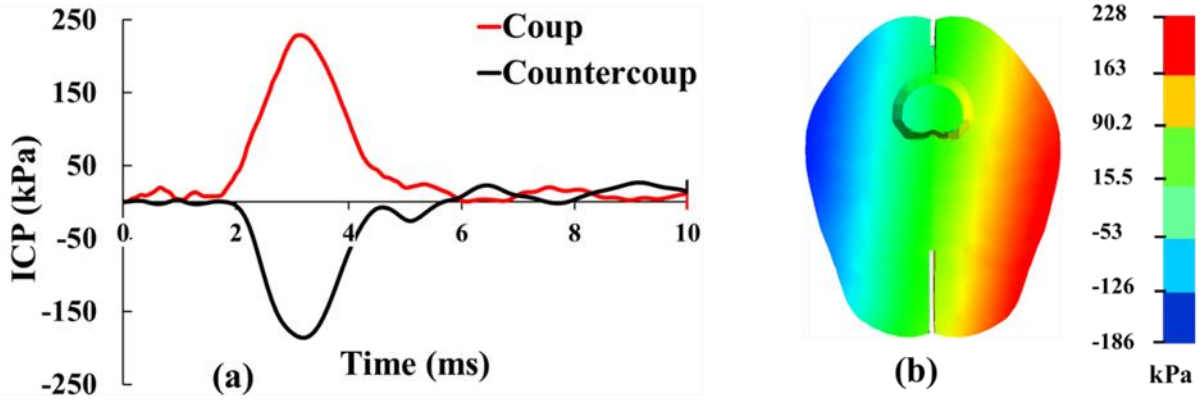

Figure 4.3. ICP response for the side impact: (a) time history of coup-countercoup pressure; (b) pressure profiles developed in different lesions of the brain

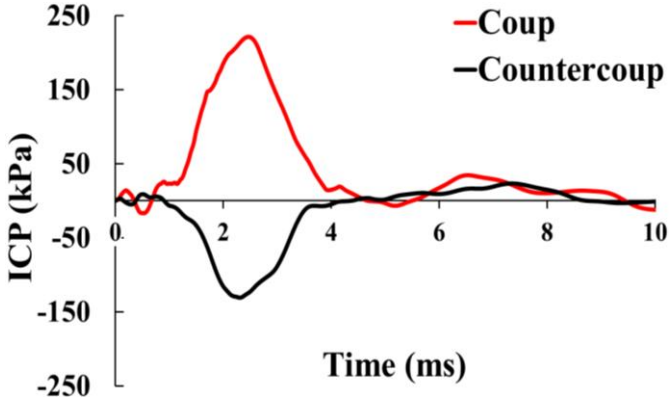

Figure 4.4. Time history of coup-countercoup pressure for the back impact

4.2.2. Shear Stress Distribution

The maximum shear stress time history for all impact scenarios at the brain stem are shown and compared in Figure 4.5. As reported in different studies (Ruan et al. 1994; Willinger et al. 1999; Zhang et al. 2001b; Zhang et al. 2004), the corpus callosum and the brain stem are the regions that are highly susceptible to high shear stresses and therefore, undergo shear deformations when subjected to dynamic loads. Accordingly, the distribution of the local stresses was monitored inside these two regions but the results are only provided for the brain stem where the maximum values were observed. The comparison between the maximum shear stresses in

Figure 4.5 revealed that while the pressure level in the back impact was not much different from the pressure levels in the front and side impacts, the shear stress peak value in the back impact was about 22% less than the ones predicted in the other impact scenarios. However, like the ICP levels in the front and side impacts which showed very similar values, the shear stresses were nearly the same for these two directions. The maximum shear stress for the front, side, and back impacts were 6.9 kPa, 7.2 kPa, and 5.5 kPa.

The shear stress development and distribution inside the brain at different lesions, such as the midbrain, corpus callosum, thalamus, and the brain stem, is shown for all impact scenarios in Figure 4.6. It can be easily seen that, as mentioned before, the maximum shear stress was observed at the brain stem for all three impacts. Figure 4.6 also vividly depicts the difference in stress wave propagation based on the location of impact and therefore, imposing the brain to different levels of severity.

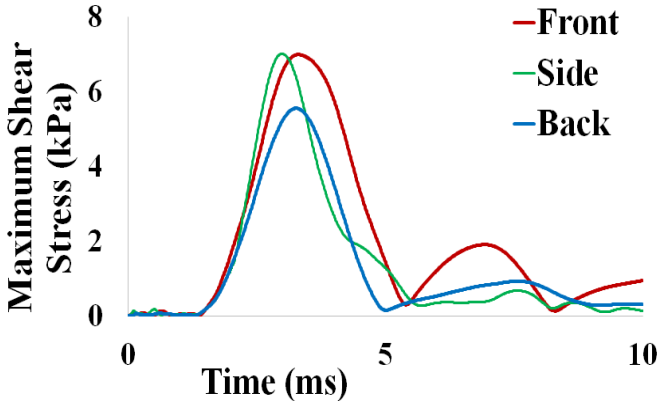

Figure 4.5. Time history of average maximum shear stress distribution in the brain stem for all impact scenarios: comparison of shear stress response for front, back, and side impacts

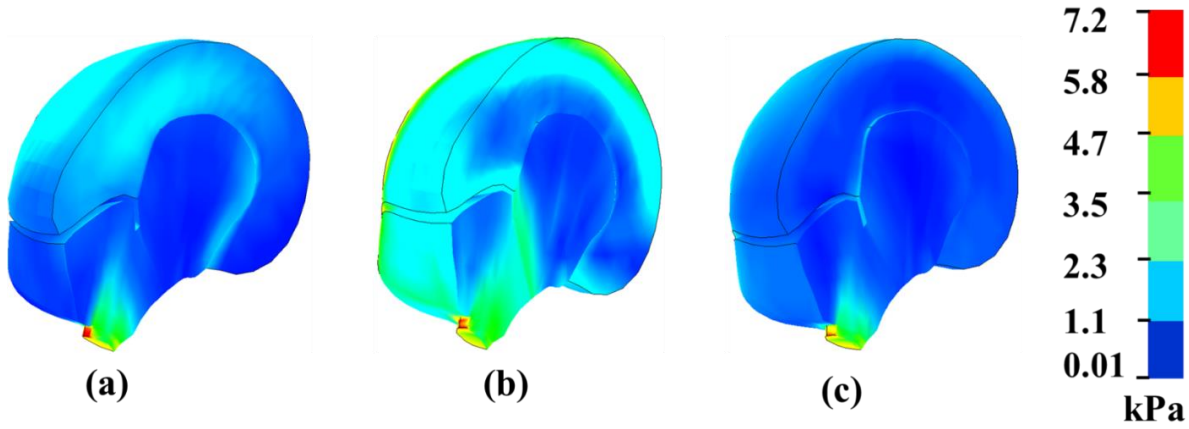

Figure 4.6. Local shear stress distribution at different lesions of the brain for (a) front; (b) side; and (c) back impacts at t = 4.1 ms

4.2.3. Brain Acceleration

The resultant linear brain center mass acceleration was evaluated in all simulations. This was performed, particularly, to examine the relationship between the head kinematic and the tissue response. The brain accelerations were found to be 268 g, 293g, and 276g in the front, side, and back impact scenarios, respectively. It was observed that while at the tissue level, the responses predicted in the back impact were less than the tissue parameters in the front and side impacts, the peak value of linear acceleration was the least for the front impact. As shown in Figure 4.7, all accelerations followed a similar pattern. The complexity of the head geometry was assumed to be the main reason for the difference in peak acceleration values.

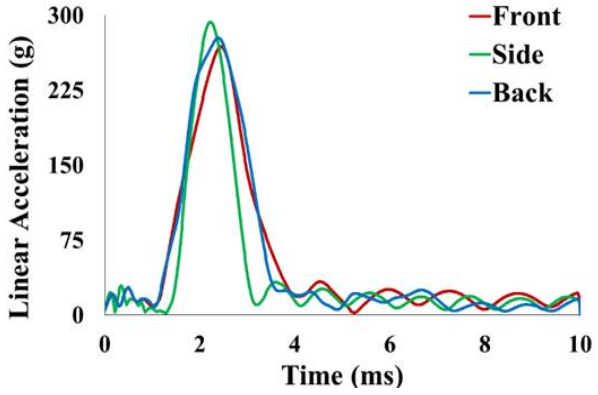

Figure 4.7. Comparison of brain acceleration in front, back, and side impacts

4.3. Discussion

A detailed FE head model was used in this study to investigate the brain injury level when the head impacts a rigid body such as the wall from different directions. It is known that the structural complexity, material inhomogeneity, and the variable tolerance limits of head components can affect the head response at tissue and kinematical levels. To this end, impact of our validated head model against the rigid wall in front, back, and side directions were performed. The tissue parameters, such as ICP and shear stress, as well as the kinematical parameters, such as the brain linear center mass acceleration, were recorded for all of the scenarios. It was observed that while tissue responses of the brain in front and side impact were quite similar in terms of coup-countercoup ICPs and the shear stress, the brain acceleration for the front impact was 8.5% less than the one predicted for the side impact. On the other hand, while it was asserted that the back impact conditions were to be the safest in terms of shear stress and coup-countercoup pressures, the predicted brain acceleration in the back scenario was nearly 5% more than what was predicted for the front impact. This brings to question the evaluating measures based only on the head, or brain kinematics. The impact directions were the same as the ones used in the work of Ruan et al. (1994) and also as the front and side impacts used in the work of Zhang et al. (2001b). It should be mentioned that these works used impactors for modeling their impact, while in our the study the head was impacted against a rigid wall and the head velocity was chosen so that it reached the critical injurious conditions based on the available injury threshold in the literature. The predicted coup-counter coup pressure gradients, as well as the shear stress in the front and side impacts, were higher than those recorded in the back impact. This finding is in good agreement with the computational results of Ruan et al. (1994). Referring to clinical observations, they asserted that the probability of countercoup injury

in back impacts is higher than other impact directions due to higher negative countercoup pressure. Their simulations also predicted the highest countercoup pressure in the occipital impact, while in our study, the lowest countercoup injury was observed for the back impact. However, it should be noted that the differences in the FE head models, mesh refinement, exact impact location, and the impact force are crucial parameters which can significantly affect the results. In all impact scenarios, the compressive (positive) and tensile (negative) peak pressures were observed at the coup and countercoup regions, respectively, and occurred at about the same time. All the pressures were found to follow a similar pattern and nearly symmetrical behaviors were observed for the pressure histories in the front and side impacts. This finding was in good agreement with the computational results of Ruan et al. (1994). However, it was opposite to the finding of Zhang et al. (2001b) for the side impact in which they observed a lag between the peak coup and countercoup pressures. They declared that the increase of absorbed impact energy of the soft tissues due to the structural loading of the outer shell under a dynamic load, can contribute to such a lag. They also reported higher tissue response for the brain in the side impact in comparison to the front impact. Although in our findings, the results in front and side impacts were quite similar, but still the front impact, predicted higher peak values in terms of coup-counter coup pressure, as well as the maximum shear stress.

According to the injury threshold proposed by Ward et al. (1980), a 234 kPa coup pressure and a -86 kPa countercoup pressure are perceived as the tolerance level for serious brain injuries such as contusion. Based on the results obtained for the cases analyzed in the current work, the front impact can place the brain at the 100% risk of coup and countercoup injuries as it produces ICP levels as high as 236 kPa at the coup site and -196 at the countercoup site. However, for side and back impacts, the peak estimated value was lower than the threshold even

though the chance of coup injury was very high. However, based on Ward's threshold, the countercoup injury would happen in all scenarios.

Based on the studies performed on animal tissues, and also using numerical simulations, it has been postulated that diffuse brain injury is a main outcome of shear deformation of brain axons and that the brain stem and corpus callosum are the regions that are most prone to diffuse injuries (Adams et al. 1982; Margulies and Thibault 1992).Zhang et al. (2004) proposed a tolerance level for 50% probability of mild TBI based on the shear stress. They suggested the threshold value as 7.8 kPa. Comparing the results in all impact directions, it was found that the directionality of impact significantly altered the impact response of the head in the back impact scenario. Increased tolerance to both focal and diffuse injuries was observed for the back impact while the brain showed a decreased tolerance to diffuse injuries in the front impact. Although the peak value of shear stress in the front (7.2 kPa) and side impacts (6.9 kPa) was lower than the proposed injury threshold, it was postulated that they can still have significant damage to the brain axonal tissues. Based on results from the study presented here, it was concluded that the front and side impacts would impose more severe diffuse injuries. This finding is, to some extent, in agreement with the computational results of Zhang et al. (2001b) as they reported a decreased tolerance level to concussive injuries in the lateral direction in comparison to frontal and lateral impacts. They also reported decreased tolerance level in the lateral direction.

Based on the brain kinematical data, it was observed that for the cases considered, there wasn't an essential correlation between the kinematical and tissue level responses. The numerical results for the study presented here revealed that while the tissue level parameters were lowest for the back impact, (221 kPa coup pressure, -131 kPa countercoup pressure and a maximum shear stress of 5.5 kPa), the brain acceleration was higher than that of the front impact.

4.4. Conclusion

A parametric analysis was performed to reveal the effect of impact directionality on the response of the human head at the tissue and kinematical levels. The main idea was to investigate the directional dependence of the mechanical response of the head and to examine the correlational behavior of tissue and kinematic responses. The FE head model for the study presented here was validated against the experimental results of Nahum et al. (1977). As a more realistic impact scenario, the head was impacted against a rigid wall in front, back and side directions at a velocity of 2.2 m/s to produce the injurious conditions. The anatomical plane of the head was inclined at 45 degrees. Based on the specific results obtained for the case studies performed in this research, It was found that while the predicted tissue responses in the front and side impacts were quite close, the brain response to the back impact was significantly lower than those predicted in other scenarios, especially in terms of the shear stress. The highest brain acceleration was observed for the front impact signifying that the front impact is counted as the most severe case of head impact. The directional dependence of the head response was confirmed as it was observed that for the back impact, the head was less prone to severe injuries, while front and side impacts predicted severe injury conditions. The head showed increased tolerance to the diffuse injuries in the back impact while decreased tolerance to diffuse axonal injury (DAI) was observed for both front and side impacts. The maximum shear stress was predicted in the brain stem in all three impact conditions. The coup-countercoup pressure, shear stresses, and brain accelerations followed similar patterns for all impact scenarios. It was concluded that the biomechanics of the head impact can be altered by many parameters such as the impact velocity, the location of impact and the geometry of the head. Moreover, it is believed that due to the complicated behavior of the human head under dynamic loads, the tissue level

parameters serve as more reliable predictors in defining the injury criteria. The authors of the study presented here believe that the findings of such studies could help the future design of the protective headgears. The authors would suggest further validation of the current head model against experimental shear stress/strain data available in the literature, to provide more confident results. Future studies are required, however, for defining a new injury threshold based on the tissue response of the head. The research presented here can be further employed to study the effect of impact directionality upon accurate modeling of the human neck. This research is also an emphasis on the fact that based on different head models used in the literature, different conclusions can be made for similar boundary conditions. Hence, the future studies should vitally employ several accurate FE human head models to verify the concluding results. Also, this work is among the first researches mentioning the need for correlative analysis of human head response in terms of tissue and kinematic responses.

CHAPTER 5. EXAMINATION OF THE PROTECTIVE ROLES OF HELMET/FACESHIELD AND DIRECTIONALITY FOR HUMAN HEAD UNDER BLAST

To account for the blast directionality effects on the response of the brain, interaction of the human head with blast-induced shockwaves approaching from the front, back, top, and bottom sides were simulated (Figure 5.1). Moreover, a major part of the study was devoted to examine the protective effect of the helmet and faceshield on the mitigation of brain injury risk with respect to the blast orientation. Accordingly, the three protection levels, (unprotected head, helmeted head, and 3) explained in section 3.3.3 were exposed to blast loading (Figure 3.7).

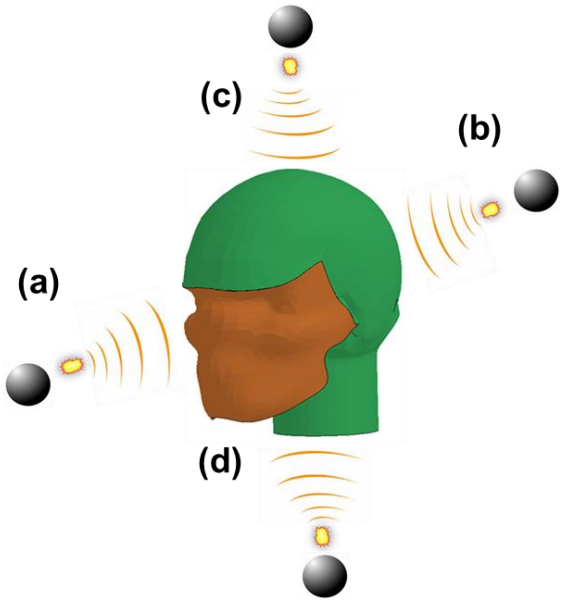

Figure 5.1. Different blast scenarios used for the study: (a) Front; (b) Back; (c) Top; and (d) Bottom blasts

All surfaces of the media, except for the ambient surface facing the detonation, were modeled as non-reflecting boundaries to allow for the outflow of the propagating shockwaves in an open space blast scenario. Jazi et al. (2013a) studied the effect of three different boundary conditions, fixed neck, free neck, and neck attached to the body on the brain response in front and back blasts, and found no difference between the tissue responses in the first 5 milliseconds.

The reason is that due the very short duration of blast the relative motion of the head doesn't transfer to neck in the first few milliseconds. Hence it was concluded that using either fixed or free boundary conditions doesn't impact the brain response significantly.

To ensure the stated assumption, however, the simulations were performed using both boundary conditions and no difference was observed in the brain tissue responses. Accordingly, a fixed boundary condition was chosen and the inferior surface of the neck was constrained in all degrees of freedom. The discretized ALE media enveloping the Lagrangian components, as well as the time history of blast overpressure around the head, are shown in Figure 5.2. The Lagrangian parts, head-helmet-faceshield assembly, was inserted into a Eulerian domain represented by a 50×50×50 cm cubic domain in which the air flow and the propagating blast waves were included. For more details readers can refer to sections 3.3.1 and 3.3.2.

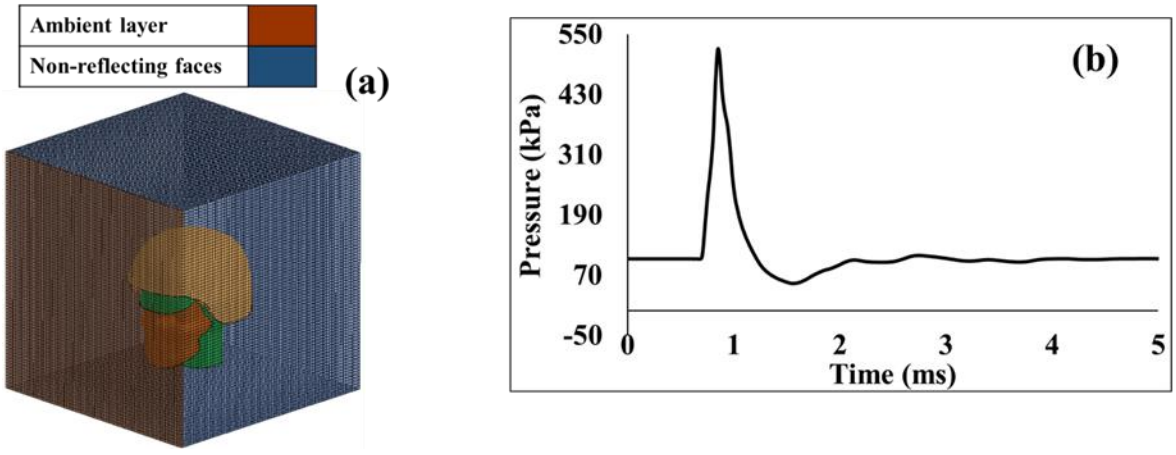

Figure 5.2. (a) ALE media and the boundary conditions; (b) Time history of the shockwave generated around the head

5.1. The Effect of Blast Direction on the Mechanical Response of the Head

5.1.1. Tissue Response of the Brain

The peak maximum pressure at coup and countercoup sites of the head are compared for all four blast scenarios in Figure 5.3(a). Based on the results, the back blast predicted the highest peak coup (650 kPa) and countercoup (-256 kPa) pressures. While the front blast predicted the lowest coup pressure (325 kPa), however, the brain sustained the lowest countercoup pressure in the bottom scenario (-150 kPa). The difference in brain response to the incoming shockwaves approaching from the different directions revealed the directional dependence of the brain tolerance to dynamic loads. In terms of the coup pressure, top (622 kPa) and bottom (538) blasts also predicted pretty high peak values. With respect to the back blast, coup pressure decreased by100%, 4.3 % and 17.2 % and the countercoup pressure decreased 9.4%, 30.4%, and 41.5%, in front, top, and bottom blast scenarios, respectively.

Figure 5.3(b) compares the average maximum shear stress at different lesions of the brain that are more prone to injury, namely the corpus callosum and the brainstem (Figure 5.4) in all four blast scenarios. The peak values of shear stresses in both the brainstem (6.39 kPa) and the corpus callosum (1.7 kPa) were predicted for the bottom blast. The predicted shear stress values in the brainstem for the back, front, and top blast scenarios were 27.3%, 30.7%, and 35% less than that obtained in the bottom blast.

Figure 5.3(c) compares the peak values of average maximum principal strains at the corpus callosum and brainstem regions when the unprotected head was exposed to blast from different directions. The bottom and front blasts predicted the highest and lowest strain levels at brain stem (0.038 and 0.025) and corpus callosum (0.01 and 0.005), respectively. The level of evaluated strains in the corpus callosum was in the range of 0.005-0.006 in all other directions,

which was an order of magnitude less than the values obtained in the brain stem at the same directions. Accordingly, based on the current results, the brain stem was realized as the region dictating the injury upon a blast insult. In terms of the blast directionality, it was observed that with respect to the bottom blast, strain reduced by 34.2% in the front, 21% in the back, and 31.5% in the top blasts.

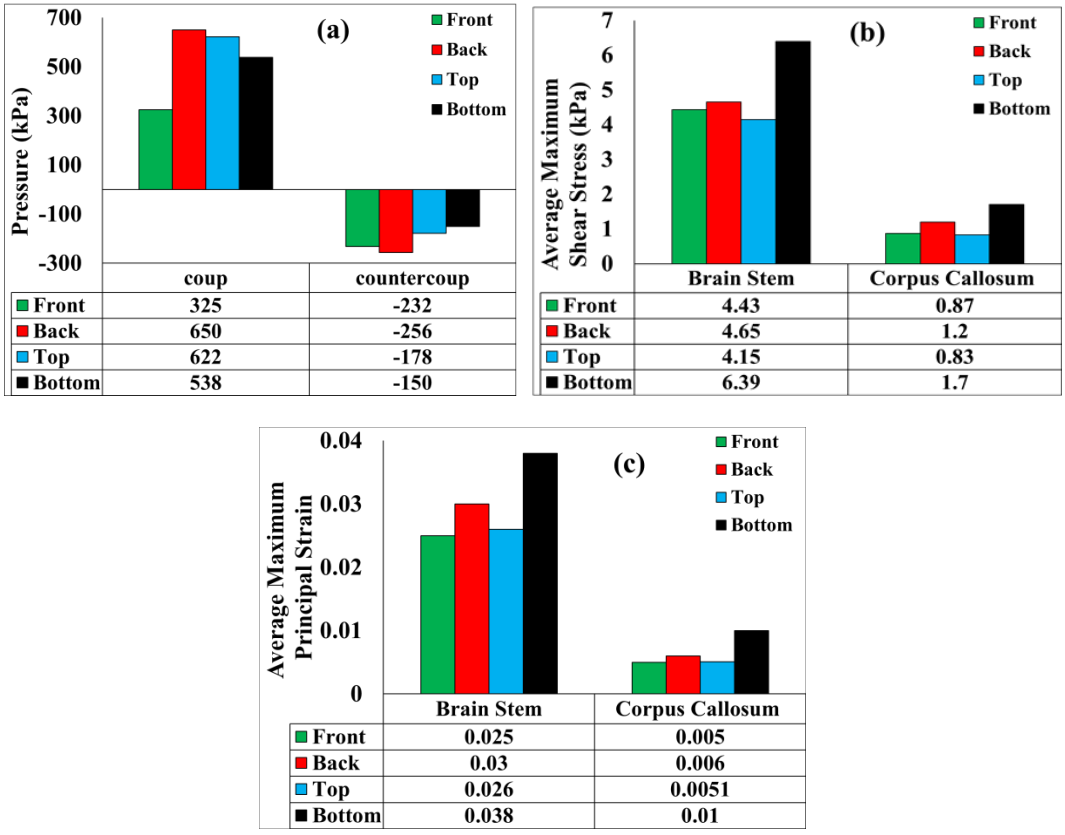

	coup	countercoup
Front	325	-232
Back	650	-256
Top	622	-178
Bottom	538	-150

	Brain Stem	Corpus Callosum
Front	4.43	0.87
Back	4.65	1.2
Top	4.15	0.83
Bottom	6.39	1.7

	Brain Stem	Corpus Callosum
Front	0.025	0.005
Back	0.03	0.006
Top	0.026	0.0051
Bottom	0.038	0.01

Figure 5.3. Comparison of the peak values of (a) coup-countercoup pressures, (b) shear stress and (c) principal strain for the unprotected head in different blast directions

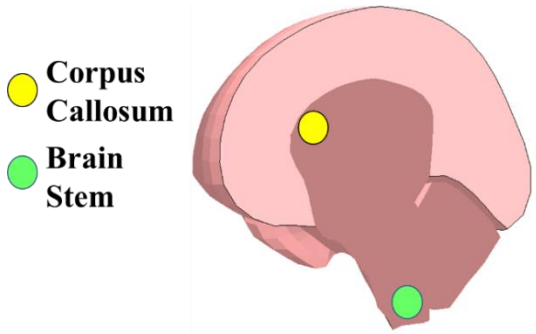

Figure 5.4. Locations where maximum shear stress was recorded inside the brain

To show the variation of ICP and maximum shear stress with time, the time traces were recorded at the coup and brainstem, respectively (Figure 5.5). The significant peaks (both negative and positive), following the major overpressure peaks, were correlated to angular and linear motions of brain inside the cranium. Development and evolution of these pressure profiles inside the brain are shown in Figure 5.6. Based on the location of blast wave impingement on the head (left column), the frontal, occipital, parietal and temporal lobes of the brain sustained the highest ICP level for the front, back, top, and bottom blasts, respectively.

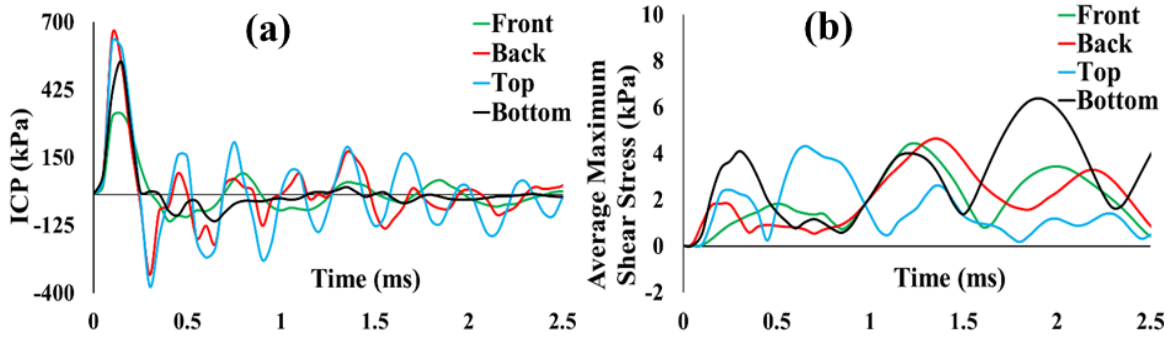

Figure 5.5. Temporal evolution of (a) ICP at the coup site and (b) maximum shear stress in the brain stem

5.1.2. Kinematic Response of the Brain

The temporal variation of the brain's kinematic response, in terms of the resultant center mass linear acceleration, are compared in Figure 5.7 for all blast directions. The highest linear acceleration was predicted in the top blast (366g) and decreased by 14.7%, 35.7% and 50.3% in the back, bottom, and front scenarios, respectively.

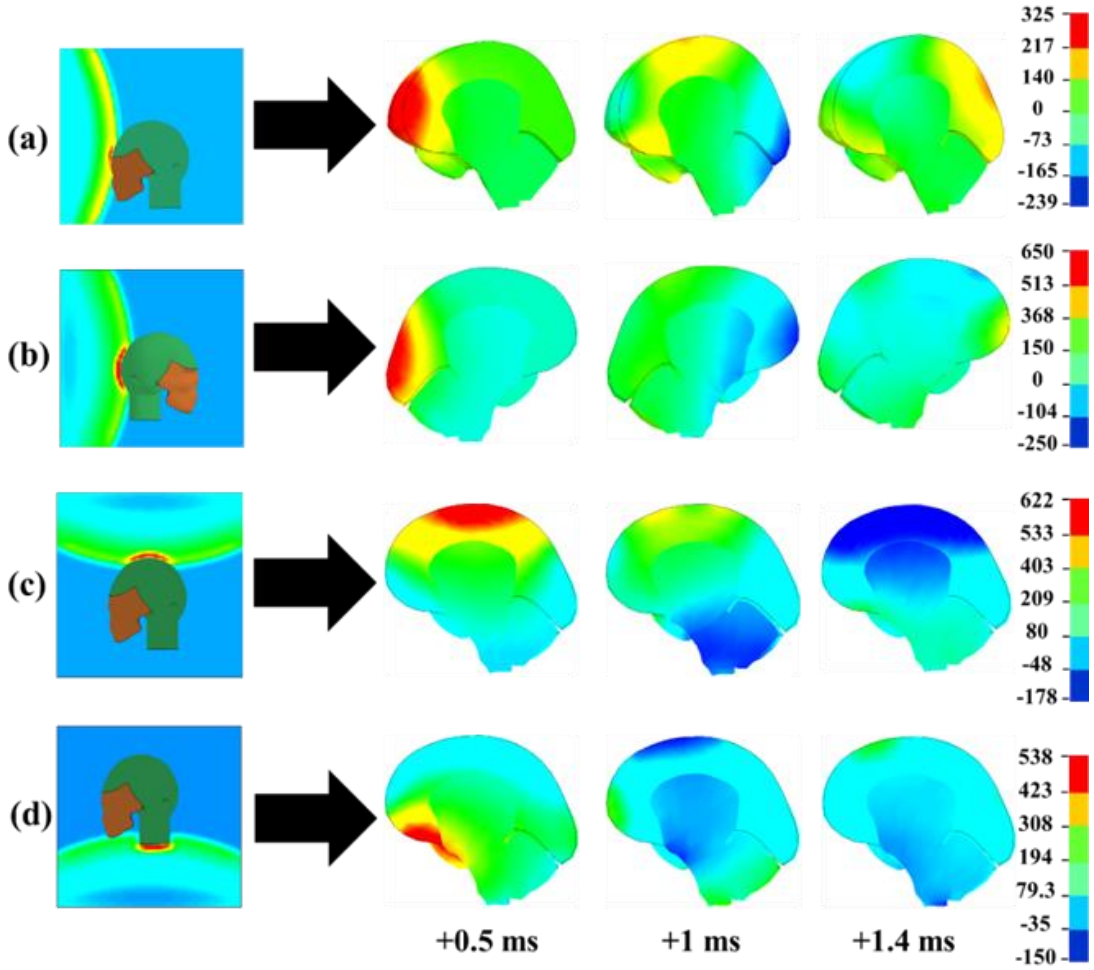

Figure 5.6. Evolution of pressure profiles (kPa) at different lesions of the brain for (a) front, (b) back, (c) top, and (d) bottom blasts at several distinct times after the impingement of blast waves on the head

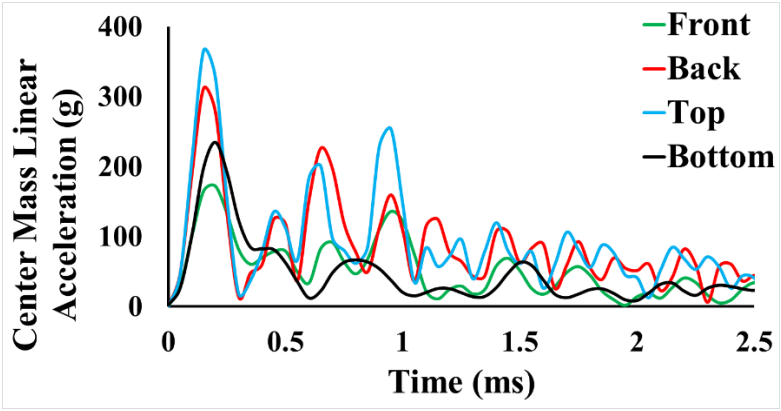

Figure 5.7. Time history of brain center mass linear acceleration for different blast directions

5.2. The Effect of Protective Headgears on the Directional Response of Head

5.2.1. Tissue Response of the Brain

Figure 5.8 highlights the effect of the helmet and the helmet-faceshield systems on the mitigation of coup-countercoup ICP in the blast scenarios studied here. It should be noted that all the reduction and increase percentages provided in this section are evaluated with respect to the unprotected head. In the front blast, it was observed that the fully-protected system reduced the peak coup ICP by 76.7 % which was more than twice the reduction achieved through helmeted system (31%). While the helmeted system showed better protection capability in terms of the countercoup ICP (46.8% reduction), however, the fully-protected system had a similar mitigation efficiency (74.1%). The faceshield did not affect the pressure response of the brain in the other three directions. Due to the maximum coverage area by the helmet-faceshield assembly, the fully-protected system predicted the highest percentage reduction in coup and countercoup ICP peak values for the top (83.1%) and front (74.1%) blasts, respectively. For the back blast, identical results were obtained upon using both protection assemblies, (i.e., 58.5% and 54.6% percentage reduction in coup and countercoup pressures was observed, respectively). However, the bottom scenario showed completely different results as both protection systems had adverse effects and increased the coup-countercoup ICPs.

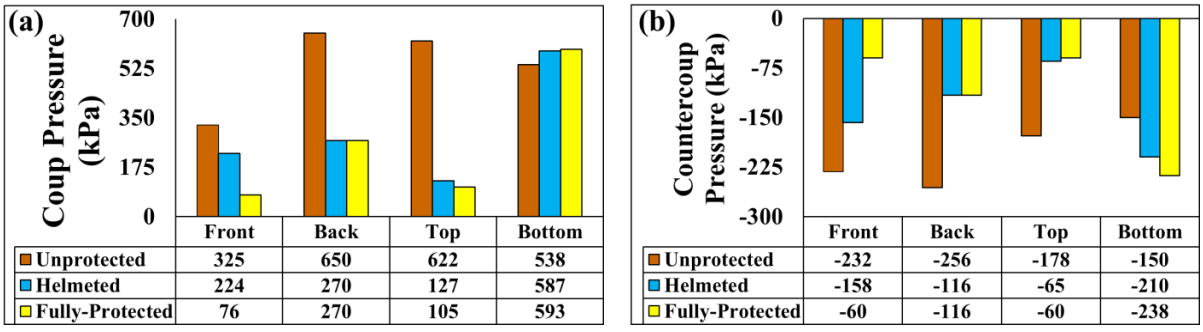

	Front	Back	Top	Bottom
Unprotected	325	650	622	538
Helmeted	224	270	127	587
Fully-Protected	76	270	105	593

	Front	Back	Top	Bottom
Unprotected	-232	-256	-178	-150
Helmeted	-158	-116	-65	-210
Fully-Protected	-60	-116	-60	-238

Figure 5.8. Comparison of (a) coup and (b) countercoup peak pressures in different blast directions for unprotected, helmeted, and fully-protected head models

The peak average maximum deviatoric stresses, developed inside the brain due to the hyper- viscoelasticity of the brain tissue, were observed to occur in the brain stem for all cases. Figure 5.9(a) illustrates the comparison of the peak shear stress values in the brain stem for different protection systems with respect to the blast direction. It was observed that in situations where most of the shockwaves were impeded by either of the protective tools, the peak shear stress decreased. This was confirmed by the 14.2% reduction of shear stress in the front blast by using a fully-protected system against the increasing effect of the helmeted system (11%). Likewise, in the top blast scenario, where nearly perfect protection was provided by both protection systems, the shear stress peak value decreased by 11.8% and 14.4% for helmeted and fully-protected systems, respectively. In other blast scenarios, peak shear stress mostly showed an increasing trend upon using the protective headgear.

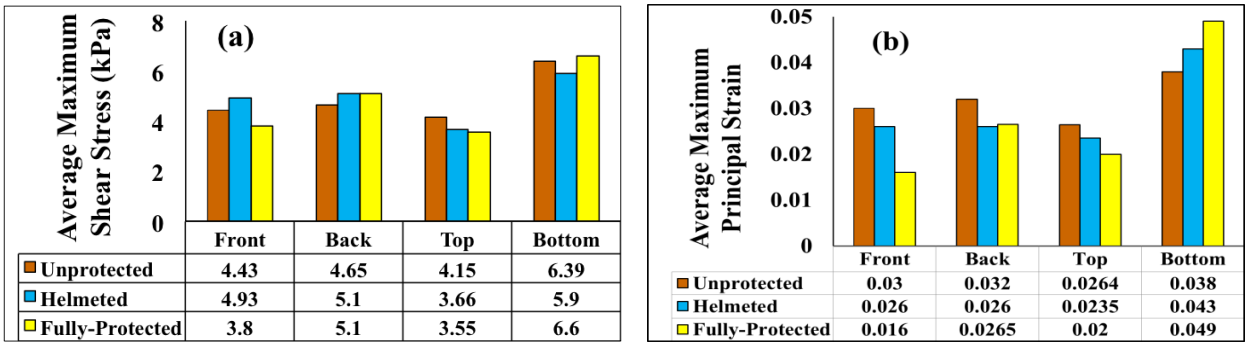

Figure 5.9. Comparison of the peak values of (a) shear stress and (b) principal strain in the brain stem in different blast directions for unprotected, helmeted, and fully-protected head models

In our directionality study presented in section 5.1, the brain stem was recognized as lesion of brain being most prone to injury under blast (Figure 5.3(c)). Hence, as shown in Figure 5.9 (b), in the protection capability study, only the peak values of principal strains in the brain stem were evaluated and compared. As expected, the fully protected system provided the highest protection efficiency (46.6% reduction) when employed in the front blast, compared to the helmeted system (13.4%). On the contrary, the fully protected assembly showed quite

adverse effects in the bottom blast (28.9% increase) while the helmeted system had less unfavorable effects (13.4% increase). In the back blast scenario, however, both helmeted and fully protected systems offered around 20% reduction in the principal strain. In the top blast, although the fully protected system showed to be more effective (20.5 % reduction) with respect to the helmeted system (11.9% reduction), but it wasn't significant.

5.2.2. Kinematic Response of the Brain

The highest mitigation efficiency was predicted by the fully-protected system in the front blast (79.6%) in terms of the center mass linear acceleration (Figure 5.10). Likewise, this protective configuration decreased the acceleration by 78.4% in the top scenario. In the back scenario, however, the helmeted system (75.9%) had a little more effect in reducing brain acceleration when compared to the fully-protected model (72.6%). Adversely, the protection assemblies increased the acceleration in the back blast (1.7% and 6.3% for helmeted and fully-protected, respectively).

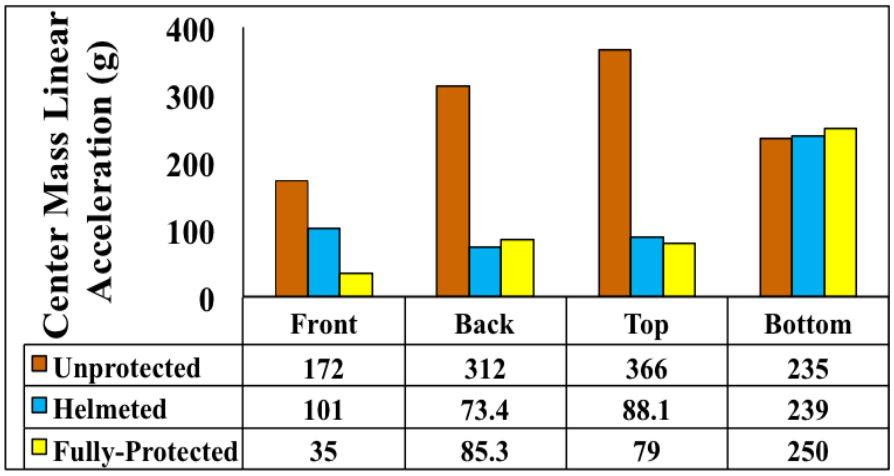

	Front	Back	Top	Bottom
Unprotected	172	312	366	235
Helmeted	101	73.4	88.1	239
Fully-Protected	35	85.3	79	250

Figure 5.10. Comparison of the peak values of brain center mass linear acceleration in different blast directions for unprotected, helmeted, and fully-protected head models

Figure 5.11 depicts the mitigation efficiency of the protection systems used in this study with respect to the orientation of the blast. The attenuation of transferred pressure waves into the brain can be vividly observed in row (a) for the front blast. Moreover, the elevated pressure region on the facial region is observed for the back and bottom blasts due to the reflection of entrapped blast waves inside the helmet and faceshield gap.

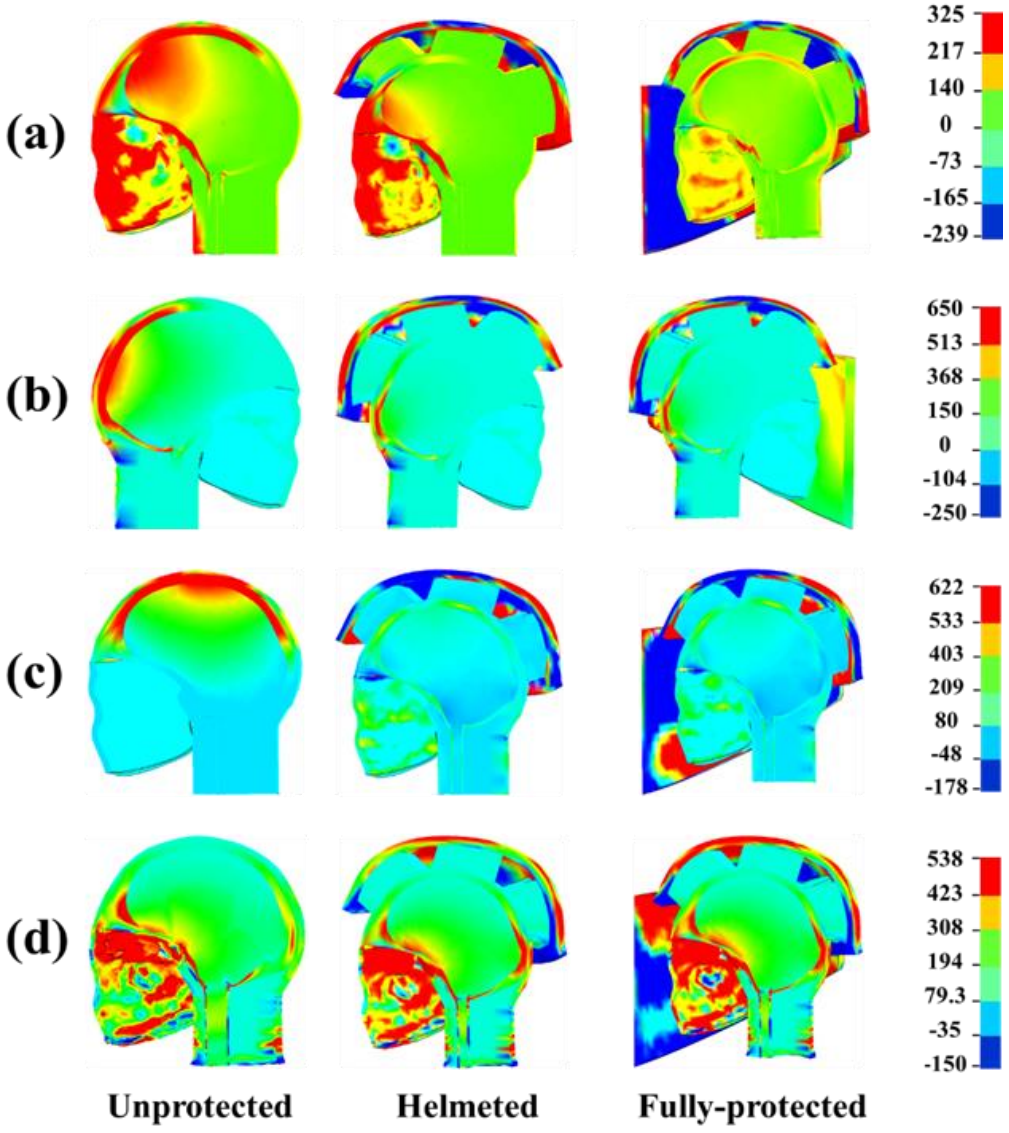

Figure 5.11. Blast mitigation capability of helmet and face shield with respect to shockwave direction at 0.5 ms after the head-blast wave interaction for (a) front; (b) back; (c) top; and (d) bottom blasts

5.3. Discussion

The directional response of the brain was observed in this study in terms of both tissue and kinematic responses. These observations are believed to greatly influence the study of different blast induced TBI mechanisms. While focal injuries are mainly correlated with peak ICP level and skull deformations, shear damages are responsible for diffuse injuries (Zhang et al. 2004). One interesting finding of the study presented here was that the two measured tissue responses in each direction were not essentially correlated, (i.e. while the back blast imposed the highest peak coup-countercoup ICP, the bottom blast predicted the peak maximum shear stress). This revealed that based on the direction of the assault to the head, the tolerance of the brain to focal and diffuse injuries may differ in terms of individual dynamic responses. This was in agreement with the results of Taylor and Ford (2009). The maximum shear stress which occurred inside the brain stem after the transition of the primary shockwave through the head, was mainly induced upon the rippling of the skull instead of the relative movement of the head, as asserted by Moss et al. (2009) and Taylor and Ford (2009). However, the relative motion of the brain inside the cranium cavity with respect to the skull contributed to the development of coup-countercoup ICP gradients. An important finding of the current directionality case study was that the kinematical responses couldn't be used as the sole injury indicator to predict the injury risk, as it indicated that the tissue level responses showed to played much important role in imposing the brain injury risk.

The directionality considerations can relate to the variable performance of PPE under impact and blast conditions. In our study, the use of personal protective equipment (PPE) showed the highest mitigation efficiency for the front blast. This was mainly due to the fact that the faceshield inhibited the direct impingement of the shockwaves on the head and hindered the

propagation of blast pressure waves inside the intracranial space through the two major pathways: the head and the face. Upon utilizing a faceshield, the approaching shock waves were diffracted around the head and hence the direct impingement of waves on the head was prevented. In terms of local shear stresses, the PPE showed adverse effects and increased the shear stress level in most directions. One possible reason could be the increase in mechanical loads on the head due to a stronger coupling between the head and helmet in the presence of the padding, as was also stated by Moss et al. (2009). Furthermore, the underwash effect of the helmet, developed upon the alteration of the blast flow inside the helmet gap, induced an amplified pressure region in the helmet subspace leading to increased pressure loading on the head, which confirmed the computational conclusions of Ganpule et al. (2012). These two incidents were believed to cause amplification of the stress wave inside the cranial space and to increase the stress level in the brain stem. In terms of the head kinematics, it was concluded that in all blast scenarios, except for the bottom blast, the enhanced surface area of the blast wave incidence counteracted the elevated inertial forces due to the added mass of both helmet and faceshield and resulted in a remarkable attenuation of the brain acceleration. However, it was postulated that for the bottom blast, the trapped turbulent shock in the head-faceshield gap applied a sudden displacement on the head, pushed the faceshield and helmet, and resulted in an increase in the brain acceleration. The results showed that adding a faceshield to the helmeted protection system was only effective in front blast situations, as it had either adverse or no effects in other directions. Based on these results, it was postulated that the employment of faceshield in the protection system should be further studied, especially with the consideration of blast directionality effects.

Several injury thresholds have been proposed in the literature based on brain tissue and kinematic responses. Ward et al. (1980) proposed an injury threshold based on the coup ICP (234 kPa) while (Zhang et al. 2004) proposed 80% mild TBI injury threshold based on the shear stress (10 kPa) and linear acceleration (106g), as well as an injury threshold of -76 kPa based on the countercoup ICP. If the aforementioned criteria can provide a tolerance level for the diffuse and focal injuries, the pressure results from the study presented here predicted 100% focal (coup-countercoup and contusion) injury risk in all blast scenarios for the unprotected head, with the front blast imposing the highest injury risk. Based on Zhang's criterion, the shear stress peak values predicted no injury risk in any direction in terms of 80% probability of mTBI. The bottom and top blasts, however, showed the lowest and highest tolerance to the diffuse injury. Except for the bottom blast where PPE showed an adverse effect and increased the ICP levels, the evaluated tissue responses were predicted to be either much lower or comparable to the injury thresholds in other directions. While the predicted peak linear accelerations for the unprotected head, in all directions, exceeded the proposed brain tolerance level (106 g), the PPE effectively reduced the acceleration to below the 80% mTBI threshold, except for the bottom blast.

It was observed that while the variation of the peak values of the ICPs and principal strains showed similar trends with respect to the directionality and protection level, the shear stresses didn't show such behavior. In other words, it was observed in Figure 5.8(a) that upon increasing the protection level (helmeted and then fully protected), the ICP levels at the coup site started to decrease for the front blast and increased in the bottom blast. Likewise, the same behavior was observed in the variation of principal strain peak values (Figure 5.9(b)).

5.4. Conclusion

A parametric study was carried out to examine the effect of blast directionality on the mechanical response of the brain, as well as evaluate the protection capability of protective head/facial gears (helmet and faceshield) in different blast scenarios. The generation, propagation, and interaction of blast waves with our unprotected, helmeted, and fully protected heads were successfully simulated for 10 ms in front, back, top, and bottom blast scenarios using an integrated arbitrary Lagrangian Eulerian method in conjunction with a penalty-based algorithm. The tissue level parameters (ICP, shear stress), as well as the kinematic response (linear center mass acceleration) were monitored for all cases. Based on the results obtained in the study presented here, it was concluded that due to the differences in geometry, function and tolerance of various brain components, directionality effects of blast played an important role in defining the brain response under impulsive loading. The protective headgears showed different mitigation capabilities based on the blast orientation. The fully-protected and helmeted systems were shown to be most efficient in front and top blasts, respectively. This was due to impediment of most of the shockwaves. The tissue response of the head was altered upon using the PPE and the bottom blast was found to impose the most severe conditions in terms of transferred mechanical loads to the head. Based on current results, it was determined that the faceshield was only effective in front blast, as it imposed either adverse or no effects in other directions. The current findings suggested the need for incorporating the directional dependency of the brain response to dynamic loads in the modular design of military helmets.

5.5. Investigation of Possible Correlation between Brain Tissue Response and Head Kinematics for Blast-Induced Brain Injury

To the authors' best knowledge, the studies on the correlative relationship of brain's tissue response and the head kinematics have mainly been performed for head injuries under impact. However, as the injury mechanism for the bTBI is different from impact induced TBI, evaluation of head and brain biomechanics under blast shockwaves is of great importance.

Accordingly, in the research presented here, a computational approach was taken to investigate possible correlation between the brain's tissue response and head kinematics to find out whether the linear acceleration can be used as a sole injury predictor is defining brain injury for bTBI. The significance of such a study is that it can help improve the design and material of the current military helmets for enhanced blast protection as well as develop state of the art equipment to evaluate the risk of injury for the soldiers.

To this end, the NDSUFEHM was exposed to an identical shockwave overpressure of 520 kPa from front, back, top, and side directions.

The tissue response of the brain as well as the linear acceleration of the head was evaluated in all directions and were compared against each other. Propagation and interaction of blast waves with the head and the development of the resulting maximum pressure profile at the coup site and the shear stress at the brainstem is shown in Figure 5.12 for front blast. The peak linear acceleration for the head as well as the highest peak values for ICP and shear stress were observed for the blast from the side.

Figure 5.13 show the variation of peak ICP and shear stress values in each direction with the linear acceleration. An important finding was the direction dependent response of the head to an identical loading in different directions in terms of both tissue and kinematical responses.

Moreover, undergoing a higher linear acceleration did not necessarily impose higher tissue responses (blast from top). Time histories of brain ICP and head's linear acceleration showed similar patterns in all directions in terms of the peak duration while shear stress pattern varied with changing the direction. Compared to maximum shear stress, much better correlation was found between the ICP peak ICP values and the head acceleration.

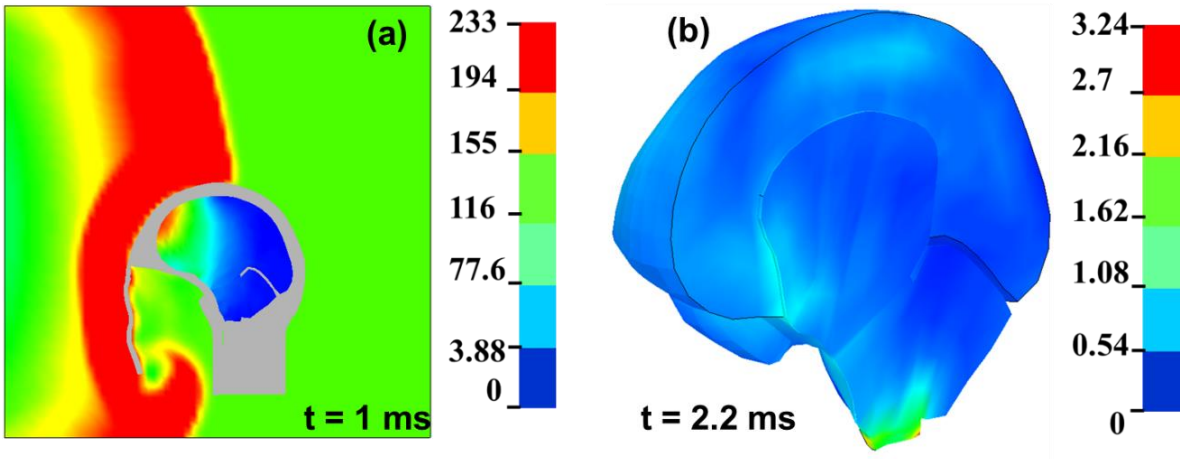

Figure 5.12. (a) Blast wave propagation and ICP (kPa) development (b) Maximum shear stress at brainstem

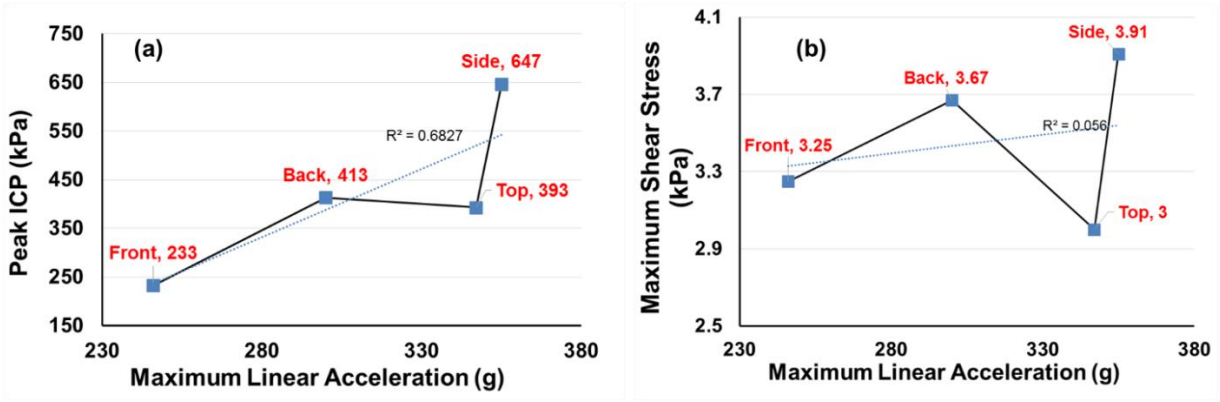

Figure 5.13. Relationship between acceleration of head and (a) Peak ICP (b) maximum shear stress

Human head and its components-specifically brain- are composed of different constitutive parts with different shapes, functions, and materials. It mean that the response of the

head would differ based on the location of impact. Accordingly, the idea behind the present research was to investigate the accuracy of considering linear acceleration as a sole injury predictor by finding the response of the head to an identical blast load from four different directions. Regarding the injury thresholds introduced by Ward et al. (1980) (peak coup ICP = 235 kPa), the head was marginally in the safe zone only for the front blast (ICP = 233 kPa). However, based on Zhang et al. (2004) criterion (max. shear stress = 7.8 kPa), the brain was far from mild TBI in all scenarios. However, the range of linear acceleration of head (>200 g) puts the head in the severe and critical injury range based on the threshold introduced by St Clair and Chinn (2007). These discrepancies between the head kinematics and brain's response is an indication of the lack of credibility of linear acceleration to be a sole indicator of brain injury. As shown in Figure 5.13(a), the variation of ICP levels showed an acceptable correlation with linear acceleration, while shear stress basically showed no effective correlation with that (Figure 5.13(b)). This would be in agreement with the results of King et al. (2003) relating linear acceleration variations to pressure gradient. While the acceleration of the head differed in each direction due to the directional behavior of the head, still for pretty close peak values of acceleration in top and side blasts, the brain predicted a much higher peak ICP value in side blast (647 kPa), nearly 64% more than that in top blast (393 kPa). However, the shear stress was only 30% higher in side blast and was still small (3.9 kPa). Accordingly, another disadvantage of using only the linear acceleration as the injury predictor is that in cases like the one mentioned, it would not be possible to discern different types of injury as the pressure gradients mainly relates to concussion and contusion injuries while shear stress is associated with diffuse injuries such as the diffuse axonal injury (DAI) which can be more critical than concussion.

The results of this specific case study showed that the tissue response of the brain, such as shear stress, strain, and ICP, are much more viable injury predictors compared to head acceleration. The reason lies within the fact that the brain response is an indicative of the local response of the brain tissue to the applied load. It was observed that while linear acceleration may be able to help define the generality of pressure-related injuries such as concussion, but it is unable to predict the extent and level of injury. Moreover, due to very weak correlation with shear stress variation, it might not be able to accurately predict the diffuse and shear related injuries.

The relationship between head kinematics and the brain response would be of significance in designing the protective tools such as helmet for head protection. The possibility of any correlation among these parameters would be lower as the application of helmet on the head would increase the complexity of the head response.

CHAPTER 6. THE EFFECT OF PROTECTIVE TOOLS ON THE MECHANICS OF BLAST WAVES: A NUMERICAL STUDY ON THE DEVELOPMENT AND IMPACTS OF THE UNDERWASH EFFECT USING FEA AND CFD MODELING

6.1. CFD Study on the Blast Flow Mechanics and the Underwash Effect

Shockwaves are defined as supersonic waves which travel in a fluid medium at velocities greater than the speed of sound. Propagating through the media they are traveling in, they carry high levels of energy and lead to sudden changes in pressure, density, and temperature of the media. A blast wave is defined as a shockwave which is generated as a result of the release of huge amounts of energy confined a small volume in a timeframe of microseconds. Blast waves which are generated upon detonation of high explosives develop a high-pressure shock front which is followed by a negative blast wind. Understanding the flow mechanics of blast waves and their interaction with structures has always been a big challenge. Upon growing use of Improvised Explosive Devices (IEDs) in the battlefields, protection of soldier's lives against blast explosions is of great concern. Blast-induced traumatic brain injury (bTBI) caused by the interaction of blast shockwaves with the human head occurs mainly in four different forms: primary resulting from direct impact of shockwaves, secondary due to strike of fragmentations propelled by the blast waves, tertiary resulting from the impacts induced by environmental means, and quaternary caused by the toxic gases. The Defense and Veterans Brain Injury Center (DVBIC) recently reported that 287,861 deployed servicemembers have been diagnosed with TBI from 2000 to 2013, a high percentage (~ 69%) of those being as a result of blast (Taylor and Ford 2009). There has been a great attempt in improving the survivability of the soldiers against blast threats by enhancing the current protective equipment. Military helmets serve as the most efficient tool in safeguarding the head against ballistic impacts, while their efficiency against

blast shockwaves is still not well recognized. This would probably be due to the complex mechanics of the blast wave propagation and interaction with helmet and head. The blast mechanics, as well as the shockwave-head interaction analysis are essential to grasp a qualitative evaluation of biomechanical response of the head. Due to limitations and moral issues regarding the exposure of human head and body to explosives, there is a lack of experimental literature in this area. Accordingly, numerical methods such as finite element (FE) and finite volume codes have been developed to provide real-time assessment of the current problem. Military helmets, while significantly effective in mitigating the blast shockwaves, have reported to cause a problem due to the flow of the shockwaves in their gap. Underwash effect, referred to as the adverse effect of helmets, is defined as the development of a local high pressure region inside the helmet gap and at a location opposite to where incoming waves enter the gap. This amplified pressure region can induce elevated surface pressure on the head, causing elevated loads to be transferred to the head. There are several computational studies that have introduced the importance of studying the blast flow mechanics and the underwash effect in evaluating the efficiency of the protective tools, especially combat helmets. These studies have employed the FE analysis to evaluate the flow mechanics of blast waves upon interaction with unprotected and helmet protected human heads. Mott et al. (2008) studied the flow dynamics of the blast waves around a helmeted head and found a locally amplified pressure region in the head-helmet with a pressure gradient close to that of an unprotected head. In another computational study, Moss et al. (2009) carried out a FE analysis and introduced this phenomenon as the underwash effect of the helmet imposed upon the interaction of coincident blast waves under no-padding conditions and in the head-helmet gap. Ganpule et al. (2012) verified this effect through both experimental and numerical studies. They investigated the effect of helmet on the blast wave mechanics and

the pressure field around the head and reported the attenuating effect of padding system on the underwash impulse. Varas et al. (2011) used a gelatin filled surrogate of skull/brain and carried out the shock tube simulation using a fluid-solid interaction (FSI) approach. They simulated the airblast through CFD modeling of inviscid compressible flow of an ideal gas and found the pressure and strain response of the surrogate using FEA. Przekwas et al. (2011) used the CFDRC CoBi solver code to perform FSI analyses on the blast wave interaction with unprotected and helmeted head. In their CFD model, they studied the behavior of blast flow upon interacting with helmeted head and reported underwash as a localized high-pressure region at the opposite side of entering shockwaves. However, they didn't discuss about possible reasons and mechanisms of this effect. There are a few other studies that have used a combination of CFD (for modeling the airblast) and FEA (modeling the human head/body) to evaluate the injury biomechanics of human head and body under blast ((Gupta and Przekwas 2014; Gupta and Przekwas 2015)). In terms of assessing the brain injury risk in different blast theatres, many researchers have investigated the mechanical response of the human head and brain to dynamic loads such as blast ((Chafi et al. 2010a; Grujicic et al. 2011; Grujicic et al. 2010; Gu et al. 2012; Moore et al. 2009; Panzer et al. 2012; Rezaei et al. 2014b; Taylor et al. 2014)). Although FEA can provide efficient approaches for modeling the blast waves and their interaction with the head and helmet, CFD analysis is required to find out the mechanism leading to the underwash effect of the helmets through studying the supersonic shockwave flow around the head and the helmet. The current literature on this subject such as Ganpule et al. (2012) and Moss et al. (2009) have not been substantiated with any fluid flow study, and the works of (Gupta and Przekwas 2014), Gupta and Przekwas (2015) and Przekwas et al. (2011) have just introduced the effect and hasn't looked into the mechanism behind it. To this end, for the very first time, the current research takes

advantage of the capabilities of CFD for investigating the supersonic turbulent flow dynamics around and inside the military helmets to elaborate on the underwash effect. The main focus of the current study is to carry out a qualitative investigation on the mechanisms leading to underwash effect by analyzing the flow characteristics such as the streamlines, velocity vector fields, and the pressure profiles upon the interaction of the airflow (blast-like waves) approaching the rigid unprotected/helmeted head. Additionally, the incidence of underwash overpressure in the head-helmet gap is verified in different directions namely, front, back, side, and bottom flow directions. The CFD modeling is performed using ANSYS CFX 14.5 (ANSYS 2012a) to carry out a concise 3D finite volume (FV) flow analysis. Modeling scheme and numerical method are discussed in section 6.1.1. The CFD results for all cases are provided in section 6.1.2, followed by a discussion on the results in section 6.1.3 and finally the concluding remarks are presented in section 6.1.4.

6.1.1. Numerical Methods

6.1.1.1. Geometry and Mesh Generation

The first step in every computational study is the generation of the geometry or the computational domain. A rigid approximation of a simplified head model, created using Solidworks, as well as the real ACH helmet model obtained via 3D scanning were used, as shown in Figure 6.1. To study the underwash effect, the standard gap size (d = 2.5 cm) was considered between the head and the helmet (Figure 6.1). The head-helmet assembly was enclosed by a very large cube ($286 \times 220 \times 75$ cm) filled with air (as an ideal gas) as the fluid medium for propagation of the shockwaves, with the head and helmet subtracted from it. A very small domain($8 \times 220 \times 75$ cm) was connected to the main domain for the release of the high-

pressure, supersonic compressible flow. Due to the symmetry of the model, only half of the computational domain was discretized and modeled to reduce the computational cost.

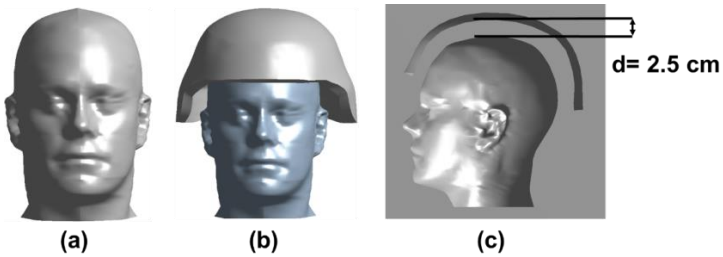

Figure 6.1. (a) Unprotected; (b) Helmeted head models; (c) The gap size between head and helmet

The grid generation was performed using the Meshing tool in ANSYS Workbench platform (Release 2012). The meshing procedure takes advantage of the "sizing" feature, which discretizes the volume with unstructured tetrahedral volume elements. To improve the elements quality, advanced size function was activated in order to keep a smooth growth rate between the regions of proximity/curvature. Moreover, inflation layers, e.g. hybrid tetrahedral elements, were generated on the boundary surfaces to provide a hybrid tetrahedral mesh in order to better capture the flow physics near the walls. The meshing algorithm generated a total of 545214 and 734023 tetrahedral elements for the unprotected and helmeted models, respectively. Based on the sensitivity analysis data (Table 6.1), the mesh was appropriately refined around the head-neck model to better capture the flow dynamics of the shockwaves.

Table 6.1. Mesh sensitivity analysis based on the surface pressure analysis on the back of the head in the front blast scenario (the underwash induced overpressure)

Mesh Type	Min. element size (mm)	Max. element size (cm)	Surface Pressure on Head (MPa)
Coarse Mesh	5.9	33.5	0.98
Medium Mesh	2.3	28.2	1.18
Fine Mesh	0.486	16.2	1.5
Very Fine Mesh	0.05	10.2	1.51

6.1.1.2. Governing Equations

All the simulations in the current research were performed using ANSYS CFX (ANSYS 2012a). CFX is a finite volume based transient solver which is used for solving the laminar or turbulent, transonic/supersonic flows of compressible gases. The CFD codes such as CFX utilizes the unsteady Navier-Stokes equations in their conservation form. The compressible, unsteady, viscous and turbulent airflow is described by the governing equations for conservation of mass, momentum, and energy, as follow (White and Corfield 2006):

$$\frac{\partial \rho}{\partial t} + \text{div}\, \rho \mathbf{V} = \mathbf{0} \tag{6-1}$$

$$\rho \frac{D\mathbf{V}}{Dt} = \rho \mathbf{g} + \boldsymbol{\nabla} \cdot \boldsymbol{\tau}'_{ij} - \boldsymbol{\nabla} p \tag{6-2}$$

$$\rho \frac{Dh}{Dt} = \frac{Dp}{Dt} + \text{div}(k\, \boldsymbol{\nabla T}) + \boldsymbol{\tau}'_{ij} \frac{\partial u_i}{\partial x_j} \tag{6-3}$$

where ρ is density, $\mathbf{V}$ is the velocity vector, $\mathbf{g}$ is the gravity, p is the pressure, t is the time, h is enthalpy, T is the temperature, and k is the thermal conductivity. However, the stresses are defined as follow for a viscous Newtonian fluid:

$$\boldsymbol{\tau}'_{ij} = \mu \left(\frac{\partial u_i}{\partial x_j} + \frac{\partial u_j}{\partial x_i} \right) + \delta_{ij} \boldsymbol{\lambda}\, \text{div}\, \mathbf{V} \tag{6-4}$$

where μ is the dynamic viscosity, $\boldsymbol{\tau}'_{ij}$ is the stress tensor, δ_{ij} is the Kronecker delta and u_i and x_i represent the Cartesian velocity components and Cartesian coordinates, respectively. In general, to obtain the compressible flow solution, equations (6-1) to (6-4) are solved simultaneously along with the air equation of state (EOS), $p = \rho RT$ and the turbulence equations. Unlike low-speed flows, the effect of kinetic energy can't be neglected in supersonic flows or when shockwaves are present. Accordingly, a heat transfer model should be employed to evaluate the heat transfer. The major available models in ANSYS for prediction of heat transfer are "Total

Energy" and "Thermal Energy" models (Ansys 2012b). Total Energy model that was used in the present study, is implemented in the CFX code to evaluate the heat transfer in the domain due to the convection, conduction, and turbulence mixing.

6.1.1.3. Turbulence Modeling

In fluid dynamics, turbulence flow is referred to a flow regime which undergoes chaotic and random properties changes. Characterized by the temporal and spatial fluctuation of the flow field, this complex process occurs as the inertia forces outweigh the viscous effect in the fluid and is usually distinguished by the Reynolds number. In order to include the turbulence effects in the flow field solution, several eddy-viscosity and Reynolds stress models have been introduced to solve the modified transport equations by introducing time varying and averaged components in original transport equations (Rigas and Sklavounos 2005; Sklavounos and Rigas 2004)

Based on the velocity of the air and the characteristic length of the domain, the Reynolds number is calculated as $\mathrm{Re} = 1.3 \times 10^8$ implying the dominance of turbulent flow regime in the domain. CFX offer a wide range of turbulence models for solving the compressible flows. Shear Stress Transport (SST) was used as the turbulence model in our simulations (Ansys 2012b). SST is not only economical like the commonly used k-ε model, but also provides greater fidelity in terms of predicting the characteristics of the separated flows such as the onset and amount of separation upon development of the adverse pressure gradient. SST model significantly improves the prediction capability of flow separation and heat transfer and offer exact solutions for near wall mesh conditions (Menter 1994).

6.1.1.4. Discretization and Solution Scheme

The discretization of the computational domain was carried out using the finite volume method (FVM), which has shown to be efficient for supersonic or shockwave flows with

unstructured triangular grid (Rigas and Sklavounos 2005; Sklavounos and Rigas 2004). In this method, the spatial domain is divided into finite volume controls using elements (mesh), and the Navier-stokes governing (equations (6-1) to (6-4)) are integrated over each control volume in a way that the associated quantities such as mass, momentum, and energy are conserved for each volume. The fluid properties and solution variables such as pressure and velocity are stored in a node enclosed by each volume control. Then, the integral form of the governing equations is obtained and a system of algebraic equations is developed by approximating different terms (diffusion and convection) in the integral equations. Using an iterative process, the diffusion source terms are solved at all nodal points in an attempt to minimize the root mean square (RMS) to satisfy the convergence criteria (10^{-6}).

Using a coupled solver, CFX employs a fully implicit method to discretize the equations and solve for the velocity and pressure components at any given timestep. This method has the advantage of reducing the number of iterations required to satisfy the convergence. The detailed solution algorithm can be found in (ANSYS 2012a). To solve for the unsteady terms, the time-stepping algorithm was implemented using the backward Euler transient scheme which has a second order accuracy in time. However, first order backward Euler scheme, with a first order accuracy in time, was employed to solve for the solving the turbulence equations. This solution algorithm is fully implicit, robust and conservative time and is appropriate for bounded quantities such as turbulence components (unlike the second order backward Euler). High resolution advection scheme was employed to solve for the advection terms in the discrete finite volume equations (Ansys 2012b).

6.1.1.5. Problem Formulation and Boundary Conditions

The main objective of the current research was to investigate the behavior of the turbulent, supersonic compressible shockwaves over a head-helmet assembly. To this end, an interactive approach was developed to generate the shockwaves. A very small domain, referred to as domain 1, was interfaced with a very large domain, referred to as domain 2, including the head/helmet assembly. The initialization of domain 1 was carried out by filling it with air (as an ideal gas) at a pressure of 700 kPa, a temperature of 25 C, with a velocity of 400 m/s (Mach number of 1.32). Domain 2 was kept at ambient setting (pressure of 101.32 kPa and 0 velocity and 25 C). To allow for the release of supersonic flow into the at-rest domain 2, a fluid-fluid interface was defined at the interface of two domains. As mentioned before, the Total Energy heat transfer model and SST turbulence models were used to predict the heat transfer and turbulence effects.

For the boundary conditions, all the surfaces of both domains, as well as the head and helmet surfaces were considered as no-slip walls except for the right surface of domain 2, for which the Entrainment opening was considered with a relative static pressure of zero. Due to symmetric geometry of the head-helmet assembly and the domains, the symmetric condition was applied to reduce the computational cost. The details of the computational domain as well as the initial and boundary conditions are shown in Figure 6.2(a). The simulations were carried out for an identical incident shockwave approaching the unprotected and helmeted assemblies from front, back, side, and bottom directions (Figure 6.2(c)). Transient simulations were run for 6 milliseconds with timesteps of 2.5×10^{-6} seconds which took about 48 hours of clock time for execution on a 2.93 GHz Intel Core i7 with 8 GB of RAM.

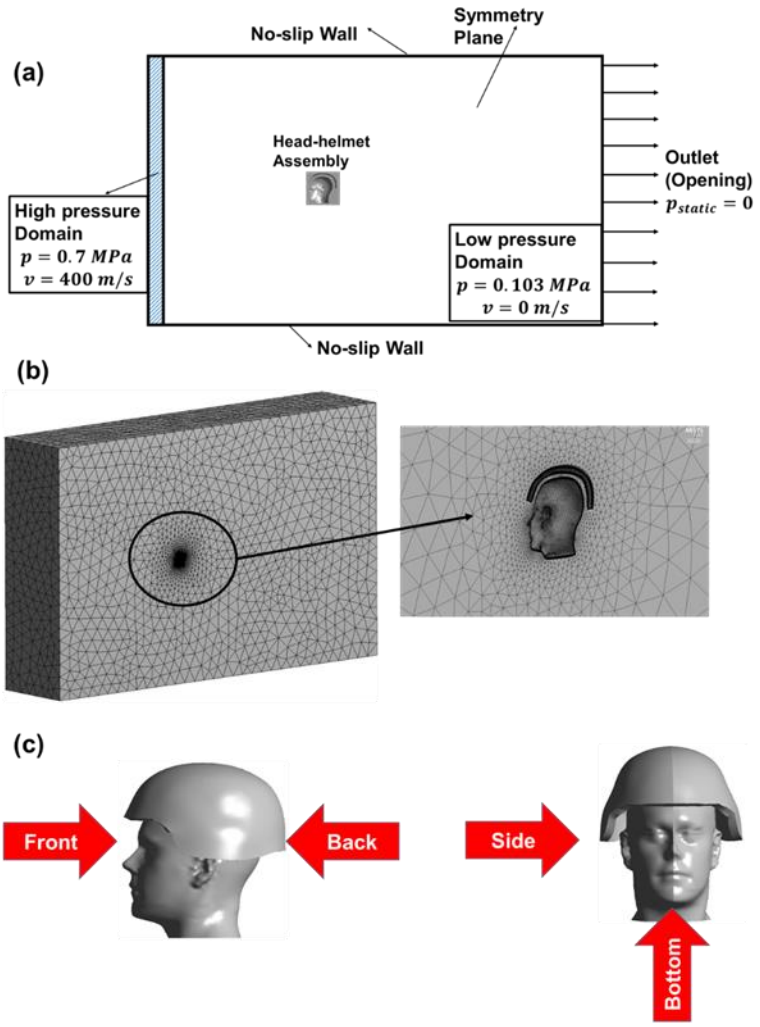

Figure 6.2. (a) Computational domain and boundary conditions (b) Mesh generation; (c) Problem formulation and the direction of incoming shockwaves

6.1.2. Results

6.1.2.1. Development of Underwash Effect

In this section, first the development of the underwash effect is investigated through studying the front shockwave flow around and inside the unprotected and helmeted assemblies. To this end, the pressure profile, as well as the flow visualizations in terms of the velocity streamlines and vector fields are obtained and presented to discuss the mechanisms leading to underwash. Due to the irregular geometry of the helmet, the shockwave flow is believed to be highly affected by the impact location of the waves on the helmet. Accordingly, in the second

part of the study, the effect of shockwave parameters such as its direction and intensity on the incidence of underwash is sought. Figure 6.3 shows the interaction and propagation of the front shockwaves, as well as the separation of these waves from the boundaries, and finally the reunion of the waves at the opposite side, along with the Mach contours, at different time instances. While the shockwaves flow followed a similar pattern in both protection cases, the propagation of these wave inside the helmet gap led to an elevated pressure region at the opposite side of the helmet (at 1.25 ms). The observation of the flow behavior revealed that the nasal regions of the face and the eye provided possible locations for the concentration of the shockwaves. The underwash induced overpressure at the back of the head in the helmeted case (1.5 MPa) was observed to be about 3.4 times the overpressure generated upon the reunion of the waves at the back of the unprotected case (0.44 MPa). The exterior shockwave flow (flow outside and around the helmet gap) was observed to propagate faster than the interior flow (flow inside the helmet gap). This caused a backflow of exterior waves towards the outgoing interior flow from the back of the helmet. The backpressure applied by this backflow caused a flow blockage inside the backside curve of the helmet which resulted in a rapid deceleration of the flow and development of a high pressure region. A recirculating region was observed to form at the front region of the helmet due to the geometrical discontinuity of the helmet. Accordingly, the wake region was narrowed and increased flow velocity. This would explain the supersonic region developed at the front region at the first three time instants, as shown by the Mach contours Figure 6.3(c).

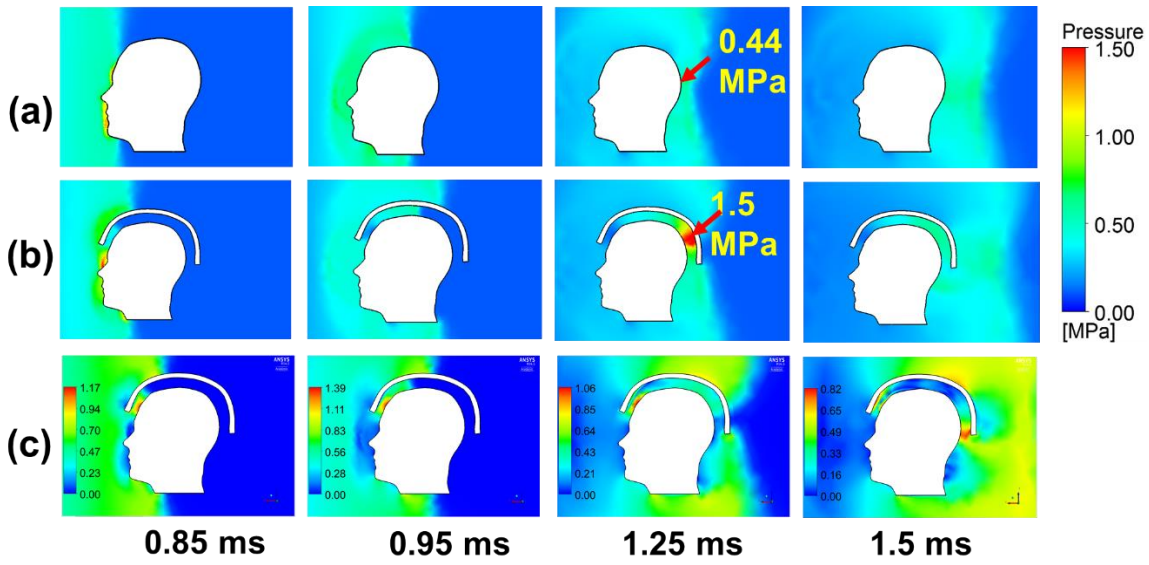

Figure 6.3. Interaction, separation, and reunion of the front shockwave flow for (a) unprotected and (b) helmeted heads; (c) the Mach contours for the helmeted head

The temporal variation of the shockwave overpressure was recorded at 5 different locations on the sagittal plane of the head (along the symmetry plane), as shown in Figure 6.4. It was observed that around the frontal region of the head (points 1 & 2), the helmet provided a significant protection against the shockwaves by diffracting the waves and preventing them from entering the gap and impacting the head. For example the overpressure of 1 MPa for the unprotected head at point 1 was reduced in half to 0.5 MPa in the helmeted case. However, from the mid-sagittal plane towards the back of the head (points 3-5), the pressure started to increase instead of gradually decreasing and reaching to the ambient pressure. As pointed out before, in events such as explosion, a large amount of energy is released which increases the pressure, velocity, and the temperature of the fluid it is traveling in. In a matter of few milliseconds, a sudden increase in the overpressure occurs and afterwards, the aforementioned fluid properties gradually decrease as the shockwaves travel. While at the top of head (point 3), the overpressure inside the helmet gap (0.56 MPa) slightly exceeded the one in the unprotected case (0.47 MPa), it significantly increased at point 4 where the underwash was reported (1.5 MPa for helmeted and

0.44 MPa for unprotected). However, after the underwash, the overpressure started to decrease and approached to the value of unprotected overpressure at point 5. This observation confirmed the incidence of the high pressure region. Moreover, streamlines were plotted in the sagittal plane to visualize the air flow in and around the unprotected and helmeted head in Figure 6.5.

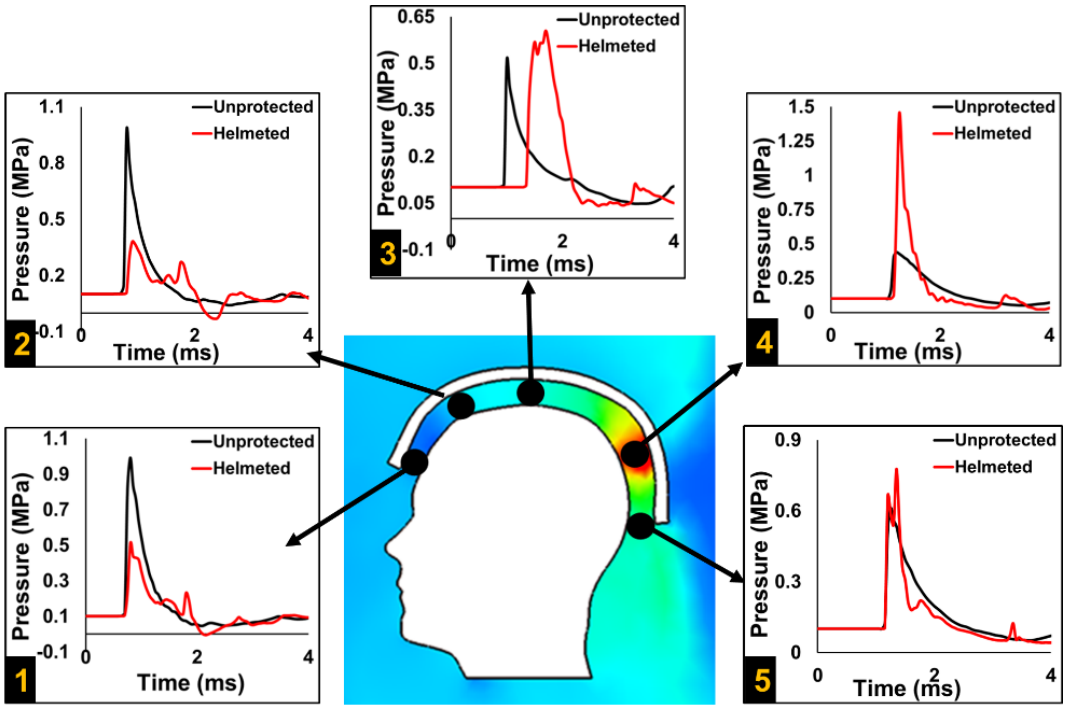

Figure 6.4. Temporal variation of overpressure at different locations on the sagittal plane of the head

The flow streamlines are shown at two different instants, i.e., before (a & c) and at the time of underwash overpressure (b & d) for the helmeted and unprotected heads. For the unprotected head, no separation at the surface of the head was observed. However, for the helmeted head, at the time of the underwash (Figure 6.5(b)), the flow boundary layer was separated upon moving around the leading edge of the helmet. Moreover, at the back of the head and where the underwash was observed, the flow's direction changed with the change in the helmet's radius of curvature. A vortex region was developed at the front region of the helmet when the underwash occurred while, no vortex region was observed at the instant before the

underwash, as well as in the unprotected cases. While highly supersonic before underwash incidence (Figure 6.5(a)) with Mach number around 1.34, the flow approached to transonic speeds (Ma~1.1), at the time of the underwash. Another important observation during the underwash event was the momentum change of the flow. Looking at the velocity changes in the fluid as it entered the backside curve of the helmet, one can expect the momentum to change due to changes in density, velocity and area of the fluid flow. Figure 6.5(e) shows the shockwave flow visualization through the horizontal surface streamlines and the 3D streamlines inside and around the helmeted head. The velocity change, reunion of waves, as well as the interaction of shockwaves moving in different directions over and inside the helmet at the back side is obvious in this figure. Based on the unique geometry of head and helmet and the angle of attack for the approaching flow, the incoming flow was separated into two different flow paths at the leading edge of the head (forehead) and the helmet: one flowing inside the gap and the other one traveling all around the exterior surface of helmet, as shown in Figure 6.5.

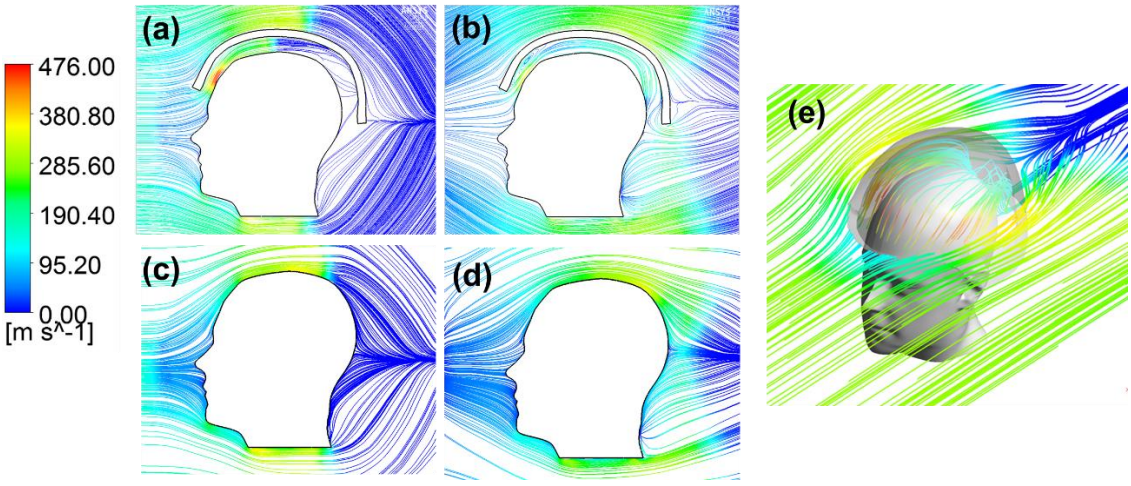

Figure 6.5. Streamline plots of shockwave flow over and inside the helmeted (a &b) and unprotected (c & d) heads; (e) 3D and surface streamlines showing the underwash incidence

6.1.2.2. Effect of Shockwave Direction on Underwash

Due to the strong dependence of underwash effect on the geometrical features of the interacting bodies, the potential for underwash also varies with the shockwave direction as a result of the non-uniform configuration of the head and helmet. As shown in Figure 6.6, both unprotected and helmeted heads were exposed to identical incident overpressures at four different flow directions, namely front, back, side, and bottom directions, and the underwash incidence was examined in all cases. In each direction, the propagation of the supersonic shockwaves around the head/helmet assembly and inside the helmet gap, as well as the development of the underwash overpressure was captured at four different instants. The bottom and back blast predicted the highest (3.5 MPa) and lowest underwash overpressure (1.15 MPa), respectively. Side shockwaves predicted the second highest overpressure (1.7 MPa) and the front shockwaves lead to an overpressure (1.5 MPa) close to the one in the side flow. The formation of the shockwaves upon the interaction of the supersonic flow with the helmet in all directions is clearly shown Figure 6.6. Moreover, side blast showed to provide much better protection for the facial parts.

Figure 6.7 compares the shockwave overpressure at three different locations between the unprotected and helmeted heads: (1) entrance of the shockwaves into the helmet gap; (2) the top of the head (or midway toward the underwash location for bottom blast); (3) the underwash location at the opposite side of the shockwave's entrance. This comparative analysis revealed the contribution of the helmet geometry in protecting the head against shockwave, as well as preventing the development of the underwash overpressure. The peak overpressures at all the locations for both unprotected and helmeted heads, as well as the percentage increase and decrease upon using the helmet are provided in Table 6.2. As expected, except for the bottom

direction in which no helmet protection was provided under the head, the overpressure at location (1) in the helmeted case was observed to be much less than the one in the unprotected case due to the diffraction of shockwaves by the helmet. It's worth mentioning the overpressure at location (1) varied based on how the geometry of the helmet in each direction altered and strengthened the shockwave flow. More than 50% mitigation was provided in front (51%), back (62%), and side (62%) directions, while a negligible mitigation was provided in the bottom direction (3%). At location (2), however, the helmeted overpressure slightly exceeded the unprotected one, except for the bottom case where there was a huge difference between the unprotected and protected overpressures (225% increase upon using helmet).

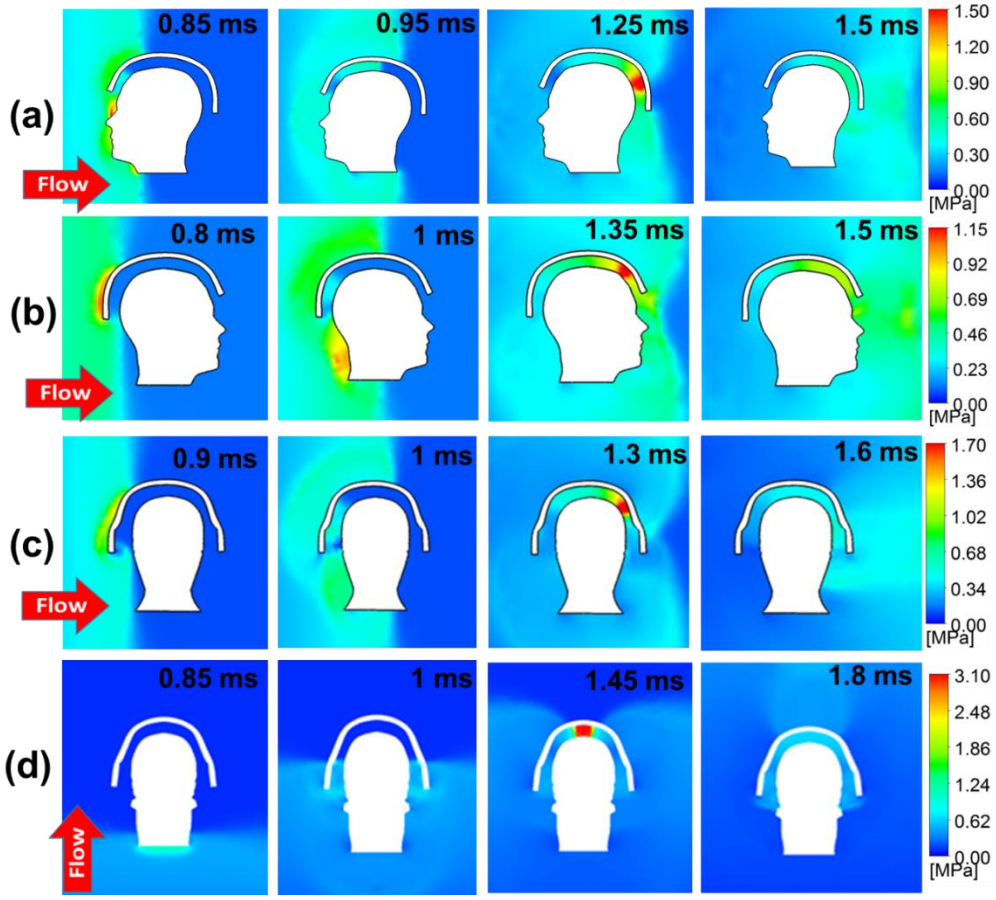

Figure 6.6. Pressure contour of supersonic shockwave around and inside the helmeted head at distinct times for (a) front (b) back (c) side (d) bottom shockwave flow

At location (3), i.e. underwash overpressure'slocation, all helmeted models predicted highly amplified overpressure with respect to those for the unprotected head. Although the highest peak overpressure was predicted in the bottom shockwave flow (3.1 MPa), the highest percentage increase was reported for the side direction (466%). The percentage increase in the peak overpressure in front (250%) and back (266%) was nearly the same.

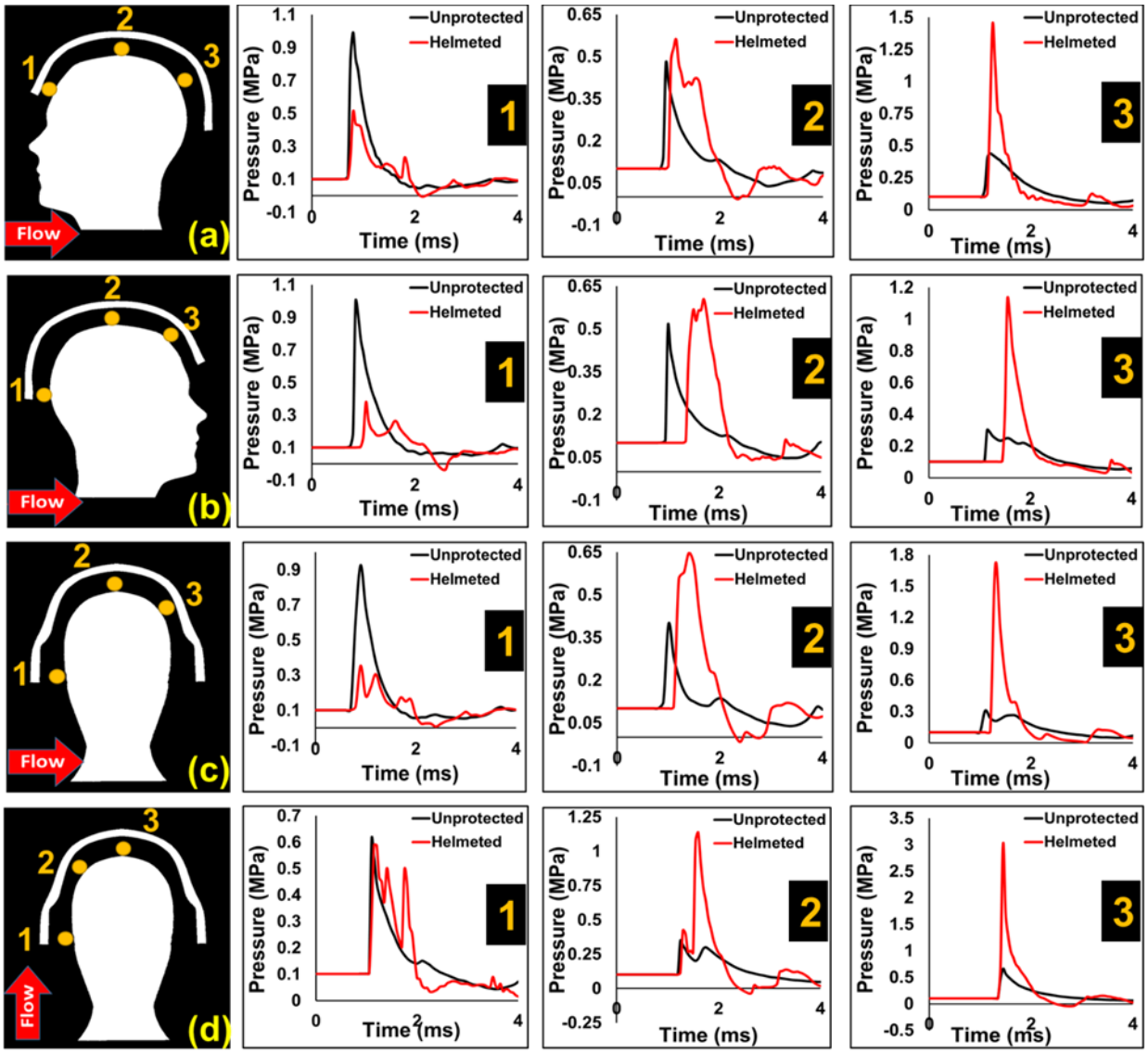

Figure 6.7. Temporal variation of pressure around unprotected and helmeted heads at three different locations for (a) front (b) back (c) side (d) bottom shockwave flow directions

Figure 6.8 represents the flow characteristics around and inside the helmeted heads in all directions. The flow streamlines illustrate a similar pattern for the front and back directions due to the partial similarity of the head-helmet configuration. Development of a vortex at the front region was observed on the inner side of the helmet in these directions. However, the flow behavior in the side and bottom directions differed significantly and no vortex region was observed.

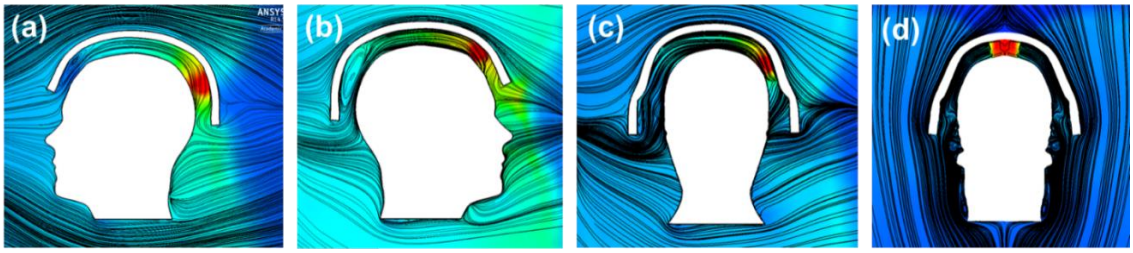

Figure 6.8. shockwave flow streamlines inside and around the helmeted head in (a) front; (b) back; (c) side; and (d) bottom shockwave flow directions

Table 6.2. Peak overpressure of shockwaves at three different locations for both unprotected and helmeted heads, as well as the percentage increase and decrease upon using the helmet in all flow directions

Flow Direction	Location	Unprotected Overpressure (MPa)	Helmeted Overpressure (MPa)	% Increase (by helmet)	% Decrease (by helmet)
Front	1	1	0.51	---	51
	2	0.485	0.56	20.61	---
	3	0.44	1.5	250	---
Back	1	1	0.38	---	62
	2	0.51	0.6	17.6	---
	3	0.3	1.1	266	---
Side	1	0.926	0.35	---	62
	2	0.4	0.65	62	---
	3	0.3	1.7	466	---
Bottom	1	0.61	0.59	---	3
	2	0.35	1.14	225	---
	3	0.66	3.1	370	---

6.1.2.3. Effect of Incident Shockwave Overpressure on Underwash

Two parametric studies were carried out to illustrate the effect of blast intensity and helmet geometrical features on the underwash induced overpressure at the back of the head in the front scenario. The purpose of this study was to investigate if there was any correlation between the incident overpressure of the incoming waves in front of the head-helmet assembly, and the helmet gap size, with the intensity of the underwash overpressure.

For the incident overpressure study, three different incident overpressures of 0.7, 1, and 1.42 MPa were generated in front of the head (yellow region), and the corresponding underwash overpressures were evaluated, as shown in Figure 6.9(a). It was found out while the underwash overpressure increased by increasing the incident overpressure, there was no certain correlation between these two overpressures. However, the increase rate of the underwash overpressure reduced by increasing the shockwave intensity. In other words, while for the 0.7 MPa shockwave, the corresponding underwash overpressure (1.5 MPa) had a 114% increase, for the 1 MPa and 1.42 MPa shockwaves, the underwash peak overpressure increased by 79% and 77%, respectively.

In the gap size study, for an identical incident overpressure of 0.7 MPa in the front scenario, three different gap sizes, namely 2 cm, 2.5 cm (used for this study), and 3 cm gaps, were considered for the helmet and the corresponding underwash peak overpressures of 1.45 MPa, 1.5 MPa, and 1.65 MPa were recorded, respectively. The underwash overpressure was observed to increase by increasing the gap size. However, the increase rate of the peak overpressure didn't follow a specific pattern upon changing the gap size by a certain amount (0.5 cm). While the overpressure increased by 3.5 % by increasing the gap from 2 cm to 2.5 cm, it showed a 10% increase upon being increased from 2.5 cm to 3 cm. The variation of the peak

overpressure with the gap size is shown in Figure 6.9(b). However, it should be noted that more incident intensities and gap sizes should be evaluated to in order for general conclusions to be drawn.

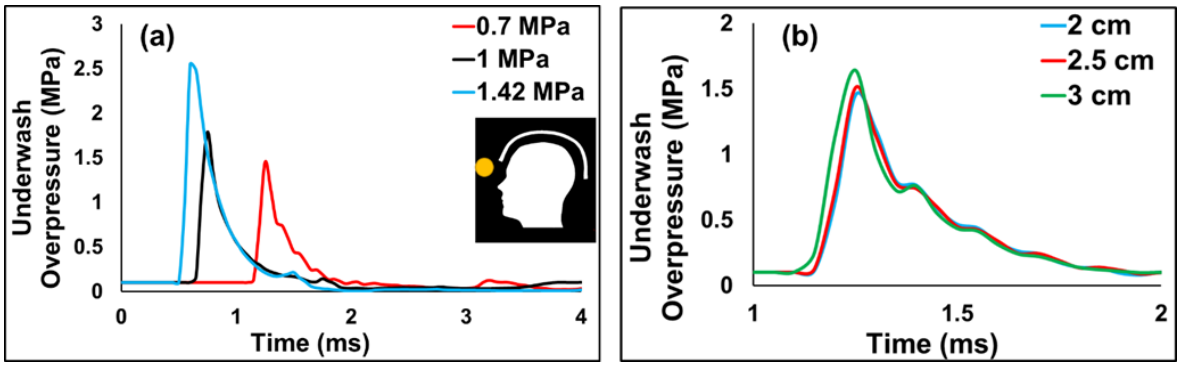

Figure 6.9. The effect of (a) incident overpressure and (b) helmet gap size on the underwash overpressure

6.1.3. Discussion

Diffracted by the leading edge of the helmet, the turbulent flow approaching the helmet formed a turbulent boundary layer, as shown in Figure 6.10(a). Due to the discontinuity imposed by the geometry of the helmet, an adverse pressure gradient was developed on the inner surface of the helmet and led to the separation of the flow from the helmet's surface. This caused the formation of the reverse flow vortex, i.e. a bubble, inside the boundary layer. Moreover, this led to the narrowing of the shockwave flow passage inside the helmet gap, hence increasing the velocity and decreasing the pressure of the flow at the front region of the helmet gap.

At the backside curve in Figure 6.10(a), a sharp redirection of flow was observed, which was followed by another diversion at the trailing edge of the helmet due to its sharp angle. It was observed that the velocity, as well as the density of the fluid changed noticeably as it entered this curve from the top of the helmet gap. The fluctuating flow pattern at the underwash site was believed to be due to the backflow caused by the exterior flow on the outgoing interior flow at the trailing edge of the helmet.

To analyze the flow behavior as well as investigate the effect of the helmet curvature on the underwash incidence, the assumption of a 2D flow was made (Figure 6.10b) and the momentum equations were written in x and z direction to solve for the forces that were applied on the head at the helmet backside curvature. Applying the momentum equation on a control volume (CV) shown in Figure 10(b), along with the continuity equation, a relationship was obtained between the pressure forces and the angle θ. It was concluded that based on the assumptions made, the underwash overpressure increased by increasing the angle.

3D simulations performed in the current research, allowed us to look for the mechanism of the underwash by studying the development of pressure profiles in all anatomical planes. First to evaluate whether the maximum elevated pressure was certainly happening at the location introduced as the underwash location in sagittal plane, we looked for the elevated pressure region in horizontal and coronal planes as well. All three planes with the elevated overpressure region (underwash) is shown in Figure 6.10(c). The underwash-induced overpressure was observed to occur at the same location in all planes. This confirmed that the blockage of the shockwave flow was imposed by the backflow of exterior flow in all planes.

The variation of the underwash incidence and overpressure with the flow direction confirmed the importance and role of the helmet geometry on the flow mechanics of shockwaves. It was observed that based on the geometry of the helmet in each direction, the smaller the helmet outlet, the less backflow entered the helmet gap, and hence, smaller overpressure was generated. This can be clearly seen in Figure 6.6(a-c). The highest overpressure among these, was for the side waves (due to the largest outlet of helmet in this direction) and the lowest was for the back side due to the smallest outlet. The highly amplified underwash overpressure in the bottom flow was postulated to be due the fact the majority of the shockwaves

entered the helmet gap and a small part of them were deviated by the helmet edges. Moreover, the shockwaves were intensified by the interior surface of the helmet like what happens in confined space blasts. This amplification of shockwaves along with the high impulses imposed by two huge bulks of shockwave flows on each other upon meeting on top of the head, led to an incredibly high overpressure, as shown in Figure 6.6(d).

The increase of the underwash overpressure with increasing the incident overpressure and the gap size in the front scenario further confirmed the large dependence of the underwash overpressure on both the flow dynamics and helmet geometry. It was asserted that upon increasing the incident shockwave intensity, a stronger shock front was developed and moved inside and outside of the helmet. Accordingly, the corresponding back pressure by the exterior flow on the outgoing interior flow increased the underwash overpressure increases. However, the increase rate of the underwash overpressure decreased upon increasing the incident overpressure.

Increasing the gap size caused the helmet to have a bigger outlet at the backside. Hence, a similar explanation to what was stated for the high overpressures in the side flow, can be used here. The greater the outlet, the larger the backflow of exterior shockwaves, and the greater the underwash overpressure. Interestingly, the underwash overpressure for a gap size of 3cm approached to the value recorded for the side shockwaves.

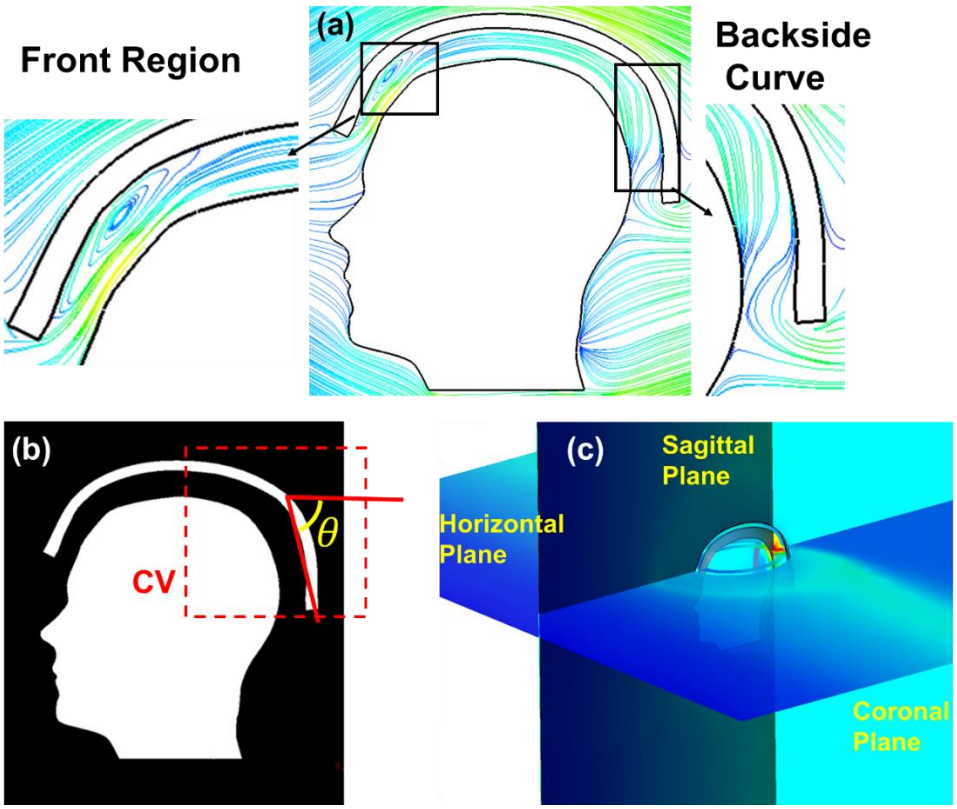

Figure 6.10. (a) The flow field inside the helmet gap at the time of underwash (b)The underwash overpressure location in all anatomical planes of the head; (c) The backside curvature of the helmet

6.1.4. Conclusions

A CFD study was carried out to investigate the mechanism leading to the development of a high pressure region developed at the opposite side of the entering shockwaves inside a helmet gap, called the underwash overpressure. The development of this phenomenon was investigated through studying the supersonic turbulent shockwave flow around and inside the unprotected and helmeted head models by evaluating the flow streamlines, velocity vectors, and the pressure distribution for the shockwaves approaching the heads from the front direction. Furthermore, two parametric studies were performed to evaluate the effect of parameters such as shockwave flow direction and intensity on the underwash. The following summarize the key findings of the current work:

- Regions of concavity, such as nasion, were observed to provide locations for the reflection and amplification of the incoming shockwaves.
- For shockwaves approaching from front, back, and side directions, underwash was postulated to occur as a result of the backpressure imposed by the backflow of the exterior flow on the outgoing interior flow. Moreover, in the directional study of the underwash, it was observed that the smaller outlet for the shockwave out of the helmet (based on the geometry of the helmet in each direction) would lead to lower underwash overpressure due to less backflow of the exterior flow.
- For the shockwaves approaching from the bottom, majority of the shockwaves entered the helmet gap and a small part of them were deviated by the helmet edges. Moreover, the shockwaves were intensified by the interior surface of the helmet like what happens in confined space blasts and along with the high impulse two huge bulks of shockwave flow imposed on each other upon meeting on top of the head, led to an incredibly high overpressure.
- The geometrical discontinuity caused by the helmet edge in the front and back cases, resulted in the development of a reverse flow vortex region (bubble) on the interior surface of the helmet at the front region of the helmet, and consequently increased the flow velocity and formed a supersonic flow region.
- The shockwave flow was observed to go through a momentum change at the backside curve of the helmet in case of the front, back, and side flows. Using the momentum and continuity equation in 2D, a relationship was developed between the applied force on the head in the helmet's curve and the angle of the helmet's curve (Figure 6.10). It was found that the higher the angle, the greater the underwash overpressure would be.

- The parametric study on the effect of the incident shockwave overpressure on the underwash induced overpressure revealed that while the underwash overpressure increased by increasing the incident intensity, the increase rate of the underwash overpressure decreased by increasing the incident overpressure.
- The underwash overpressure increased upon increasing the gap size of the helmet in the front scenario, as a larger backside outlet was generated for the helmet, and hence larger backpressure was applied by the exterior shockwave flow.
- There are some limitations in the current work which should be addressed in future studies, such as studying the effect of helmet pads on preventing the underwash incidence and role of faceshield on underwash and shockwaves flow mechanics.

6.2. Effect of Underwash Overpressure on the Mechanical Response of Brain in bTBI

6.2.1. Rationale for Incorporating Directionality Effects

In this chapter some abbreviated expressions are used to describe the overpressure and ICPs tolerated by the head and brain, respectively. U-skull, U-ICP, and Coup-ICP refer to the underwash induced skull pressure, underwash induced ICP, and the peak ICP imposed on the protected heads by the primary shockwaves, respectively. Before studying the underwash, a rationale for incorporation of the directionality effects in the study of underwash is presented. Figure 6.11 shows the variation of maximum brain ICP, underwash impulse, and U-ICP with the location of TNT along the vertical axis (z-axis) of the sagittal plane of the head in the front blast. For the current study, the explosive was located at z = 25 cm (in front of the forehead) and was moved up to z = 32 cm (in front of the top of the head) as well as moved down to z = 12 cm (in front of the chin). The results, recorded for every centimeter of displacement, clearly showed that changing the explosive location significantly affected the underwash impulse, the U-ICP, and the

brain ICP. The brain ICP showed an 18% decrease, while underwash impulse and U-ICP decreased by 30% and 23%, respectively. This showed that due to the inhomogeneity of the head components as well as the irregular shape of the head, the interaction of blast waves with the head can be alternated based on the origin of the explosion. This would definitely raise the need for investigating the brain response with respect to the blast location. To this end, n the study presented here, the head was exposed to blast waves from different directions so more realistic conclusions can be made based on the results of the study.

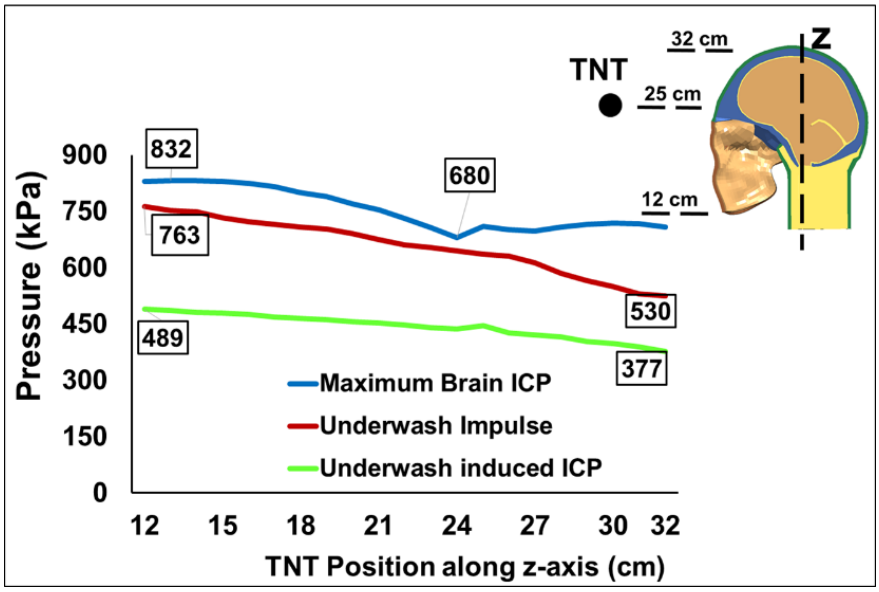

Figure 6.11. Variation of maximum brain ICP, underwash impulse, and uICP with the location of explosive along the z-axis for the front blast

To better observe the incidence of underwash effect and evaluate its possible effects, the two protection systems shown in Figure 3.7, were used and the padding system was removed from the helmet. To account for the blast directionality effect on the incidence of the underwash and the corresponding brain response, the protected head models were exposed to an identical blast overpressure from front, back, side, and bottom directions (Figure 6.12).

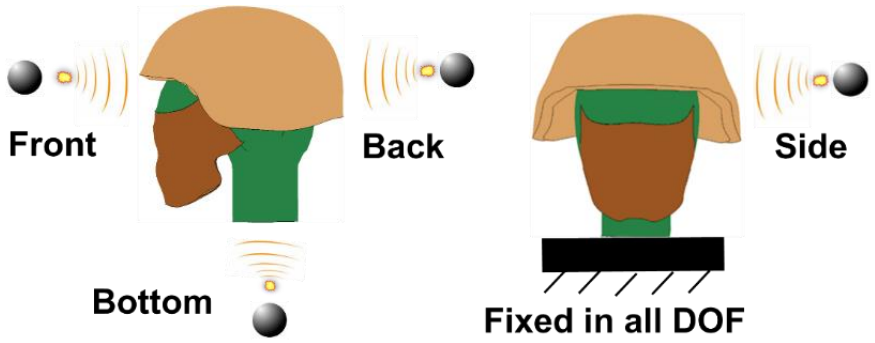

Figure 6.12. Different blast scenarios: front, back, and bottom; side blast along with boundary condition for the neck

6.2.2. The Effect of Blast Direction on the Underwash Overpressure

The genesis of underwash has been shown to be due to the helmet-faceshield protection assemblies used for protection of the head (Ganpule et al. 2012; Sarvghad-Moghaddam et al. 2014a). Based on the geometry and configuration of protective tools assemblies, the blast flow mechanics can alter and hence change the incidence and intensity of the underwash overpressure. Figure 6.13 manifests the blast directionality effects on the underwash incidence under different protection systems. In all directions, i.e., front, back, side, and bottom blasts, the helmeted and fully-protected heads were exposed to an identical blast overpressure of 520 kPa. The underwash phenomenon in each direction showed its own unique feature. Figure 6.13(a) shows that in the front blast, while the fully-protected system mainly inhibited the underwash (370 kPa), the helmeted system led to an underwash overpressure of 580 kPa, slightly more than the 520 kPa incoming pressure waves. The back blast, on the other hand, predicted a much higher underwash overpressure for the fully protected system (665 kPa) which was significantly higher than that predicted by the helmeted system (460 kPa), as shown in Figure 6.13 (b). In the side blast (Figure 6.13 (c)), however, the great coverage provided by fully-protected system, led to an overpressure as low as the one seen for the front blast (367 kPa) and prevented the underwash. The underwash induced pressure by the helmeted system in this case was also lower than those

obtained in other directions. Finally, the bottom blast (Figure 6.13 (d)) predicted the highest underwash overpressure for both helmeted (1053 kPa) and fully-protected systems (1220 kPa). This overpressure was observed to be more than twice that of the approaching shockwaves. The reason was recognized to be mainly due to the larger interior spacing for the entrapment of shockwaves as no impediment was provided by both helmet and faceshield.

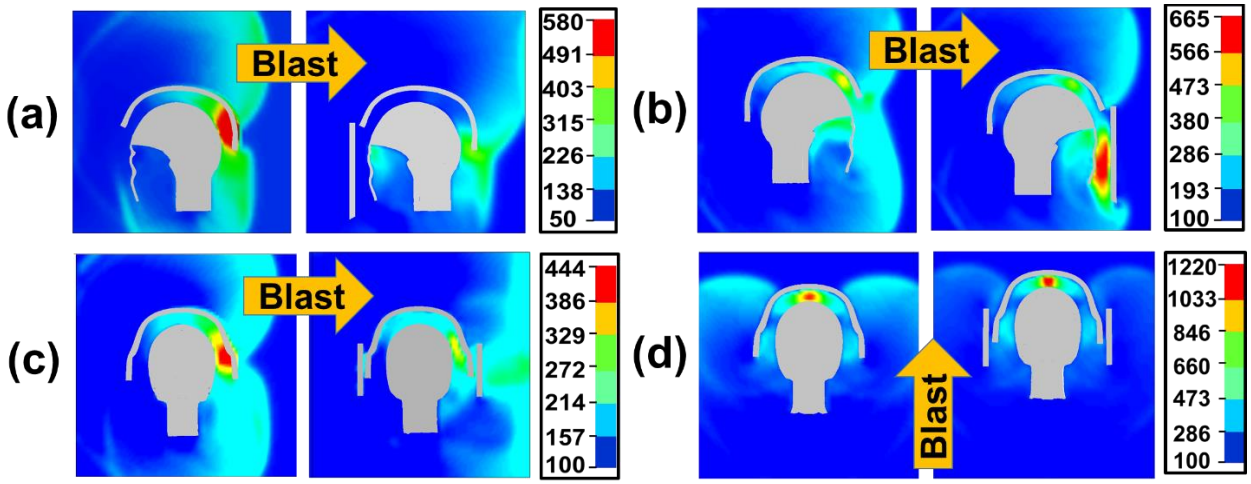

Figure 6.13. Evaluation of underwash incidence of helmeted (left column) and fully-protected head (right column) with respect to blast direction for (a) front; (b) back; (c) side; and (d) bottom blasts

6.2.3. The Effect of Underwash on Skull Pressure and U-ICP

The time history of underwash induced skull pressure (U-skull) and the corresponding U-ICP were evaluated at the underwash locations for all blast directions. This was done to observe the protection potential of the skull at different locations. As shown in Figure 6.14, the U-ICP and skull pressure time history graphs showed to be out of phase with respect to each other, except for the maximum peaks (first peaks) which were observed to be in-phase in all directions. The attenuation of overpressures by the skull showed dependency on both the location of localized pressure waves and the intensity of the waves. Another observation was that the skull pressure time histories for helmeted and fully-protected cases followed a pretty similar pattern in back and bottom blasts, while they showed a minor phase lag in case of the front and bottom

blasts. For the front blast, as shown in Figure 6.14(a), the U-skull (843 kPa) by the helmeted system was attenuated by 60% and induced a U-ICP of 333 kPa. However, for the fully-protected system, the highly attenuated U-skull (267 kPa) decreased by 64% and led to a U-ICP of 96 kPa. Figure 6.14 (b)confirms the assertions of Sarvghad-Moghaddam et al. (2014a) that faceshield has no effect on the tissue response of the brain for the blast from the back. The U-skull for the helmeted (564 kPa) and the fully-protected (538 kPa) systems decreased by 63% and 59% and imposed a U-ICP of 198 kPa and 235 kPa, respectively. However, for the side blast (Figure 6.14 (c)), while the elevated U-skull for the helmeted system (748 kPa) was attenuated by 53% and imposed a U-ICP of 335 kPa, the U-skull in the fully-helmeted system (441 kPa) decreased only by 34% and imposed a U-ICP of 293 kPa. Finally, in the bottom blast (Figure 6.14(d)), the highly-elevated U-skull in both helmeted (1240 kPa) and fully-protected systems (1737 kPa) decreased significantly. They were reduced by 67% and 72% and imposed U-ICPs of 411 kPa and 482 kPa, respectively. These comparisons clearly revealed that due to the geometrical non-uniformity of the skull, it attenuated the underwash induced pressure on its surface to different extents. The highest skull pressure reduction was observed for the fully-protected head in the bottom blast (72%).

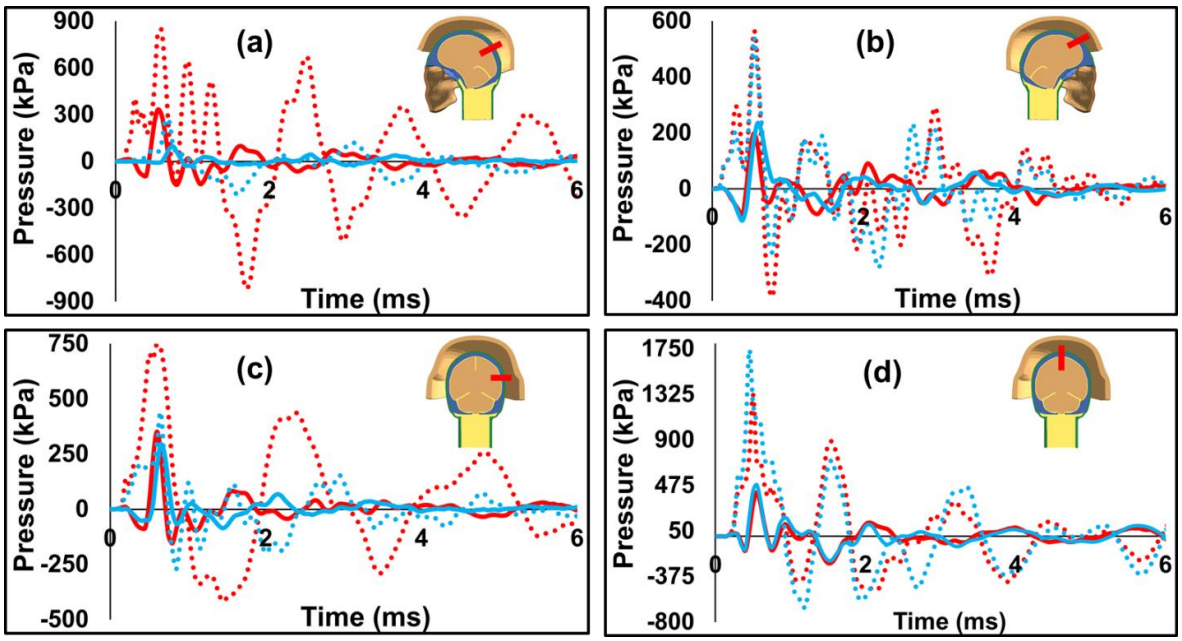

Figure 6.14. The U-Skull (dashed lines) at the countercoup site and the subsequent brain U-ICP (solid lines) due to underwash for (a) front; (b) back; (c) side; and (d) bottom blasts (Red: helmeted, Blue: fully-protected; the red pointer shows the location of underwash induced overpressure on the skull surface and brain)

When a protected head is exposed to blast waves, it may encounter two different types of blast induced peak ICPs; (1) ICP induced upon exposure of head to the incoming primary blast waves which usually happens at the coup site and is measured as the peak ICP (Coup-ICP); (2) ICP that is induced due to the underwash, which was defined earlier as U-ICP, and occurs at the countercoup site. To better delineate the effects of the underwash on the brain response, the U-ICP was compared against the Coup-ICP of the protected heads in Figure 6.15. For the helmeted case, the U-ICP was lower than both the unprotected head's peak ICP and the Coup-ICP of the helmeted head in front, back, and bottom blasts. However, in the side blast, while U-CP (351kPa) was significantly lower than the unprotected head's peak ICP (848 kPa), it was greater than the Coup-ICP (324 kPa), highlighting the importance of underwash considerations in the helmet design. The bottom blast predicted the highest U-ICP (411 kPa) due to the highest underwash overpressure (1053 kPa) in this direction. Moreover, the Coup-ICP of the helmeted

head was greater than that of the unprotected head Sarvghad-Moghaddam et al. (2014a). For the fully-protected head, the variation trend was very similar to the helmeted case, except for the front blast, in which the U-ICP (107 kPa) was very close to the Coup-ICP (96 kPa) due to the reflection of blast waves from the interior surface of the faceshield.

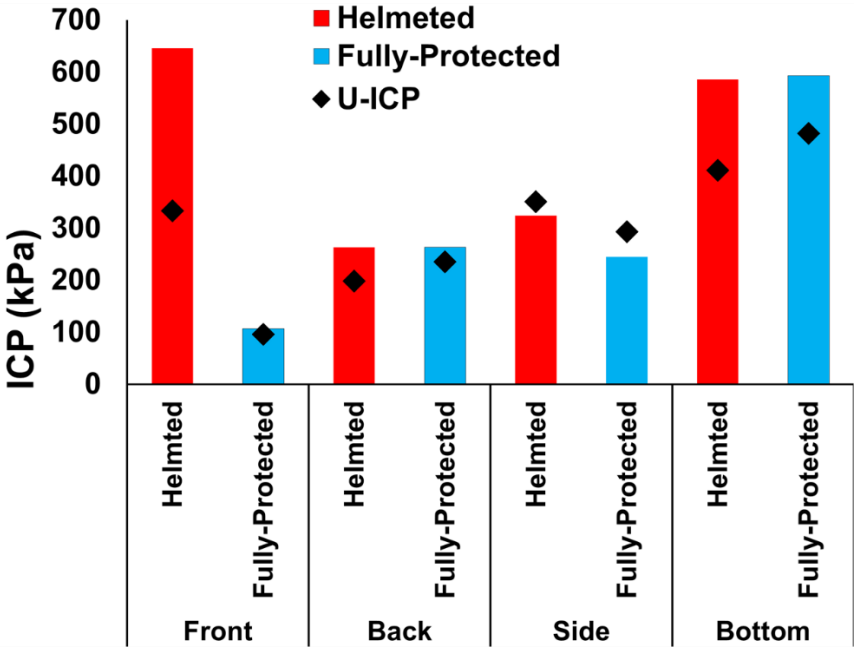

Figure 6.15. Comparison of the peak Coup-ICP of heads due to primary blast waves against the U-ICP due to underwash (diamond markers represent U-ICP)

6.2.4. The Effect of Underwash on the Brain Maximum Shear Stress

Temporal variation of the maximum shear stress (MSS) is shown in Figure 6.16 for all protection levels in all four blast directions, where the location of the MSS in each direction is shown with a colored bullet for each protection level; black, red, and blue bullets represents the unprotected, helmeted, and the fully-protected cases, respectively. Except for the bottom blast (Figure 6.16(d)) in which the MSS for all protection levels occurred at the brain stem, the location of MSS varied in other directions. As shown in Figure 6.16(a), for the front blast, while the MSS was observed at the parietal lobe for the unprotected case, it occurred at the brain stem for both protected heads. Moreover, while the MSS for the fully-protected head was lower than

the one for unprotected head, it was greater than the one for the helmeted system. As shown in Figure 6.16(b) for the back blast, while the MSS was found at the frontal lobe for both unprotected and fully-protected heads, the helmeted head's MSS occurred at the brain stem. Both helmeted and fully-protected systems contributed to the reduction of shear stress in the back blast with respect to the unprotected head. Adversely, these protection systems increased the MSS in the side blast, as shown in Figure 6.16(c), confirming the low tolerance of the head to diffuse injuries for lateral assaults (Sarvghad-Moghaddam et al. 2014a; Zhang et al. 2001b). In the side blast, unlike the unprotected case in which the MSS was seen at the occipital lobe, it was found to be at the brain stem for both protected cases. Finally, the fully-protected case predicted the highest MSS in the bottom blast with respect to all other cases. Although all MSSs were found at the brain stem, the unprotected and helmeted cases predicted pretty close peaks (Figure 6.16(d)) in this direction.

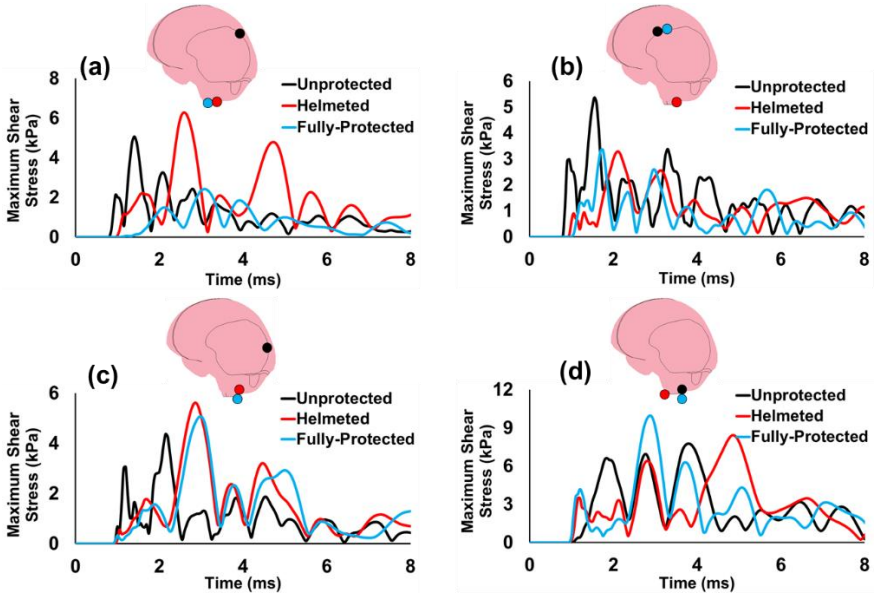

Figure 6.16. Maximum shear stress in brain in (a) front; (b) back; (c) side; (d) bottom blasts

6.2.5. Discussion

The underwash effect of the protective tools and its effects on the tissue response of the brain were investigated. The interaction of unprotected, helmeted, and fully-protected heads with blast shockwaves, with an overpressure (520 kPa) complying with 50% LD_{50} (lethal dose) of lung injury survival, from front, back, side, and bottom directions were simulated. Based on the protection level and the blast direction, while the underwash caused comparable ICP responses in front, back, and bottom blasts, it even increased the peak ICP of the brain in the side blast. For the cases studied, the underwash was observed to not only alter the peak tissue response, but also exacerbate the conditions in some cases, leading to increased chances of concussive injuries.

Ganpule et al. (2012) asserted in their 2-D study that the underwash effect occurred due to the interaction of blast waves inside the helmet gap with those propagating outside. However, our 3D study showed that underwash mainly occurred as the shockwaves scattered in different directions upon entering the gap and interacted at a point inside the gap at the countercoup site and formed a localized pressure region. Using a CFD study, two major phenomena were recognized to affect the formation of underwash region: (1) change of blast flow's momentum due to the change of the flow direction in the helmet curvature (varying radius of curvature); (2) flow separation on the head surface due to the reversed flow region, caused by adverse pressure gradient at this point. The non-uniform geometry of the helmet and faceshield caused different cross-section areas of protective tools to face the incoming waves in each blast direction, and hence the flux of blast waves entering and exiting the gap changed. This implies that the blast directionality effects should be studied in conjunction with protection configurations, i.e., helmeted and fully-protected assemblies.

The study of the underwash overpressure and U-ICP in all blast directions (Figure 6.17) showed that in none of the blast directions, the U-ICP exceeded the peak brain ICP predicted by the unprotected head. As shown in Figure 6.17, the highest and lowest underwash overpressures were predicted for the bottom and side blasts, respectively. In the front blast, while helmet didn't provide much underwash prevention, the fully-protected system prevented underwash by obstructing the shock waves' path into the gap. In the back blast, due to the larger coverage area and the high curvature of the back side of the helmeted system, the influx of the blast waves reduced and caused a lower underwash overpressure. However, for the fully-protected system, an elevated underwash overpressure in the facial region was observed. The reflection of the outgoing waves from the interior surface of the faceshield, the concentration of the pressure waves in nasal and ocular cavities intensified by the reflected waves, and accordingly, transition of more pressure waves into the cranium space were realized as the main reasons. Ganpule et al. (2012) considered three different curvatures for the back of the helmet in a front blast scenario, and observed that the underwash overpressure decreased at lower curvatures. In the current study, the underwash overpressure was found out to be the lowest in the side blast. It was concluded that the step-like structure of helmet sides significantly weakened the incoming shockwaves by diffracting the shockwaves and dissipating their kinetic energy, which in result developed an underwash overpressure lower than the primary blast waves' overpressure. For the bottom blast, however, the entrapment of shockwaves inside both helmet and faceshield at the top of the head was recognized as the main reason for the highest underwash overpressure among the studied directions. Moreover, it was found out that the reflected waves from the shell surface moved towards the localized pressure region and intensified that. That is why the

underwash overpressure in the bottom blast for the fully-protected head was more than twice the incoming blast's overpressure.

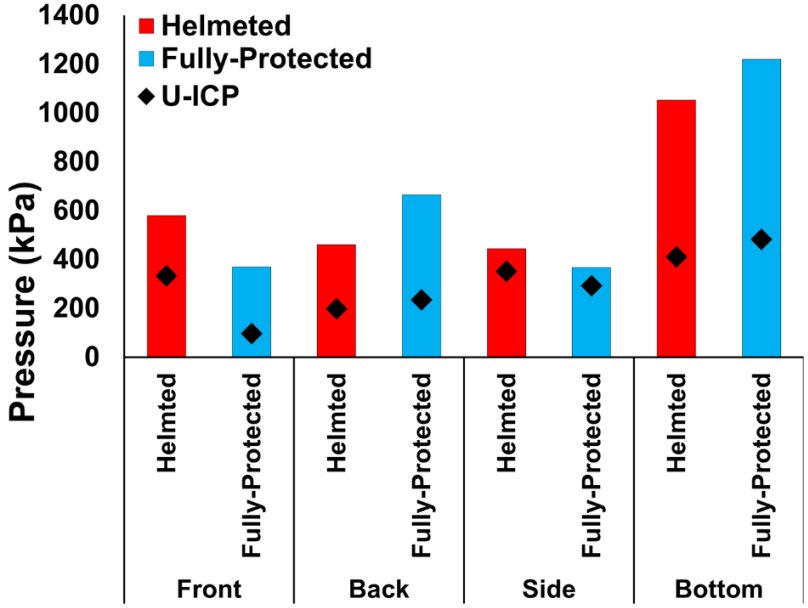

Figure 6.17. Comparison of the underwash overpressure on the head and the corresponding U-ICP in all blast directions (diamond markers represent U-ICP)

The angular and linear accelerations of the head, peak ICP, maximum shear and tensile stresses and strains, skull flexure, cavitation, and the acoustic impedance mismatch have been mentioned as major factors in evaluating the injury risk and level of bTBI (Ganpule et al. 2013; Goeller et al. 2012; Grujicic et al. 2010; Grujicic et al. 2012a; Gu et al. 2012; Moss et al. 2009; Nakagawa et al. 2011; Panzer et al. 2012; Selvan et al. 2013; Zhang et al. 2013a). Hence, two major tissue parameters, ICP and MSS that are responsible for the concussive and diffuse injuries, respectively, were studied in all blast scenarios. Concussive injuries such as contusion mainly occur due to the relative displacement of the brain with respect to skull when the brain collides the skull as the head undergoes acceleration/deceleration (Chafi et al. 2010a; Grujicic et al. 2011; Grujicic et al. 2010; Moore et al. 2009; Zhang et al. 2013a). Diffuse or shear injuries, on the other hand, occur due to the tearing and shear damage of axons as a result of the blast

shear waves (Chafi et al. 2010b; Zhang et al. 2001b).Upon impingement of blast pressure waves on the head, the shear stress waves are induced on the skull and brain tissues, where they are intensified at material interfaces such as skull/CSF and CSF/brain. The stress waves start to travel in the intracranial space from the coup site towards the countercoup site and are weakened as they travel due to reflections that occur at the interfaces of different head components. Loading of the brain tissue is governed by a direct mechanism happening due to transmission of stress waves from the skull, as well as an indirect mechanism occurring as a result of the flexure or deflection of the skull (Selvan et al. 2013). A quick look at Figure 6.14 clearly confirms the effect of underwash overpressure on the response of the skull. For all directions, the helmeted head predicted high pressure profiles on the skull with large oscillations and high positive and negative peaks. This was significantly attenuated for the fully-protected system in front and side blasts as the compressions waves were damped by the faceshield and led to lower skull deformations. Bolander et al. (2011) and Leonardi et al. (2011) stated that ICP oscillations after the initial peak may be linked to the skull deformation. This implies that for the cases studied here, the helmeted head caused more deflections of the skull in most of the cases. Bolander et al. (2011) concluded that the likelihood of neurotrauma within the first 2 ms of exposure to the blast is the highest. Figure 6.14 shows that for the current study, the skull and brain pressure responses were highly affected in this time period due to the underwash. Furthermore, the skull thickness has shown to significantly affect the pressure wave transmission; the thicker the skull, the lower the transmitted waves will be (Selvan et al. 2013) .The skull thickness has a remarkable variation through the head structure (Jue and Masuda 2013). This was clearly observed in our study as the induced surface pressure on the skull at different locations (front, back, side, and top) of the head (due to underwash) was attenuated differently. Skull flexure has been suggested as a major brain

injury mechanism by many researchers (Bolander et al. 2011; Grujicic et al. 2012b; Moss et al. 2009; Selvan et al. 2013; Zhang et al. 2013a). The skull transverse deflections and strains at the underwash locations in the current research (not shown for brevity), showed elevated deformations in all directions. The skull was observed to undergo inward and outward deflections at these locations which was believed to give rise to the extreme positive and negative pressure profiles in the brain. While the inward flexures of the skull imposed increased ICP in the brain, the outward flexures led to the cavitation in CSF and subsequently in the brain tissue. Cavitation has also been introduced as another major brain injury mechanism (Goeller et al. 2012; Grujicic et al. 2011; Panzer et al. 2012).While cavitation mainly occurs at countercoup lesions due to the negative pressure profiles imposed by compressive stress waves, coup cavitation has also been reported for severe pressure waves inside the cranium (El Sayed et al. 2008). Due to underwash, much higher negative pressures profiles were observed at the coup site, i.e., underwash induced more severe coup cavitation injury risks.

The maximum and minimum U-ICPs were found for the bottom, and front blasts, respectively (Figure 6.17). Assuming real-life conditions in which soldiers always protect their heads at least with a helmet, the U-ICP showed comparable, if not greater values (such as in side blast), than the peak Coup-ICP predicted by the protected heads due to primary blast waves (Figure 6.15). Accordingly, it was concluded that while both protection assemblies provided protection in some directions (Grujicic et al. 2010; Nyein et al. 2010; Sarvghad-Moghaddam et al. 2014a; Zhang et al. 2013a), they induced adverse effects in others (Sarvghad-Moghaddam et al. 2014a). The higher U-ICP in the side blast with respect to the Coup-ICP of both protected system due to primary blast waves (despite the lowest underwash overpressure in this direction) was recognized to be due to the decreased tolerance of the brain tissue to lateral assaults. This is

in agreement with the results of several numerical and experimental studies on the brain response to blast and impact loading from different directions (Hodgson et al. 1983; Zhang et al. 2013a; Zhang et al. 2001b). However, the peak U-ICP values in other directions were reported to be comparable to the Coup-ICP of both protected systems. Elkin and Morrison Iii (2007) reported in their experimental study that the brain has a region-specific tolerance. Hence, it was concluded that besides the injury risk due to the Coup-ICP, these comparable U-ICPs could elevate the concussive injury risk at countercoup sites, as well. The blast-induced peak Coup-ICP for the protected heads due to the primary blast overpressure in this study, exceeded the concussive injury threshold of 235 kPa, introduced by Ward et al. (1980), except for the fully-protected head in the front blast. While the recorded U-ICPs also exceeded this pressure threshold in most cases, marginal values for U-ICP were predicted for both protected heads in the back blast. Moreover, while the Coup-ICP was slightly higher than the threshold in the side blast (245 kPa), the underwash elevated the injury risk by increasing the peak ICP to 293 KPa. These two observations implied that underwash may exacerbate the pressure response of the brain at threshold values.

Due to the complicated geometry of the head and protective tools, it is difficult to exactly ascertain the impact of underwash on the shear response of brain. The shear stress pattern was significantly altered upon using the protection systems (Figure 6.16). Except for the fully-protected system in the back blast, the MSS was observed at the brain stem. Clinical studies and pathological researches have shown that the brainstem and corpus callosum are the regions that are most prone to DAI (Adams et al. 1982; Gennarelli et al. 2003). Hence, for the cases studied in this research, the protected heads were observed to be more susceptible to diffuse injuries in

all directions. The shear stress in the bottom blast was observed to be the highest due to higher shear forces induced by the elevated focal pressure region.

The brain acceleration was seen to reduce upon using protection assemblies in all cases. The reason was believed to be due to the backward counter pressure induced by underwash to resist the forward accelerating motion imposed by the primary waves. Moreover, this resulted in lower relative displacement of the brain with respect to the skull for protected cases in all directions. The higher the protection, the lower was the relative displacement.

6.2.6. Conclusion

The underwash effect was realized to occur mainly due to the change of momentum of the blast flow as a result of the curvature change of the helmet in the exit side, as well as the interaction of the travelling waves inside the helmet/faceshield gap at the countercoup site. The underwash overpressure was found to be the highest for the fully-protected head in the bottom blast due to the entrapment of most of the pressure waves in the helmet/faceshield gap, as well as the reflection of these waves from the interior surface of the helmet shell and the faceshield. The faceshield was observed to significantly decrease the underwash overpressure in front and side blasts as it impeded the shockwaves path into the gap. Due to the decreased tolerance of the brain tissue to dynamic loads from lateral sides, the U-ICP was observed to exceed the Coup-ICP in the side blast. Skull showed to significantly attenuate the shockwaves in the bottom blast where the localized pressure waves were formed on top of the head due to underwash. The bottom blast showed to have the highest U-ICP for both protection levels. The back blast, on the other hand, predicted the lowest U-ICP compared to other directions except for the fully-protected case in the front blast. MSS was observed for the bottom blast in which the shear forces of blast were realized to be the highest due to the high pressure region on the skull. It was suggested that

underwash clearly altered the tissue response of the brain as it led to increased ICP levels, imparted elevated skull flexure, and induced high negative pressure which increased the chance of coup-cavitation. Based on the results for the cases studied in this research, it was concluded the directionality considerations should be incorporated in the helmet/faceshield design especially for the sides of the helmet from where the head is most prone to injury. The application of faceshield should be further investigated, as it can induce higher underwash overpressure and even lead to facial injuries.

CHAPTER 7. CONCLUSIONS AND FUTURE WORKS

7.1. Conclusion

The increases of traffic accidents, assaults, and military conflict have raised major concerns about the risk of traumatic brain injury among both civilians and military service members. Moreover, the increase of the explosive devices in the battlefields requires a great attention in developing highly efficient protective tools to protect the soldiers against blast threats. Current protective tools such as helmet and faceshield have shown to be highly effective against high speed projectiles. However, due to the complex mechanics of the blast waves, their efficiency against explosive blast is still not very well-known. The current research employed a novel and comprehensive computational approach to study the mechanical response of the human head and brain to both blunt impacts and blast loads using finite element and computational fluid dynamics analyses. To this end, North Dakota State University Head Model, a detailed 3D FE head model was used and the tissue response if the brain in terms of ICP and shear stress and strains, as well as the head and brain kinematics in terms of the linear acceleration were evaluated. The generation and propagation of the blast wave were accurately simulated in LS-DYNA, and their interactions with the human head were carried out through penalty-based fluid-structure interaction algorithms. The major focus of this research was on exploring the effect of loading conditions such as loading direction and intensity on the mechanical response of the human head and brain; Evaluating the protection efficiency of the head protective tools such as military helmets and faceshields under blast loading, with and without considering the blast parameters such as blast direction; and Understanding the flow mechanics of the blast around the unprotected and protected heads to investigate the mechanism

of the underwash effect of the head protective tools through CFD modeling, and evaluate any possible effect of underwash on brain response through FEA.

The major finding of the research in each category can be summarized as:

1- Effect of Loading Directionality on Brain Response

- While the predicted tissue responses in the front and side impacts were quite close, the brain response to the back impact was significantly lower than those predicted in other scenarios, especially in terms of the shear stress.
- The highest brain acceleration was observed for the front impact signifying that the front impact is counted as the most severe case of head impact.
- The directional dependence of the head response was confirmed as it was observed that for the back impact, the head was less prone to severe injuries, while front and side impacts predicted severe injury conditions.
- The head showed increased tolerance to the diffuse injuries in the back impact while decreased tolerance to diffuse axonal injury (DAI) was observed for both front and side impacts. The maximum shear stress was predicted in the brain stem in all three impact conditions.
- The coup-countercoup pressure, shear stresses, and brain accelerations followed similar patterns for all impact scenarios. It was concluded that the biomechanics of the head impact can be altered by many parameters such as the impact velocity, the location of impact and the geometry of the head.
- Moreover, it was postulated that due to the complicated behavior of the human head under dynamic loads, the tissue level parameters serve as more reliable predictors in defining the injury criteria.

2- Protection Efficiency of Helmet and Faceshield against Blast

- Due to the differences in geometry, function and tolerance of various brain components, directionality effects of blast played an important role in defining the brain response under impulsive loading.
- Protective headgears showed different mitigation capabilities based on the blast orientation. The fully-protected and helmeted systems were shown to be most efficient in front and top blasts, respectively. This was due to impediment of most of the shockwaves. In the bottom blast, the space under the helmet and faceshield accommodated the majority of the blast waves which was also intensified upon reflection from the interior face of the helmet and led to increased pressure on the head and higher ICP and shear stress inside the brain
- The tissue response of the head was altered upon using the protective tools and the bottom blast was found to impose the most severe conditions in terms of transferred mechanical loads to the head.
- Based on current results, it was determined that the faceshield was only effective in front blast, as it imposed either adverse or no effects in other directions. The current findings suggested the need for incorporating the directional dependency of the brain response to dynamic loads in the modular design of military helmets.

3- Mechanics of Shockwave Flow and Underwash Effect Mechanism (CFD Study))

- Regions of concavity, such as nasal regions, were observed to provide suitable locations for the reflection and amplification of the incoming shockwaves.
- For shockwaves approaching from front, back, and side directions, underwash was postulated to occur as a result of the backpressure imposed by the backflow of the exterior flow on the outgoing interior flow. Moreover, in the directional study of the underwash, it was observed

that the smaller outlet for the shockwave out of the helmet (based on the geometry of the helmet in each direction) would lead to lower underwash overpressure due to less backflow of the exterior flow.

- For the shockwaves approaching from the bottom, majority of the shockwaves entered the helmet gap and a small part of them were deviated by the helmet edges. Moreover, the shockwaves were intensified by the interior surface of the helmet like what happens in confined space blasts and along with the high impulse two huge bulks of shockwave flow imposed on each other upon meeting on top of the head, led to an incredibly high overpressure.
- The geometrical discontinuity caused by the helmet edge in the front and back cases, resulted in the development of a reverse flow vortex region (bubble) on the interior surface of the helmet at the front region of the helmet, and consequently, which increased the flow velocity and formed a supersonic flow region
- The shockwave flow was observed to go through a momentum change at the backside and side curve of the helmet in case of the front, back, and side flows. Using the momentum and continuity equation in 2D, a relationship was developed between the applied force on the head in the helmet's curve and the angle of the helmet's curve. It was found that the higher the angle, the greater the underwash overpressure would be.
- The parametric study on the effect of the incident shockwave overpressure on the underwash induced overpressure revealed that the increase rate of the underwash overpressure decreased by increasing the incident overpressure.

- There are some limitations in the current work which should be addressed in future studies, such as studying the effect of helmet pads on preventing the underwash incidence, role of faceshield on underwash and shockwaves flow mechanics.

4- Effect of Underwash on Brain's Mechanical Response (FEA Study)

- The underwash overpressure was found to be the highest for the fully-protected head in the bottom blast due to the entrapment of most of the pressure waves in the helmet/faceshield gap, as well as the reflection of these waves from the interior surface of the helmet shell and the faceshield.
- The faceshield was observed to significantly decrease the underwash overpressure in front and side blasts as it impeded the shockwaves path into the gap. Due to the decreased tolerance of the brain tissue to dynamic loads from lateral sides, the U-ICP was observed to exceed the Coup-ICP in the side blast.
- Skull showed to significantly attenuate the shockwaves in the bottom blast where the localized pressure waves were formed on top of the head due to underwash.
- The bottom blast showed to have the highest U-ICP for both protection levels. The back blast, on the other hand, predicted the lowest U-ICP compared to other directions except for the fully-protected case in the front blast. MSS was observed for the bottom blast in which the shear forces of blast were realized to be the highest due to the high pressure region on the skull.
- It was suggested that underwash clearly altered the tissue response of the brain as it led to increased ICP levels, imparted elevated skull flexure, and induced high negative pressure which increased the chance of coup-cavitation.

- Based on the results for the cases studied in this research, it was concluded the directionality considerations should be incorporated in the helmet/faceshield design especially for the sides of the helmet from where the head is most prone to injury. The application of faceshield should be further investigated, as it can induce higher underwash overpressure and even lead to facial injuries.

7.2. Future Works

The current research provided highly promising outcomes in the study of bTBI. Although the results of the current study contribute to the development of new methods and ideas in the brain injury studies, but there are still many potential area for research.

First of all, development of a more detailed FE head model could greatly help to investigate the mechanism of bTBI as the discretization parameters can significantly affect the pressure and especially shear response of the brain. Moreover, each head model possesses its own unique features, and hence to be able to draw more general conclusions, several head models should be exposed to identical blast loading and the results should be compared.

This study used the most commonly used helmet model by the US military, the Advanced Combat Helmet. Our results showed that while this helmet greatly reduces the risk of the injury, there is still so much room for improvement as the gap of the helmet can help develop unfavorable high pressure region. The mitigation efficiency of the new helmet model (Enhanced Combat Helmet) should be evaluated to assess the replacement of current helmets with that. Moreover, parametric studies should be developed and performed on the effect of geometry and material modification and optimization of the helmet in order to improve its efficiency against blast. Some possible areas include development of a modular design of the helmets based on the injury threshold of the brain in each direction, optimization and improvement of the helmet

padding layout and material by using fluid filler, mixture of foams with different densities, and changing the pad thickness.

Moreover, to better visualize the shockwave flow behavior, interaction of shockwaves generated by the shock tube with the head front different directions and with different helmet geometries in terms of the helmet curvature, inclusion of padding, and gap size can be performed to optimize to develop ideas for the improvement of the helmet design.

Furthermore, as soldiers are encounters with both ballistic and blast threats in the battlefield, one possible to study could be the assessment of the helmet protection when head goes under an identical acceleration due to the ballistic impact and the blast waves. By studying the difference of the mechanism of injury in these two cases, the importance of the tissue responses as injury predictor can be emphasized.

Finally, more attention should be paid to studying different injury mechanisms caused upon the interaction of blast waves with the head, such as cavitation, skull deformation, as well as concussion and diffuse axonal injury through multi-scale analysis of the brain. This could greatly help to understand the post-traumatic stress disorders that bTBI victims are suffering from.

REFERENCES

Aare M, Kleiven S (2007). Evaluation of head response to ballistic helmet impacts using the finite element method. International Journal of Impact Engineering 34:596-608.

Abel JM, Gennarelli TA, Segawa H (1978). Incidence and severity of cerebral concussion in the rhesus monkey following sagittal plane angular acceleration. SAE Technical Paper.

Abolfathi N, Naik A, Sotudeh M, Karami G, Ziejewski M. Diffuse Axonal Injury and Degradation in Mechanical Characteristics of Brain White Matter. In: ASME 2008 Summer Bioengineering Conference, 2008. American Society of Mechanical Engineers, pp 229-230.

Adams JH, Graham DI, Murray LS, Scott G (1982). Diffuse axonal injury due to nonmissile head injury in humans: an analysis of 45 cases Annals of neurology 12:557-563.

Al-Bsharat AS, Hardy WN, Yang KH, Khalil TB, Tashman S, King AI (1999). Brain/skull relative displacement magnitude due to blunt head impact: new experimental data and model. SAE Technical Paper.

Alexander MP (1995). Mild traumatic brain injury: pathophysiology, natural history, and clinical management Neurology, 45:1253-1260.

Anderson RJ (2008). Shell shock: an old injury with new weapons Molecular interventions 8:204.

Anderson RW, Brown C, Blumbergs P, Scott G, Finney J, Jones N, McLean A. Mechanisms of axonal injury: an experimental and numerical study of a sheep model of head impact. In: Proceedings of the International Research Council on the Biomechanics of Injury conference, 1999. International Research Council on Biomechanics of Injury, pp 107-120.

ANSYS C (2012a). Ansys CFX Realease 14.5 User Guide ANSYS Inc.

Ansys C (2012d). Solver Theory Guide, Release 14.5 Ansys Inc, Canonsburg.

Antona-Makoshi J, Davidsson J, Ejima S, Ono K, Brolin K, Anata K. Correlation of Global Head and Brain Tissue Injury Criteria to Experimental Concussion derived from Monkey Head Trauma Experiments. In: IRCOBI Conference, 2013. vol IRC-13-55. pp 509-522.

Anzelius A (1943). The effect of an impact on a spherical liquid mass.

Arundine M, Chopra GK, Wrong A, Lei S, Aarts MM, MacDonald JF, Tymianski M (2003). Enhanced vulnerability to NMDA toxicity in sublethal traumatic neuronal injury in vitro Journal of neurotrauma 20:1377-1395.

Axelsson H, Hjelmqvist H, Medin A, Persson J, Suneson A (2000). Physiological changes in pigs exposed to a blast wave from a detonating high-explosive charge Military medicine 165:119-126.

Bain AC, Meaney DF (2000). Tissue-level thresholds for axonal damage in an experimental model of central nervous system white matter injury. Journal of biomechanical engineering 122:615-622.

Baker WE (1973). Explosions in the Air. University of Texas Pr., Austin

Bala S (2001). Contact Modeling in Ls-Dyna Livermore Software Technology Corporation and FEA Information Inc, Livermore, CA

Bauman RA et al. (2009). An introductory characterization of a combat-casualty-care relevant swine model of closed head injury resulting from exposure to explosive blast. Journal of neurotrauma 26:841-860

Belanger HG, Curtiss G, Demery JA, Lebowitz BK, Vanderploeg RD (2005). Factors moderating neuropsychological outcomes following mild traumatic brain injury: a meta-analysis.

Journal of the International Neuropsychological Society : JINS 11:215-227 doi:10.1017/s1355617705050277.

Belingardi G, Chiandussi G, Gaviglio I. Development and validation of a new finite element model of human head. In: Proc. 19th International Technical Conference of the Enhanced Safety of Vehicle (ESV), Washington, DC, 2005.

Bogo V, Hutton R, Bruner A (1971). The effects of airblast on discriminated avoidance behavior in rhesus monkeys. DTIC Document.

Bolander R, Mathie B, Bir C, Ritzel D, VandeVord P (2011). Skull flexure as a contributing factor in the mechanism of injury in the rat when exposed to a shock wave Annals of biomedical engineering 39:2550-2559.

Bowen IG, Fletcher ER, Richmond DR (1968). Estimate of man's tolerance to the direct effects of air blast.

Boyer D (1960). An experimental study of the explosion generated by a pressurized sphere. Journal of Fluid Mechanics 9:401-429.

Bradshaw D, Morfey C. Pressure and shear response in brain injury models. In: Proceedings of the 17th international technical conference on the enhanced safety of vehicles, Amsterdam, The Netherlands, 2001.

Cater HL, Gitterman D, Davis SM, Benham CD, Morrison B, Sundstrom LE (2007). Stretch-induced injury in organotypic hippocampal slice cultures reproduces in vivo post-traumatic neurodegeneration: role of glutamate receptors and voltage-dependent calcium channels. Journal of neurochemistry 101:434-447.

Cernak I et al. (2011). The pathobiology of blast injuries and blast-induced neurotrauma as identified using a new experimental model of injury in mice. Neurobiology of disease 41:538-551.

Cernak I, Noble-Haeusslein LJ (2010). Traumatic brain injury: an overview of pathobiology with emphasis on military populations Journal of cerebral blood flow and metabolism. official journal of the International Society of Cerebral Blood Flow and Metabolism 30:255-266 doi:10.1038/jcbfm.2009.203.

Cernak I, Radosevic P, Malicevic Z, Savic J (1995). Experimental magnesium depletion in adult rabbits caused by blast overpressure Magnesium research. official organ of the International Society for the Development of Research on Magnesium 8:249-259.

Cernak I, Savic J, Malicevic Z, Zunic G, Radosevic P, Ivanovic I, Davidovic L (1996). Involvement of the central nervous system in the general response to pulmonary blast injury. Journal of Trauma and Acute Care Surgery 40:100S-104S.

Chafi M, Karami G, Ziejewski M (2010a). Biomechanical assessment of brain dynamic responses due to blast pressure waves. Annals of biomedical engineering 38:490-504.

Chafi MS (2009). Biomechanical Analysis of Blast-induced Traumatic Brain Injury Using Multiscale Brain Modeling. ProQuest.

Chafi MS, Dirisala V, Karami G, Ziejewski M (2009). A finite element method parametric study of the dynamic response of the human brain with different cerebrospinal fluid constitutive properties. 223:1003-1019.

Chafi MS, Karami G, Ziejewski M (2010c). Biomechanical assessment of brain dynamic responses due to blast pressure waves. 38:490-504.

Chan HS (1974). Mathematical model for closed head impact. SAE Technical Paper.

Chelluru SK (2007). Finite element simulations of ballistic impact on metal and composite plates.

Claessens M, Sauren F, Wismans J. Modeling of the human head under impact conditions: a parametric study. In: 41st Stapp Car Crash Conference41st Stapp Car Crash Conference, 1997. pp 315-328.

Coats B, Eucker SA, Sullivan S, Margulies SS (2012). Finite element model predictions of intracranial hemorrhage from non-impact, rapid head rotations in the piglet. International Journal of Developmental Neuroscience 30:191-200.

Courtney A, Courtney M (2009). A thoracic mechanism of mild traumatic brain injury due to blast pressure waves. Medical Hypotheses 72:76-83.

Damon EG, Gaylord CS, Hicks W, Yelverton JT, Richmond DR (1966). The Effect of Ambient Pressure on Tolerance of Mammals to Air Blast. DTIC Document.

Daneshvar DH, Baugh CM, Nowinski CJ, McKee AC, Stern RA, Cantu RC (2011). Helmets and mouth guards: the role of personal equipment in preventing sport-related concussions. Clinics in sports medicine 30:145-163.

Daniel RW, Rowson S, Duma SM (2012). Head impact exposure in youth football. Annals of biomedical engineering 40:976-981.

Deck C, Willinger R (2008). Improved head injury criteria based on head FE model. International Journal of Crashworthiness 13:667-678.

DePalma RG, Burris DG, Champion HR, Hodgson MJ (2005). Blast injuries N Engl J Med 352:1335-1342.

Dirisala V (2009). A Biomechanical finite element analysis of head and neck under external loadings: A parametric study of brain response. North Dakota State University.

Dirisala V, Karami G, Ziejewski M (2012). Effects of neck damping properties on brain response underimpact loading. International Journal for Numerical Methods in Biomedical Engineering 28:472-494.

Dwivedi A, Bradley J, Casem D (2012). Mechanical Response of Polycarbonate with Strength Model Fits. DTIC Document.

El Sayed T, Mota A, Fraternali F, Ortiz M (2008). Biomechanics of traumatic brain injury. Computer Methods in Applied Mechanics and Engineering 197:4692-4701.

Elkin BS, Ilankovan A, Morrison B (2010). Age-dependent regional mechanical properties of the rat hippocampus and cortex. Journal of biomechanical engineering 132:011010.

Elkin BS, Morrison Iii B (2007). Region-specific tolerance criteria for the living brain. Stapp Car Crash J 51:127-138.

Faul M, Xu L, Wald MM, Coronado V (2010). Traumatic Brain Injury in the United States Atlanta, GA: Centers for Disease Control and Prevention, National Center for Injury Prevention and Control.

Finnie J, Blumbergs P (2002). Traumatic brain injury Veterinary Pathology Online 39:679-689.

Franklyn M, Fildes B, Zhang L, Yang K, Sparke L (2005). Analysis of finite element models for head injury investigation: reconstruction of four real-world impacts. Stapp Car Crash J 49:1-32.

Fritz HG, Walter B, Holzmayr M, Brodhun M, Patt S, Bauer R (2005). A pig model with secondary increase of intracranial pressure after severe traumatic brain injury and temporary blood loss. Journal of neurotrauma 22:807-821.

Gadd CW (1966). Use of a weighted-impulse criterion for estimating injury hazard. SAE Technical Paper.

Galbraith J, Thibault L, Matteson D (1993). Mechanical and electrical responses of the squid giant axon to simple elongation. Journal of biomechanical engineering 115:13-22.

Ganpule S, Alai A, Plougonven E, Chandra N (2013). Mechanics of blast loading on the head models in the study of traumatic brain injury using experimental and computational approaches. Biomechanics and Modeling in Mechanobiology 12:511-531.

Ganpule S, Gu L, Alai A, Chandra N (2012). Role of helmet in the mechanics of shock wave propagation under blast loading conditions. Computer methods in biomechanics and biomedical engineering 15:1233-1244 doi:10.1080/10255842.2011.597353.

Geddes DM, Cargill RS (2001). An in vitro model of neural trauma: device characterization and calcium response to mechanical stretch. Journal of biomechanical engineering 123:247-255.

Gennarelli T, Adams J, Graham D (1981). Acceleration induced head injury in the monkey. I. The model, its mechanical and physiological correlates. In: Experimental and Clinical Neuropathology. Springer, pp 23-25.

Gennarelli TA, Pintar FA, Yoganandan N. Biomechanical tolerances for diffuse brain injury and a hypothesis for genotypic variability in response to trauma. In, 2003 2003. Association for the Advancement of Automotive Medicine, p 624.

Gilchrist MD, O'Donoghue D, Horgan T (2001). A two-dimensional analysis of the biomechanics of frontal and occipital head impact injuries. International Journal of Crashworthiness 6:253-262.

Goeller J, Wardlaw A, Treichler D, O'Bruba J, Weiss G (2012). Investigation of cavitation as a possible damage mechanism in blast-induced traumatic brain injury. Journal of neurotrauma 29:1970-1981.

Goldsmith W (2001). Impact. Courier Corporation.

Goldstein LE, McKee AC, Stanton PK (2014). Considerations for animal models of blast-related traumatic brain injury and chronic traumatic encephalopathy. Alzheimer's research & therapy 6:64.

Got C, Patel A, Fayon A, Tarriere C, Walfisch G (1978). Results of experimental head impacts on cadavers: the various data obtained and their relations to some measured physical parameters. SAE Technical Paper.

Greenwald RM, Gwin JT, Chu JJ, Crisco JJ (2008). Head impact severity measures for evaluating mild traumatic brain injury risk exposure. Neurosurgery 62:789.

Grujicic M, Bell WC, Pandurangan B, Glomski PS (2011). Fluid/Structure Interaction Computational Investigation of Blast-Wave Mitigation Efficacy of the Advanced Combat Helmet. Journal of Materials Engineering and Performance 20:877-893.

Grujicic M, Bell WC, Pandurangan B, He T (2010). Blast-wave impact-mitigation capability of polyurea when used as helmet suspension-pad material. Materials & Design 31:4050-4065.

Grujicic M, d'Entremont BP, Pandurangan B, Runt J, Tarter J, Dillon G (2012a). Concept-Level Analysis and Design of Polyurea for Enhanced Blast-Mitigation Performance. Journal of Materials Engineering and Performance 21:2024-2037.

Grujicic M, Pandurangan B, Bell WC, Bagheri S (2012b). Shock-Wave Attenuation and Energy-Dissipation Potential of Granular Materials. Journal of Materials Engineering and Performance 21:167-179.

Gu L, Chafi MS, Ganpule S, Chandra N (2012). The influence of heterogeneous meninges on the brain mechanics under primary blast loading. 43:3160-3166.

Gupta RK, Przekwas AJ (2014). multiscale modeling of blast induced traumatic brain injury: from whole body responses to brain microdamage.

Gupta RK, Przekwas AJ (2015). A Framework for Multiscale Modeling of Warfighter Blast Injury Protection.

Gurdjian E, Lissner H, Latimer F, Haddad B, Webster J (1953). Quantitative Determination of Acceleration and Intracranial Pressure in Experimental Head Injury. Preliminary Report Neurology 3:417-417.

Hallquist JO (2007). LS-DYNA keyword user's manual Livermore Software Technology Corporation 970.

Hardy CH, Marcal PV (1973). Elastic analysis of a skull. Journal of Applied Mechanics 40:838-842.

Hardy WN, Foster CD, Mason MJ, Yang KH, King AI, Tashman S (2001). Investigation of Head Injury Mechanisms Using Neutral Density Technology and High-Speed Biplanar X-ray. Stapp Car Crash Journal 45:337-368.

Hardy WN et al. (2007). A study of the response of the human cadaver head to impact. Stapp car crash journal 51:17.

Ho J, Kleiven S (2007). Dynamic response of the brain with vasculature: a three-dimensional computational study. Journal of Biomechanics 40:3006-3012.

Hodgson VR, Thomas LM, Khalil TB (1983). The role of impact location in reversible cerebral concussion. SAE Technical Paper.

Horgan TJ, Gilchrist MD (2003). The creation of three-dimensional finite element models for simulating head impact biomechanics. 8:353-366.

Hosey RR, Liu YK (1982) A homeomorphic finite element model of the human head and neck. Finite elements in biomechanics:379-401.

Jacobs MJN, Van Dingenen JLJ (2001). Ballistic protection mechanisms in personal armour. 36:3137-3142.

Javid S, Rezaei A, Karami G (2014). A micromechanical procedure for viscoelastic characterization of the axons and ECM of the brainstem journal of the mechanical behavior of biomedical materials. 30:290-299.

Jazi MS, Rezaei A, Karami G, Azarmi F, Ziejewski M (2013a). A computational study of influence of helmet padding materials on the human brain under ballistic impacts. Computer methods in biomechanics and biomedical engineering:1-15 doi:10.1080/10255842.2012.748755.

Jazi MS, Rezaei A, Karami G, Azarmi F, Ziejewski M (2013h). A computational study on biomechanics of brain of a helmeted human head model exposed to blast waves from different orientations.

Jazi MS, Rezaei A, Karami G, Azarmi F, Ziejewski M. Effects of Attached Body on Biomechanical Response of the Helmeted Human Head Under Blast. In: ASME 2013 International Mechanical Engineering Congress and Exposition, 2013i. American Society of Mechanical Engineers, pp V03AT03A077-V003AT003A077.

Jean A, Nyein MK, Zheng JQ, Moore DF, Joannopoulos JD, Radovitzky R (2014). An animal-to-human scaling law for blast-induced traumatic brain injury risk assessment. Proceedings of the National Academy of Sciences 111:15310-15315.

Ji S et al. (2014). Parametric comparisons of intracranial mechanical responses from three validated finite element models of the human head. Annals of biomedical engineering 42:11-24.

Jue T, Masuda K (2013). Application of near infrared spectroscopy in biomedicine. Springer.

Kabadi SV, Hilton GD, Stoica BA, Zapple DN, Faden AI (2010). Fluid-percussion-induced traumatic brain injury model in rats Nature protocols 5:1552-1563.

Kang H-S, Willinger R, Diaw BM, Chinn B (1997). Validation of a 3D anatomic human head model and replication of head impact in motorcycle accident by finite element modeling. SAE Technical Paper.

Karami G (2011) Blast and the Consequences on Traumatic Brain Injury-Multiscale Mechanical Modeling of Brain. DTIC Document.

Kenner V, Goldsmith W (1972) Dynamic loading of a fluid-filled spherical shell. International Journal of Mechanical Sciences 14:557-568.

Khalil TB, Hubbard RP (1977). Parametric study of head response by finite element modeling. Journal of Biomechanics 10:119-132.

Kilbourne M et al. (2009) Novel model of frontal impact closed head injury in the rat. Journal of neurotrauma 26:2233-2243.

King AI, Yang KH, Zhang L, Hardy W, Viano DC. Is head injury caused by linear or angular acceleration. In: IRCOBI conference, 2003. pp 1-12.

Kleiven S (2007). Predictors for traumatic brain injuries evaluated through accident reconstructions. Stapp Car Crash J 51:81-114.

Kleiven S, Hardy WN (2002). Correlation of an FE Model of the Human Head with Local Brain Motion--Consequences for Injury Prediction. Stapp Car Crash Journal:123-144.

Kramer F, Appel H. Evaluation of protection criteria on the basis of statistical biomechanics. In: International IRCOBI Conference on the Biomechanics of Impacts, 1990, Bron, France, 1990.

Kulkarni SG, Gao XL, Horner SE, Zheng JQ, David NV (2013). Ballistic helmets – Their design, materials, and performance against traumatic brain injury. Composite Structures 101:313-331.

Kumaria A, Tolias C (2008). In vitro models of neurotrauma. British journal of neurosurgery 22:200-206.

Laker SR (2011). Epidemiology of concussion and mild traumatic brain injury. PM&R 3:S354-S358.

Lamy M, Baumgartner D, Willinger R, Yoganandan N, Stemper BD. Study of mild traumatic brain injuries using experiments and finite element modeling. In: Annals of Advances in Automotive Medicine/Annual Scientific Conference, 2011. Association for the Advancement of Automotive Medicine, p 125.

LaPlaca MC, Thibault LE (1998). Dynamic mechanical deformation of neurons triggers an acute calcium response and cell injury involving the N-methyl-D-aspartate glutamate receptor Journal of neuroscience research 52:220-229.

Lee H, Gong S (2010). Finite element analysis for the evaluation of protective functions of helmets against ballistic impact. Computer methods in biomechanics and biomedical engineering 13:537-550.

Lee M-C, Melvin JW, Ueno K (1987). Finite element analysis of traumatic subdural hematoma. SAE Technical Paper.

Leonardi ADC, Bir CA, Ritzel DV, VandeVord PJ (2011). Intracranial pressure increases during exposure to a shock wave Journal of neurotrauma 28:85-94.

Li K, Cao Y-X, Yang Y-Q, Yin Z-Y, Zhao H, Wang L-j (2012). Establishment of a blunt impact-induced brain injury model in rabbits. Chinese journal of traumatology 15:100-104.

Liu H, Kang J, Chen J, Li G, Li X, Wang J (2012). Intracranial Pressure Response to Non-Penetrating Ballistic Impact: An Experimental Study Using a Pig Physical Head Model and Live Pigs. International journal of medical sciences 9:655.

Long JB, Bentley TL, Wessner KA, Cerone C, Sweeney S, Bauman RA (2009). Blast overpressure in rats: recreating a battlefield injury in the laboratory Journal of neurotrauma 26:827-840.

Löwenhielm P (1974). Strain tolerance of the Vv. Cerebri Sup.(bridging veins) calculated from head-on collision tests with cadavers .Zeitschrift für Rechtsmedizin 75:131-144

Löwenhielm P (1975). Mathematical simulation of gliding contusions. Journal of Biomechanics 8:351-356.

LS-DYNA (2007). LS-DYNA keyword user manual, Version 971. Livermore Software Technology Corporation, Livermore, California.

Macnab A, Smith T, Gagnon F, Macnab M (2002). Effect of helmet wear on the incidence of head/face and cervical spine injuries in young skiers and snowboarders. Injury prevention 8:324-327.

Mao H, Zhang L, Yang KH, King AI (2006). Application of a finite element model of the brain to study traumatic brain injury mechanisms in the rat. Stapp car crash journal 50:583-600.

Margulies SS, Thibault LE (1992). A proposed tolerance criterion for diffuse axonal injury in man. Journal of Biomechanics 25:917-923.

Marjoux D, Baumgartner D, Deck C, Willinger R (2008). Head injury prediction capability of the HIC, HIP, SIMon and ULP criteria. Accident Analysis & Prevention 40:1135-1148.

Martini F (2005). Human anatomy-/Frederic H. Martini, Michael J. Timmons, Robert B. Tallitsch; with William C. Ober...[etc.]. San Francisco, PA [etc.]: Pearson/Benjamin Cummings.

McElhaney JH, Mate PI, Roberts VL (1973). A New Crash Test Device-"Repeatable Pete". SAE Technical Paper.

McIntosh A, Kallieris D, Mattern R, Miltner E (1993). Head and neck injury resulting from low velocity direct impact. SAE Technical Paper.

Meaney DF, Morrison B, Bass CD (2014). The mechanics of traumatic brain injury: a review of what we know and what we need to know for reducing its societal burden. Journal of biomechanical engineering 136:021008.

Melvin JW, Lighthall JW (2002). Brain-injury biomechanics. In: Accidental Injury. Springer, pp 277-302.

Mendis K, Stalnaker R, Advani S (1995). A constitutive relationship for large deformation finite element modeling of brain tissue. Journal of Biomechanical Engineering 117:279.

Menter FR (1994). Two-equation eddy-viscosity turbulence models for engineering applications. AIAA journal 32:1598-1605.

Meyers MA (1994). Dynamic behavior of materials. John Wiley & Sons.

Miller K, Chinzei K, Orssengo G, Bednarz P (2000). Mechanical properties of brain tissue in-vivo: experiment and computer simulation. J Biomech 33:1369-1376.

Miller RT, Margulies SS, Leoni M, Nonaka M, Chen X, Smith DH, Meaney DF (1998). Finite element modeling approaches for predicting injury in an experimental model of severe diffuse axonal injury. SAE Technical Paper.

Moochhala SM, Md S, Lu J, Teng C-H, Greengrass C (2004). Neuroprotective role of aminoguanidine in behavioral changes after blast injury. Journal of Trauma and Acute Care Surgery 56:393-403.

Moore DF, Jérusalem A, Nyein M, Noels L, Jaffee MS, Radovitzky RA (2009). Computational biology—modeling of primary blast effects on the central nervous system. Neuroimage 47:T10-T20.

Morrison B, Cater HL, Benham CD, Sundstrom LE (2006). An in vitro model of traumatic brain injury utilising two-dimensional stretch of organotypic hippocampal slice cultures. Journal of neuroscience methods 150:192-201.

Morrison III B, Elkin BS, Dollé J-P, Yarmush ML (2011). In vitro models of traumatic brain injury. Annual review of biomedical engineering 13:91-126

Moss WC, King MJ (2011). Impact response of US Army and National Football League helmet pad systems. DTIC Document.

Moss WC, King MJ, Blackman EG (2009). Skull flexure from blast waves: a mechanism for brain injury. with implications for helmet design 103:108702.

Mott D, Schwer D, Young T, Levine J, Dionne J-P, Makris A, Hubler G. Blast-induced pressure fields beneath a military helmet for non-lethal threats. In: APS Division of Fluid Dynamics Meeting Abstracts, 2008.

Mundie TG, Dodd KT, Lagutchik MS, Morris JR, Martin D (2000). Effects of blast exposure on exercise performance in sheep. Journal of Trauma and Acute Care Surgery 48:1115-1121.

Nahum AM, Smith R (1977). Intracranial pressure dynamics during head impact. Paper presented at: Proceedings of 21st Stapp car crash conference; New Orleans, LA, USA SAE paper no 770922 Warrendale, PA: Society of Automotive Engineering.

Nahum AM, Smith R, Ward CC (1977). Intracranial pressure dynamics during head impact. SAE Technical Paper.

Nahum AM, Smith RW (1976). An experimental model for closed head impact injury. SAE Technical Paper.

Nakagawa A et al. (2011). Mechanisms of primary blast-induced traumatic brain injury: insights from shock-wave research. Journal of neurotrauma 28:1101-1119.

Newman J. A generalized acceleration model for brain injury threshold (GAMBIT). In: Proc. IRCOBI Conf, 1986. pp 121-131.

Newman J, Barr C, Beusenberg MC, Fournier E, Shewchenko N, Welbourne E, Withnall C A. new biomechanical assessment of mild traumatic brain injury. Part 2: results and

conclusions. In: Proceedings of the International Research Council on the Biomechanics of Injury conference, 2000a. International Research Council on Biomechanics of Injury.

Newman JA, Shewchenko N, Welbourne E (2000b). A proposed new biomechanical head injury assessment function-the maximum power index. Stapp car crash journal 44:215-247.

Nickell R, Marcal P (1974). In-Vacuo modal dynamic response of the human skull. Journal of Manufacturing Science and Engineering 96:490-494.

Nilsson P, Laursen H, Hillered L, Hansen A (1996). Calcium movements in traumatic brain injury: the role of glutamate receptor-operated ion channels. Journal of Cerebral Blood Flow & Metabolism 16:262-270.

Nusholtz GS, Lux P, Kaiker P, Janicki MA (1984). Head impact response—skull deformation and angular accelerations. SAE Technical Paper.

Nyein MK, Jason AM, Yu L, Pita CM, Joannopoulos JD, Moore DF, Radovitzky RA (2010). In silico investigation of intracranial blast mitigation with relevance to military traumatic brain injury. Proceedings of the National Academy of Sciences.

O'Connor WT, Smyth A, Gilchrist MD (2011). Animal models of traumatic brain injury: a critical evaluation. Pharmacology & therapeutics 130:106-113.

Okie S (2005). Traumatic Brain Injury in the War Zone. N Engl J Med 352:2043-2047.

Ommaya AK, Hirsch AE, Yarnell P, Harris EH (1967). Scaling of experimental data on cerebral concussion in sub-human primates to concussion threshold for man. DTIC Document.

Ono K, Kikuchi A, Nakamura M, Kobayashi H, Nakamura N (1980). Human head tolerance to sagittal impact reliable estimation deduced from experimental head injury using subhuman primates and human cadaver skulls. SAE Technical Paper.

Panzer MB, Myers BS, Capehart BP, Bass CR (2012). Development of a finite element model for blast brain injury and the effects of CSF cavitation 40:1530-1544.

Pena A, Pickard J, Stiller D, Harris N, Schuhmann M (2005). Brain tissue biomechanics in cortical contusion injury: a finite element analysis. In: Intracranial Pressure and Brain Monitoring XII. Springer, pp 333-336.

Pike JA (1990). Automotive safety-Anatomy, Injury, Testing and Regulation vol 103.

Post A, Oeur A, Hoshizaki B, Gilchrist MD (2013). Examination of the relationship between peak linear and angular accelerations to brain deformation metrics in hockey helmet impacts. Computer methods in biomechanics and biomedical engineering 16:511-519.

Povlishock J, Marmarou A, McIntosh T, Trojanowski J, Moroi J (1997). Impact acceleration injury in the rat: evidence for focal axolemmal change and related neurofilament sidearm alteration. Journal of Neuropathology & Experimental Neurology 56:347-359.

Prasad P, Mertz HJ (1985). The position of the United States delegation to the ISO Working Group 6 on the use of HIC in the automotive environment. SAE Technical Paper.

Przekwas A, Tan X, Harrand V, Reeves D, Chen Z, Sedberry K, Chancey V. Integrated experimental and computational framework for the development and validation of blast wave brain biomechanics and helmet protection. In: Proc. HFM-207 NATO Symposium on a Survey of Blast Injury Across the Full Landscape of Military Science, 2011.

Qiao P, Yang M, Bobaru F (2008). Impact mechanics and high-energy absorbing materials: review. Journal of Aerospace Engineering 21:235-248.

Rafaels K, Shridharani J, Bass C, Salzar R, Walilko T, Wood G, Panzer M. Blast wave attenuation: ballistic protective helmets and the head. In: Personal Armour Systems Symposium, 2010. PASS Quebec City, QC.

Ramasamy MA, Hill CAM, Masouros S, Gibb L-CI, Phillip L-CR, Bull AM, Clasper CJC (2013). Outcomes of IED foot and ankle blast injuries. The Journal of Bone & Joint Surgery 95:e25.

Release A (2012). 14.5, ANSYS Inc Canonsburg, USA.

Rezaei A, Karami G, Ziejewski M. Effect of initial ramp rate in the performance of quasi-linear viscoelastic theory on brain tissue characterization. In: brain injury, 2014a. vol 5-6. informa healthcare telephone house, 69-77 paul street, london ec2a 4LQ, ENGLAND, pp 659-659.

Rezaei A, Salimi Jazi M, Karami G (2014b). Computational modeling of human head under blast in confined and open spaces: primary blast injury International journal for numerical methods in biomedical engineering 30:69-82.

Rezaei A, Salimi Jazi M, Karami G, Ziejewski M (2014d). A computational study on brain tissue under blast: primary and tertiary blast injuries. International journal for numerical methods in biomedical engineering 30:781-795.

Richmond DR, Damon EG, Bowen IG, Fletcher ER, White CS (1966). Air-blast studies with eight species of mammals. DTIC Document.

Rigas F, Sklavounos S (2005). Experimentally validated 3-D simulation of shock waves generated by dense explosives in confined complex geometries Journal of hazardous materials 121:23-30.

Rizzetti A, Kallieris D, Schiemann P, Mattern R. Response and injury severity of the head-neck unit during a low velocity head impact. In: Proceedings of the International Research Council on the Biomechanics of Injury conference, 1997. International Research Council on Biomechanics of Injury, pp 193-206.

Rossaint J, Rossaint R, Weis J, Fries M, Rex S, Coburn M (2009). Propofol: neuroprotection in an in vitro model of traumatic brain injury. Crit Care 13:R61.

Rostami E (2012). Traumatic brain injury in humans and animal models.

Ruan J, Khalil T, King A (1991). Human head dynamic response to side impact by finite element modeling. Journal of Biomechanical Engineering 113:276-283.

Ruan J, Khalil T, King AI (1994). Dynamic response of the human head to impact by three-dimensional finite element analysis. Journal of biomechanical engineering 116:44-50.

Ruan JS, Khalil TB, King AI (1993). Finite element modeling of direct head impact. SAE Technical Paper.

Sadasivan S, Dunn WA, Hayes RL, Wang KK (2008). Changes in autophagy proteins in a rat model of controlled cortical impact induced brain injury. Biochemical and biophysical research communications 373:478-481.

Sahler CS, Greenwald BD (2012). Traumatic brain injury in sports: a review Rehabilitation research and practice 2012.

Salimi Jazi M, Rezaei A, Karami G, Azarmi F (2014). Biomechanical parameters of the brain under blast loads with and without helmets. International Journal of Experimental and Computational Biomechanics 2:223-244.

Säljö A, Bao F, Jingshan S, Hamberger A, Hansson H-A, Haglid KG (2002). Exposure to short-lasting impulse noise causes neuronal c-Jun expression and induction of apoptosis in the adult rat brain. Journal of neurotrauma 19:985-991.

Salvador E, Neuhaus W, Foerster C (2013). Stretch in brain microvascular endothelial cells (cEND) as an in vitro traumatic brain injury model of the blood brain barrier. Journal of visualized experiments: JoVE.

Sarvghad-Moghaddam H, Jazi MS, Rezaei A, Karami G, Ziejewski M (2014a). Examination of the protective roles of helmet/faceshield and directionality for human head under blast waves. Computer methods in biomechanics and biomedical engineering:1-10.

Sarvghad-Moghaddam H, Karami G, Ziejewski M. The Effects of Directionality of Blunt Impacts on Mechanical Response of the Brain. In: ASME 2014 International Mechanical Engineering Congress and Exposition, 2014j. American Society of Mechanical Engineers, pp V003T003A013-V003T003A013.

Sauaia A, Moore FA, Moore EE, Moser KS, Brennan R, Read RA, Pons PT (1995). Epidemiology of trauma deaths: a reassessment Journal of Trauma and Acute Care Surgery 38:185-193.

Scalea TM (2005). Does it matter how head-injured patients are resuscitated Neurotrauma: evidence-based answers to common questions New York: Thieme.

Selvan V, Ganpule S, Kleinschmit N, Chandra N (2013). Blast wave loading pathways in heterogeneous material systems–experimental and numerical approaches. Journal of biomechanical engineering 135:061002.

Sharma S (2011). Biomechanical analysis of blast induced traumatic brain injury---A finite element modeling and validation study of blast effects on human brain. Wayne state university.

Shepard SR, Ghajar JB, Giannuzzi R, Kupferman S, Hariri RJ (1991). Fluid percussion barotrauma chamber: a new in vitro model for traumatic brain injury. Journal of Surgical Research 51:417-424.

Shreiber DI, Bain AC, Meaney DF (1997). In vivo thresholds for mechanical injury to the blood-brain barrier. SAE Technical Paper.

Shugar T (1975). Transient structural response of the linear skull-brain system. SAE Technical Paper.

Shugar TA, Katona MG (1975). Development of finite element head injury model. Journal of the Engineering Mechanics Division 101:223-239.

Sklavounos S, Rigas F (2004). Computer simulation of shock waves transmission in obstructed terrains. Journal of Loss Prevention in the Process Industries 17:407-417.

Souli M, Ouahsine A, Lewin L (2000). ALE formulation for fluid–structure interaction problems. Computer methods in applied mechanics and engineering 190:659-675.

St Clair V, Chinn B (2007). Assessment of current bicycle helmets for the potential to cause rotational injury Published Project Report PPR213.

Stalnaker R, Melvin J, Nusholtz G, Alem N, Benson J (1977). Head impact response. SAE Technical Paper.

Stone R (2013). Advanced Combat Helmet Technical Assessment. DTIC Document,

Tabacu S (2015). Numerical model (switchable/dual model) of the human head for rigid body and finite elements applications. Computer methods in biomechanics and biomedical engineering 18:769-781.

Taber KH, Warden DL, Hurley RA (2006). Blast-related traumatic brain injury: what is known?. The Journal of neuropsychiatry and clinical neurosciences 18:141-145 doi:10.1176/appi.neuropsych.18.2.141.

Takhounts EG, Eppinger RH, Campbell JQ, Tannous RE (2003). On the development of the SIMon finite element head model. Stapp car crash journal 47:107.

Tan LB, Tse KM, Lee HP, Tan VBC, Lim SP (2012). Performance of an advanced combat helmet with different interior cushioning systems in ballistic impact: Experiments and finite element simulations. International Journal of Impact Engineering 50:99-112.

Tanielian TL, Jaycox L (2008). Invisible wounds of war: Psychological and cognitive injuries, their consequences, and services to assist recovery vol 1. Rand Corporation.

Taylor PA, Ford CC (2009). Simulation of blast-induced early-time intracranial wave physics leading to traumatic brain injury. Journal of biomechanical engineering 131:061007.

Taylor PA, Ludwigsen JS, Ford CC (2014). Investigation of blast-induced traumatic brain injury. Brain injury 28:879-895.

Tham CY, Tan VBC, Lee HP (2008). Ballistic impact of a KEVLAR® helmet: Experiment and simulations International. Journal of Impact Engineering 35:304-318.

Trosseille X, Tarriere C, Lavaste F, Guillon F, Domont A (1992). Development of a FEM of the human head according to a specific test protocol. SAE Technical Paper.

Tse KM, Lim SP, Tan VBC, Lee HP. A review of head injury and finite element head models.

Ueno K, Melvin J, Lundquist E, Lee M (1989). Two-dimensional finite element analysis of human Brain Impact Responses: Application of a Scaling Law Crashworthiness and Occupant Protection in Transportation Systems, Ed TB Khalil, AMD-Vol 106:123-124.

Van Hoof J, Cronin D, Worswick M, Williams K, Nandlall D. Numerical head and composite helmet models to predict blunt trauma. In: Proceedings of 19th international symposium on ballistics, 2001. pp 7-11.

Varas JM, Philippens M, Meijer S, Van Den Berg A, Sibma P, Van Bree J, De Vries D (2011). Physics of IED blast shock tube simulations for mTBI research Frontiers in neurology 2.

Versace J (1971). A review of the severity index. SAE Technical Paper.

Viano DC, Casson IR, Pellman EJ (2007). Concussion in professional football: biomechanics of the struck player—part 14 Neurosurgery 61:313-328.

Walsh MJ, Kelleher BJ, Severin CM (1985). Head and neck injuries in human cadavers from lateral impacts. SAE Technical Paper.

Walsh SM, Scott BR, Spagnuolo DM (2005). The development of a hybrid thermoplastic ballistic material with application to helmets. DTIC Document.

Ward C, Chan M, Nahum A (1980). Intracranial pressure–a brain injury criterion. SAE Technical Paper.

Ward CC, Thompson RB (1975). The development of a detailed finite element brain model. SAE Technical Paper.

White FM, Corfield I (2006). Viscous fluid flow vol 3. McGraw-Hill New York.

Willinger R, Baumgartner D (2003). Numerical and physical modelling of the human head under impact-towards new injury criteria International journal of vehicle design 32:94-115.

Willinger R, Kang H-S, Diaw B (1999). Three-dimensional human head finite-element model validation against two experimental impacts. Annals of biomedical engineering 27:403-410.

Willinger R, Taleb L, Pradoura P. Head biomechanics: from the finite element model to the physical model. in: proceedings of the 1995 international ircobi conference on the biomechanics of impact, september 13-15, 1995, brunnen, switzerland, 1995.

Xia Huang WT, Banghai Jiang, and Xianwen Ran (2011). Anisotropic Constitutive Model and its Application in Simulation of Thermal Shock Wave Propagation for Cylinder Shell. Composite World Academy of Science, Engineering and Technology 57:690-695.

Xing G, Barry ES, Benford B, Grunberg NE, Li H, Watson WD, Sharma P (2013). Impact of repeated stress on traumatic brain injury-induced mitochondrial electron transport chain expression and behavioral responses in rats. Frontiers in neurology 4.

Yang J, Dai J (2010). Simulation-based assessment of rear effect to ballistic helmet impact. Computer-Aided Design and Applications 7:59-73.

Yunoki M, Kawauchi M, Ukita N, Sugiura T, Ohmoto T (2003). Effects of lecithinized superoxide dismutase on neuronal cell loss in CA3 hippocampus after traumatic brain injury in rats. Surgical neurology 59:156-160.

Zhang J, Pintar FA, Yoganandan N, Gennarelli TA, Son SF (2009). Experimental study of blast-induced traumatic brain injury using a physical head model. Stapp car crash journal 53:215-227.

Zhang L, Makwana R, Sharma S (2013a). Brain response to primary blast wave using validated finite element models of human head and advanced combat helmet. Frontiers in neurology 4.

Zhang L et al. (2001a). Recent advances in brain injury research: a new human head model development and validation. Stapp car crash journal:369-394.

Zhang L, Yang KH, King AI (2001b). Comparison of brain responses between frontal and lateral impacts by finite element modeling. Journal of neurotrauma 18:21-30.

Zhang L, Yang KH, King AI (2004). A proposed injury threshold for mild traumatic brain injury. Journal of biomechanical engineering 126:226-236.

Zhang TG, Satapathy SS, Dagro AM, McKee PJ. Numerical Study of Head/helmet interaction due to blast loading. In: ASME 2013 International Mechanical Engineering Congress

and Exposition, 2013h. American Society of Mechanical Engineers, pp V03AT03A004-V003AT003A004.

Zhou C, Khalil TB, King A. A new model comparing impact responses of the homogeneous and inhomogeneous human brain. In: sae publication p-299. proceedings of the 39th stapp car crash conference, november 8-10, 1995, san diego, california, usa (sae technical paper 952714), 1995.

Zhou C, Khalil TB, King AI (1994). Shear stress distribution in the porcine brain due to rotational impact. SAE Technical Paper.

Zhou C, Khalil TB, King AI, Dragovic LJ (1997). Head injury assessment of a real world crash by finite element modeling NASA.

Zong Z, Lee H, Lu C (2006). A three-dimensional human head finite element model and power flow in a human head subject to impact loading. Journal of Biomechanics 39:284-292.